On the Observation of Tidal Gravity Variations at Syowa Station, Antarctica and the Effect of Sea Surface Height Variations

Tadahiro Sato

Doctor of Philosophy

Department of Polar Science
The Graduate University for Advanced Studies

2000

On the Observation of Tidal Gravity Variations at Syowa Station, Antarctica and the Effect of Sea Surface Height Variations

A thesis presented

by

Tadahiro Sato

Table of Contents

List of Figures

List of Tables

Abstract

The continuous gravity observation with a superconducting gravimeter (SG) #016 was started on March 22, 1993 at Syowa Station, Antarctica (69.0 N, 39.5 E). Since then, the observation is continued by Japanese Antarctica Research Expedition (JARE). This thesis mainly describes the analysis results for tidal gravity changes using the Syowa SG data and discusses the various oceanic effects on its observation. The tides treated here are those for the 12 hours to 1 year in the period. Related with the analysis for long-period tides, the gravity effects at Syowa Station due to the polar motion were reanalyzed and compared with other two SG sites in the mid latitude (i.e. Esashi, Japan and Canberra, Australia). The effect of Sea Surface Height (SSH) variations are also discussed mainly focusing into the annual gravity changes.

The thesis consists of ten chapters. In Chapter 1 (Introduction), first, the importance of gravity observation made at high latitude is described. The remaining part of Chapter 1 explains the outline of contents of this thesis. Chapter 2 reviews the tidal phenomena and the definition of several quantities appeared in the thesis. Chapter 3 describes the method to estimate the ocean effects and the computer program used in this thesis. The characteristics of SG is described in the first part of Chapter 4 related with the observation results shown in the later Chapters. The locality of Syowa Station, the procedures for setting up of the SG and the data acquisition system used in the observation are also introduced in Chapter 4. We used the computer program called BAYTAP-G and -L for the tidal analysis. The method and some problems on the actual analysis used this analysis method are mentioned in Chapter 5. The observed results are discussed in Chapters 6, 7 and 8 for the short-period tides, the long-period tides and the polar motion effect especially focusing into the annual component, respectively. The conclusions are summarized in Chapter 9 for each topics styuied in Chapter 6, 7 and 8. Finally, the concluding remarks are given in Chapter 10.

In Chapter 6, we reexamined the gravity tidal factor (δ-factor) of the diurnal and semi-diurnal tides at Syowa Station. The 2-year SG data obtained in the period from March 1993 to March 1995 were used in the analysis. The ocean tide effects (the effects of the attraction and loading due to the ocean mass) were estimated using a new global ocean tide model by Matsumoto et al. (1995). As the δ-factors corrected for the ocean tide effects, we obtained the values of 1.144, 1.127, 1.157 and 1.111 for O_1, K_1, M_2, and S_2 waves, respectively. We compared the observed mean δ-factors with the two theoretical values inferred from Wahr's (1980) theory and the Dehant's (1987) theory. The discrepancies between our values and the Wahr's theory are at about 0.2 % for both the diurnal and semi-diurnal tides and those with the Dehant's are at about 0.6 % and 2 % for the diurnal and semi-diurnal tides, respectively. The Syowa SG data indicate that the Wahr's theory is much consistent with the observation than the Dehant's theory. Judging from the consistency among the three observation results obtained by the three different gravimeters (Ogawa et al., 1991; Kanao and Sato, 1995; this study), and from the results for the computations of the ocean tide effects, it is highly probable that the large discrepancy exceeding 10 % in the δ-factors for the semi-diurnal tides at Syowa Station, which has been pointed out by Ogawa et al. (1991), is mainly caused by their inaccurate estimation of the ocean tide effects.

In Chapter 7, we examined the long-period tides (M_f and M_m waves) based on the 2 years SG data which are the same data as those used in the analysis for the short period tides (Chapter 6). The obtained amplitudes, phase lags and amplitude factors (δ- factors) are 11.642 ± 0.035 μGal, -0.12° ± 0.17° and 1.1218 ± 0.0034 for the M_f wave, and 6.143 ± 0.058 μGal, 0.33° ± 0.54° and 1.1205 ± 0.0106 for the M_m wave, respectively (1 μGal = 10^{-8} m s^{-2}). The ocean tide effects at the observation site were estimated using the five global ocean tide models: equilibrium ocean tide model, Schwiderski (1980) model, Dickman

(1989) model, CSR model (Eanes, 1995), and Desai & Wahr (1995) model. The averages of the five estimates are 0.433 μGal and 0.243 μGal in amplitude and 192.9° and 179.5° in phase for the M_f and M_m waves, respectively. The five estimates differ by a maximum of 0.057 μGal in amplitude and 18.7° in phase for the M_f wave, and by 0.033 μGal and 6.4° for the M_m wave. The estimated M_m phases are nearly 180° for the five models, and the variation of their values among the models is relatively small compared with that of the M_f phases. These indicate that the M_m wave is much close to an equilibrium tide than the M_f wave. Due to the variation of the ocean tide corrections, the corrected δ-factors were scattered within the ranges of 1.157 to 1.169 for the M_f wave and of 1.161 to 1.169 for the M_m wave. However, it is noted that the mean δ-factors of the five ocean models, i.e. 1.162 ± 0.023 for the M_f wave and 1.165 ± 0.014 for the M_m wave, prefer slightly larger value rather than those estimated from the theory of the elastic tide.

In Chapter 8, the results for the polar motion effect are described. First, the previous analysis results and the problems on the analysis for this effect, which were obtained from the analysis by Sato et al. (1997) using the two years Syowa SG data, are summarized. They discussed the two problems, i.e. on an interference problem between the annual and Chandler components and on an effect of the inaccurate estimation of step-like changes including the observed data. Based on their experiences, a revised analysis model is applied here and the analysis is carried out using the Syowa SG data much longer than those used in the previous analysis. Thus, it is revised so that (1) the annual component of the polar motion data was excluded from the IERS EOP (International Earth Rotation Service Earth Orientation Parameter) data before fitting and (2) the term to estimate the step-like changes using the Heviside's function was added to the previous model. It was shown that, by using the revised model, the analysis error for the annual component is improved by about 15 % in the case of Esashi, for example. The reliability of the analysis results is also affected by the stability of the period of Chandler component in time. We, therefore, examined this using the 22 years IERS EOP data, and we recognized that the period of Chandler component is stable within ±1.3 days during the observation period of the 17 years from 1983 to 1999. We obtained a value of 435.4 as the mean Chandler period averaged over the 17 years. This value was used for the fitting though this study.

In Chapter 8, we discussed also the results for the estimation of annual gravity changes by calculating the four effects of the solid tide, ocean tide, polar motion and SSH variations. In order to pull out the effect of mass changes in the SSH variations, it is needed to estimate the thermal steric changes in SSH variations, and to correct its effect. We evaluated the steric coefficient based on mainly the POCM (Parallel Ocean Climate Model, Stammer, 1996) SSH (Sea Surface Height) data and the SST (Sea Surface Temperature) data, and we obtained a value of 0.60×10^{-2} m/°C. The predicted annual effect at the three observation sites (i.e. Esashi in Japan, Canberra in Australia and Syowa in Antarctica) were compared with the actual data obtained from the superconducting gravimeters respectively installed at these three sites. The results of the comparison indicate that the predictions agree with the observations within 20 % in amplitude (i.e. within 0.2 μGals, where 1 μGal $=1\times10^{-8}$ ms^{-2}) and 10° in phase at each observation site, when we use the above steric coefficient. We have also tested other values for the steric coefficient, i.e. 0.0×10^{-2} m/°C and 1.0×10^{-2} m/°C, but find that the fit to observations is clearly better at 0.60×10^{-2} m/°C. For comparison, we have also evaluated the SSH effect using TOPEX/POSEIDON data (T/P data). The results from the T/P data indicate a very similar dependence on magnitude of the steric coefficients with that obtained from POCM data, although there exist some systematic differences in amplitude and phase between the two SSH data of the POCM and T/P. It is worth noting that the gravity observations favor a steric coefficient of 0.60×10^{-2} m/°C. This means that the gravity observations support the steric coefficient which was independently estimated from the SSH and SST data. This may be important on future applications of the gravity observation as a data to monitor the mass changes in the oceans which could not be detected from the precise satellite altimetry such as the T/P altimeter. We consider that the agreement between the observation and prediction shown here gives us a base to study the Earth's response to the Chandler motion and/or the excitation problem on it.

Chapter 1.
Introduction

Importance of gravity observation made at high latitude

The gravity observation at Syowa Station using a superconducting gravimeter (hereafter referred to as SG) was initiated as a part of the five-year (1993-1998) earth science program of the Japanese Antarctica Research Expedition. A model TT70 of SG (GWR Instruments: SG016) was installed there and the continuous observation started on March 22, 1993. The SG is a kind of relative gravimeter, which uses the magnetic restoring force generated by a superconducting current instead of the elastic spring force adopted in conventional metal gravimeters such as LaCoste & Romberg gravimeter (after here, LaCoste & Romberg is abbreviated to L & R). Due to remarkable stability of the restoring force and the high sensitivity, the SG is highly expected to identify the gravity signals having periods longer than one year or the signals whose amplitudes are as small as 1 nGal (1 nGal = 1×10^{-11} ms^{-2}) (Goodkind, 1999).

Figure 1 shows the SG network as of 1999, composed of 14 stations. Japanese SG group contributs to this network by developing an international SG observation network called 'GGP-Japan Network', which consists of seven sites marked with the red circles. The SG network will help clarify various geophysical phenomena as described below, by disclosing weak gravity signals covering the wide spectral range from 1 minute to 14 months or longer.

(1) Core modes (approximately 10-30 minutes period; Imanishi et al., 1992) which are characterized by the elastic strength of the inner core or by the associated anelastic structure.

(2) The Slichter mode (approximately 3-13 hours period; Slichter, 1961) which is characterized by translational motion of the inner core, or a degree of departure of the fluid core from the symmetrically layered structure being supported by

the hydrodynamic force.

(3) Fluid core resonance (FCR) in the diurnal tidal band (approximately one sidereal day period; Wahr, 1981, Sato et al., 1994) which may reflect degrees of the departure of the figure of the core-mantle boundary (CMB) and of the strength of coupling at CMB.

(4) The core undertone (approximately 13 hours period; Crossley and Rochester, 1980) which may reflect gravitational waves in the fluid core, and may provide information of the mechanical structure and associated temperature distribution in the fluid core through estimation of the density profile.

(5) The long-period tides (approximately 14 days period for example Mf tide) which are expected to give important information of frequency dependent rheological properties of the earth.

(6) Gravity changes of the periods from 12 months to 14 months due to the effect of the earth's variable rotation, which are expected to tell us the coupling dynamics between the solid parts and fluid parts of the earth.

Because the strength of the restoring force related to (2) is mainly a function of the buoyancy which is related to the distribution of density stratification inside the fluid core, the motion is probably induced by much weaker force than the earth's free oscillations. Further the motion of the fluid core may be characterized in much lower frequency bands than those of the earth's free oscillation which are mainly related to the elastic strength of the mantle. The gravity changes related to the fluid and solid inner cores are considered to be as small as 1-3 nGal (1 nGal = 1×10-3 μGal) or even smaller (Crossley, 1988), and therefore careful treatment is required to discriminate the signals from possible instrumental and environmental noises. However, these gravity changes must show some spatial characteristic, both in amplitudes and phases, depending on the geographical locations of the observation sites. Further, the amplitude spectra must have common peaks at the frequencies close to the eigenmodes of the fluid and solid inner cores. Thus it is expected to identity such weak signals when simultaneous observations are made with a global SG observation network and the obtained data are analyzed by a stacking method based on an appropriate physical model. The results for the analysis of FCR by Sato et al. (1994) is one of the example of this.

As shown in **Fig.** 1, most SG observation stations are located within a narrow latitude zone between 30°N and 50°N. This geographically biased station distribution may be a restriction of the global SG network for the purpose of drawing the maximum instrumental potential of the SG and thereby detecting weak gravity signals as mentioned above. Because the gravity signals caused by the free core resonance (FCR) appearing at the diurnal tidal band are sensitive to the shape of the CMB or by dynamical ellipticity of the core and these effects are represented with a function of latitude, for instance. Therefore, installing the SGs at high latitudes of both hemispheres and comparing them with those obtained at the mid latitudes and/or at the equatorial zone must be required to interpret the delicate signals precisely. For FCR, it will be explained in the section 2.3.

Figure 5 of Chapter 2 shows the latitude dependency of the tidal gravity amplitude. As shown in the figure, the amplitude of diurnal waves takes its maximum at ±45°, while its minimum at the equator and both poles. For semidiurnal waves, on the other hand, the maximum amplitude appears at the equator while both poles are nodes. Moreover the long-period tides become maximum at both poles and their nodal lines exist at about ±35°. The above mentioned characteristics of the spatial distribution of tidal amplitude strongly suggest some the advantages as mentioned below, to carry on the SG observation at Syowa Station in the high latitude zone (69.0°S).

(1) The amplitude of the semidiurnal tide is smaller than about 20% of its maximum. This is an advantage to search for a small signal induced by FCR which

appears in the diurnal tide band preserving 70% of the maximum amplitude at Syowa Station.

(2) Smallness of the semidiurnal tide is also an advantage to search for the core under tone signal which is believed to have a main spectral peak at 12 to 13 hours. Because these periods are very close to those of the semidiurnal tides. Thus, the signal-to-noise ratio (SNR) is expected to be highly improved in the observation at Syowa Station.

(3) SNR of the Mf long-period tide will be obviously improved compared to the observation at the mid-latitude stations.

Contents of this thesis

It is a notable thing that the incessant excitation of the earth's free oscillations of the fundamental spheroidal modes (frequency range: 0.3 to 5 mHz) was first found from the data obtained from the SG at Syowa Station (Nawa et al., 1998). After their paper was published, this phenomena has been confirmed by several analyses using the data obtained from several international seismometer networks, and the existence of this phenomena has been established (Kobayashi and Nishida, 1998, Suda et. al., 1998, Tanimoto et. al. 1998). Now the phenomena of 'incessant excitation of the earth's free oscillations' is called 'earth's background free oscillations'.

While, in this thesis, we will focus to the gravity signals in much lower frequency bands than the seismic band. It is well known that observed gravity signals are strongly affected by the effects due to the motions of atmosphere and oceans. Therefore, calculation of the effect of the oceans on the observed gravity changes is one of the important subjects of this thesis.

Chapters 2 and 3 are also introductory parts of this thesis. These chapters give a review of the tidal gravity theory and the method used here to estimation the ocean tide effects, respectively. Chapter 4 describes some characteristics of the SG and the problems on setting up the SG at Syowa Station. The tidal analysis has been performed by the two analysis programs called 'BAYTAP-G and -L'. In Chapter 5, these tidal analysis methods are introduce briefly, and gives some comments on a problem of the analysis model regarding to the analysis for the long period tides. Chapter 6 describes the results for the analysis of short-period tides using the data obtained from the SG at Syowa Station and discuss the difference between the results obtained here and those previously obtained at the same observation site by Ogawa et al. (1991) and Kanao and Sato (19 . Chapter 7 describes the results for the long-period tidal gravity changes and their implication to global ocean tide modeling. In the former part of Chapter 8, the analysis results for the polar motion effects (period: 1 year - 14 month) are described, and, in the later part of Chapter 8, the discussions mainly focusing to the observed annual gravity changes are made related with the gravity changes based on the data of the sea surface height variations. Finally, the possibility of a further application of the gravity observation as a tool to monitor the mass changes in the oceans are described.

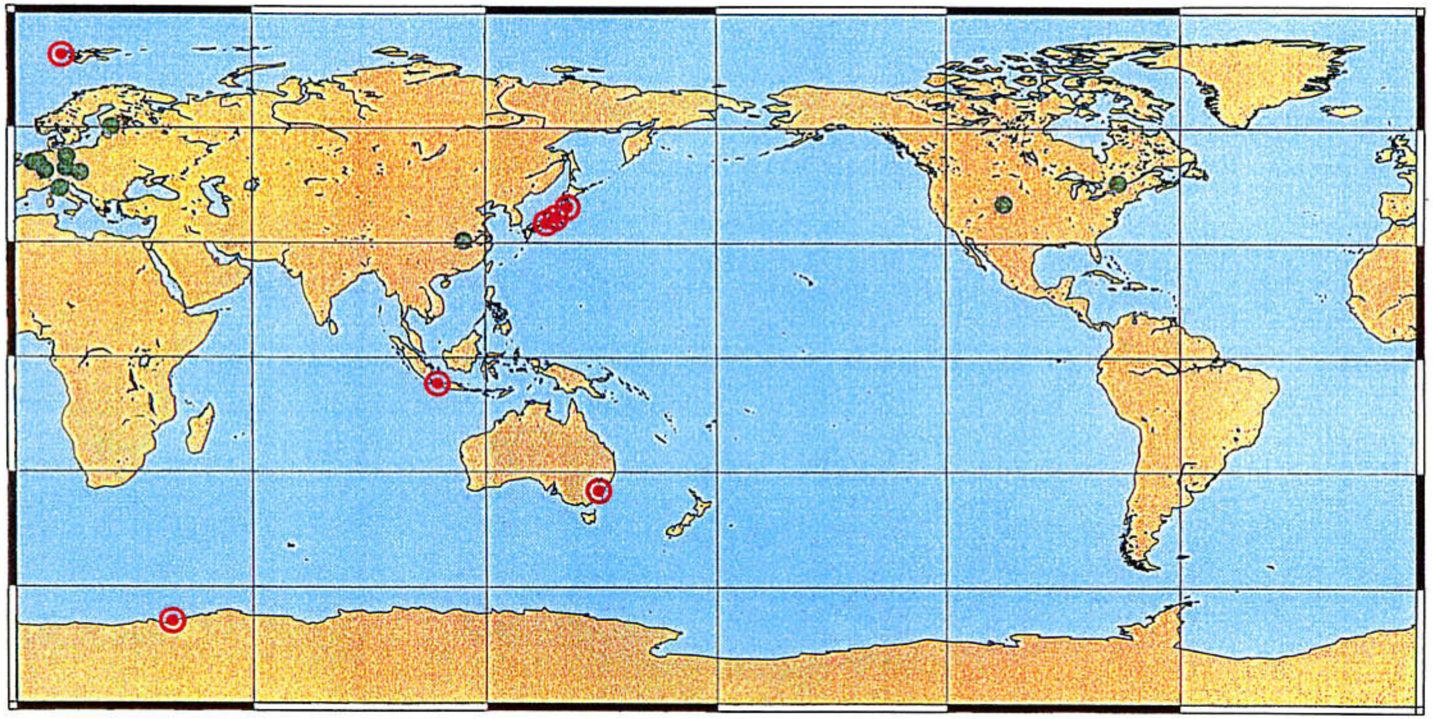

Fig. 1. GGP Network and GGP-Japan Network. This shows all superconducting gravimeter sites those which participate in GGP. The green circles show the overseas sites and the double red circles show the observation sites of GGP-Japan Network which is developing by the Japanese GGP group.

Chapter 2.
Gravity Tide on the Earth

The theory of tides and the derivation of the expression for the tide generating potential are explained in many text books (for example: Hagiwara, 1978, Melchior, 1983, Harrison, 1985 and Lambeck, 1988). We describe here their essential parts which are related with this thesis.

2.1 Tide Generating Potential

Any unit masses composing the volume (body) of the earth are affected by a force combined two of the Newtonian gravitational attraction of celestial bodies (CBs) and the centrifugal acceleration due to the orbital motion of the earth. On the meaning acting to a whole body, these forces are called the body forces. Owing to the finite size of the earth, the former is not constant throughout the earth. The difference in the Newtonian attraction by the positions causes the tidal gravity changes on the earth. We define the positional relation between the earth and the CB using an orthogonal X-Y-Z coordinate which is fixed at the earth's center and moves with the earth (see **Fig.** 2). In this figure, O and P show the center of the earth and a point on its surface, respectively. Three vectors, F_1, F_2 and F_3, show the attractions of CB acting at O and P and the centrifugal attraction induced by the earth's orbital motion, respectively. The constant attraction F_3 balances F_2. If we measure the potential with respect to the value at O, we can write the potential at P induced by the CB as

$$V = GM(1/r - 1/R - \rho \cos z / R^2) \tag{1}$$

where: G is the Newtonian gravitational constant; M the mass of CB; r the distance between earth' center and CB; R the distance between a point P on the earth and the center of the CB; ρ the earth's radius; z the angle MOP called zenith distance of the CB. The part 1/r can be developed using the zonal spherical harmonics $P_n(\cos z)$ as

$$1/\mathrm{r} = 1/\mathrm{R}\ \textstyle\sum_{n=0}^{\infty}(\rho/\mathrm{R})^n P_n(\cos z). \tag{2}$$

By substituting (2) into (1), we obtain

$$\mathrm{W} = \textstyle\sum_{n=2}^{\infty}\mathrm{V}_n = \mathrm{GM}\textstyle\sum_{n=2}^{\infty}(\rho/\mathrm{R})^n P_n(\cos z). \tag{3}$$

The potential W, which consists of the terms of n≥2, is variable with the position on the earth and this potential is called 'tide generating potential'. The main tide generating celestial bodies are the Moon and Sun.

Figure 3 shows the position of CB projected onto the celestial sphere in the equatorial coordinate system. The daily variation of W on a position fixed to the rotating earth can be represented by developing $\cos z$ with the three angles Θ, δ and ψ. Using a formula of the spherical triangle, we obtain

$$\cos(z) = \sin(\psi)\sin(\delta) + \cos(\psi)\cos(\delta)\cos(\Theta). \tag{4}$$

Here these three angles stand for: ψ geocentric latitude of the observation point; δ declination of the CB; Θ local hour angle of CB. The local hour angle Θ has a relation with the Greenwich hour angle Θ_G as

$$\Theta = \Theta_G + \lambda \tag{5}$$

where λ is the east longitude of the observation point.

In (3), the second degree potential V_2 has the largest amplitude among V_n. By substituting (4) into (3), we obtain an expression for V_2 as

$$V_2 = GM(\rho/R)^3\{3(\sin^2\delta - 1/3)(\sin 2\psi - 1/3) \\ +(\sin 2\psi \sin 2\delta \cos\Theta) + (\cos^2\psi \cos^2\delta \cos 2\Theta)\} \qquad (6).$$

From (6), we can see several characteristics of the tides. Namely, it indicates that the tidal potential V_2 consists of the three terms (tidal species). Each of them is distinguished by its time variation represented by the change in Θ, and shows its own spatial pattern of the amplitude distribution. These three tidal species, respectively, are called the long-period tide, the diurnal tide and the semidiurnal tide in the frequency domain. While, from the spatial pattern of amplitude distribution of each specie, they are called the zonal tide, the tesseral tide and the sectorial tide, respectively. Due to the dependency on δ, we see that the diurnal tide never arises, if the CB moves on the orbit which is coincident with the equator of the earth. On the other hand the semidiurnal tide never arises, if the CB moves on the orbit which is coincident with the earth's meridian. As seen in (6), the tidal potential decreases its amplitude with the factor of $(\rho/R)^n$. Since ρ/R is a small quantity of about 0.0166 for the Moon, it is enough to consider the potentials up to the 4th degree for most observation purposes.

Actually, however, the orbital motion of the CB is far from a pure circular motion. Thus, the position angles δ and Θ are represented as a superposition of a number of circular motions (harmonic motions). The angular variation in time of each harmonics is usually represented with five arguments so called Doodson's arguments. The five astronomical arguments are: τ mean lunar day; s tropic month; h tropic year; p period of revolution of the mean perigee of the Moon; N' period of revolution of lunar nodes; p_s period of revolution of the solar periherion. Each harmonics is called "tidal wave" or "tidal constituent'. The main constituents are M_f for the long-period tides, O_1 and K_1 for the diurnal tides and M_2 and S_2 for the semidiurnal tides. The period and origin of these main constituents are summarized in **Table** 1. The tidal potential tables developed by Cartwright and Tayler (1971) and Cartwright and Edden (1973, the revised table of the former) have been widely used in the study of ocean tides. While, in the study of earth tides, the potential table given by Tamura (1987) is widely used. In his table, the Doodson argument, angular speed at the year 2000 and amplitude at that epoch are given for the 1200 constituents in total, which were obtained by developing the three potentials of V_2, V_3 and V_4 by means of the FFT (First Fourie Transformation) method. The tidal analysis in this thesis is carried out using tidal analysis programs called "BAYTAP-G' for the short-period tides and "BAYTAP-L' for the long-period ones (Tamura et al., 1991). In these programs, the observed tidal components are estimated based on the Tamura's potential table.

Table 1. Main constituents in each of the three tidal species.

tidal specie	name of consitutuent	period	origin
zonal	M_f	14 days	declinational wave of M_0 (the constant lunar tide)
tesseral	O_1	25.819 hours	principal lunar daily tide
	K_1	23.934 hours	combination of the principal lunar and solar declinational tides
sectorial	M_2	12.421 hours	principal lunar semidiurnal tide
	S_2	12.000 hours	combination of the principal solar semidiurnal tide and variational tide from M_2

The mass on and in the earth is redistributed asymmetrically by the diurnal tidal force with respect to both the meridian and the equator. This produces a torque which causes the wobbles of the earth so that its mantle figure axis rotates in space (i.e. forced nutation). Any similar redistribution of the earth's mass represented spatially by the P_2^1 mode in terms of the spherical surface harmonics can also produce the similar effect on the earth's rotation (i.e. the changes in the polar motion and free core nutation, which will be described in the following chapters). This is a reason why the studies of the earth tides and the earth's rotation have close relation to each other.

2.2. Gravity Tides on the Rigid Earth

The expression of the tidal gravity changes is derived by differentiating the tidal potential with respect to the radial direction ρ, which is represented as

$$\mathbf{A} = \sum_{n=2}^{\infty} A_n = \sum_{n=2}^{\infty} \partial \mathrm{V}_n / \partial \rho, \tag{7}$$

where A_n is the n-th degree tidal force in the normal direction to the earth's surface, positive upward. (7) gives the tidal force on a rigid earth (i.e. in the sense of not taking account the effect of deformation of the earth), and **A** is usually used as the reference (i.e. a theoretical value) to measure the response of the earth to the tidal forces.

(7) is an expression using the geocentric coordinate in the spherical earth. However, the actual gravimeter is made on the earth's surface which is approximated by an ellipsoid of revolution in its shape (i.e. the reference ellipsoid) and it measures the force changes in the direction of local vertical (i.e. the changes in the force composed of combination of the self-gravitational attraction of the earth's mass and the centrifugal force due to the earth's rotation). Therefor, it is needed to convert (7) into an expression projected onto the direction of local vertical. Since the direction of a local vertical is almost coincident with the direction of the normal line of the observation point P on the reference ellipsoid, we refer this ellipsoid for expressing the theoretical value to be compared with the observation. We define the three angles ψ, λ and η and the unit vectors $\mathbf{e}_\psi$,

$\mathbf{e}_\lambda$ and $\mathbf{e}_\eta$ in the respective directions as shown in **Fig.** 4. These three angles are called as: ψ, the geocentric latitude of the observation point, λ the east longitude and η the geocentric radial component. With respect to the ψ-λ-η coordinate system, the tidal force is written as

$$\mathbf{A}' = \sum_{n=2}^{\infty}\{1/\eta\partial \mathrm{V}_n/\partial\psi \mathbf{e}_\psi + (1/\eta\cos\psi)\partial \mathrm{V}_n/\partial\lambda \mathbf{e}_\lambda + \partial \mathrm{V}_n/\partial\eta \mathbf{e}_\eta\} \qquad (8).$$

In **Fig.** 4, φ shows the geographical latitude, and ϵ is the difference between the angle ψ and φ

$$\epsilon = \varphi - \psi \qquad (9).$$

If we take the z-direction along φ and its positive direction downward, the gravity change due to tidal forces is given by

$$\Delta g = \mathbf{A}' \cdot \mathbf{e}_z = -\sum_{n=2}^{\infty}(\partial \mathrm{V}_n/\partial\eta\cos\epsilon + 1/\eta\partial \mathrm{V}_n/\partial\psi\sin\epsilon) \qquad (10)$$

where $\mathbf{e}_z$ is the unit vector in the z-direction.

Using the Doodson's normalization and arguments defined by U_i and developing V_n with the spherical harmonics function P_n^m, for the degree 2 tides, the explicit formulas for the i-th constituent are given as

$$\Delta g_0 i = -C_v(\rho_e\cos\varphi - 2\rho_p\sin\varphi)A_i\cos U_i \quad \text{for the zonal wave,} \qquad (11)$$

$$\Delta g_{1i} = -2C_v(\rho_p\cos\varphi + \rho_e\sin\varphi)A_i\cos U_i \quad \text{for the tesseral wave,} \qquad (12)$$

and

$$\Delta g_{2i} = -2C_v(\rho_e \cos\varphi)A_i \cos U_i \qquad \text{for the sectorial wave.} \qquad (13)$$

Here

$$C_v = \tfrac{3}{4}\mathrm{GM}\tfrac{\varrho^2}{c^3}\tfrac{1}{a}, \qquad (14)$$

$$\rho_e = \rho\cos\psi = \{1/\sqrt{1-f^2\sin^2\varphi}+H/a\}\cos\varphi \qquad (15)$$

and

$$\rho_p = \rho\sin\psi = \{(1-f^2)/\sqrt{1-f^2\sin^2\varphi})+H/a\}\sin\varphi, \qquad (16)$$

where: A_i is the amplitude of tidal potential for the i-th constituent; M, c and a is the mass of Moon (or Sun), the mean distance of Moon (or Sun) and the equatorial radius of the earth; ρ is the geocentric distance of the observation point P shown in **Fig.** 4, i.e. it is the sum of the two distances of the surface of reference ellipsoid measured from O and the height H of the observation point P measured from the surface of reference ellipsoid.

The computation results for the three constituents of M_f, K_1 and M_2 using (11), (12) and (13) are shown in **Fig.** 5, and **Table** 2 lists up the values of GM of the Moon or the Sun, the earth's equatorial radius a and the earth's flattening f. These values are those used in the tidal analysis programs BAYTAP-G and -L by Tamura et al. (1991).

Table 2. The constants used in BAYTAP-G and -L

quantity	value	unit
GM of the Moon	4.9027933×10^{12}	m^3s^{-2}
GM of the Sun	1.32712438×10^{20}	m^3s^{-2}
Earth's equatorial radius	6,378,136	m
Earth's flattening	1/298.257	

2.3. Gravity Tides on the Deformable Earth

2.3.1 Gravimetric Tidal Factor (δ−factor)

In addition to the direct tidal force of the celestial bodies (primary gravity tides), the gravity tides on the deformable earth is further induced by other two effects (secondary gravity tides). They are the changes induced both by the displacement of the observation position and by the redistribution of the earth's mass associated with the deformation. These additional effects (i.e. the responses of the deformable earth to the tidal force) is usually represented in terms of the dimensionless parameters so called Love's numbers h and k (Love, 1909, 1911) and Shida's number l (Shida and Matsuyama, 1912). h, k and l are related to the vertical displacement, additional potential change and the horizontal displacement, respectively. Although these three numbers h, k and l are frequently called 'Love numbers' and Lambeck (1988) also uses this word in his text book, it is not correct. Because Love introduced only the h and k in his paper written in 1909. This is pointed out also in a famous text book 'The Earth' by Jeffreys (1970).

The magnitudes of h, k and l are estimated by solving the simultaneous equations for the elastic earth being hydrodynamically balanced, which consist of the four equations, namely, the equation of motion, the constitution equation representing the stress-strain relation, the equation of continuity, and the Poisson equation representing the pressure balance. This system of the equations are usually summarized by using 6 variables so called Alterman's y-notation (Alterman et al., 1959). For the tidal deformations (i.e. for tidal Love and Shida numbers), this system is solved by assuming the stress free condition at the earth's surface. When the other boundaries exist inside the earth such as the core-mantle boundary (CMB), the boundary conditions are also taken into account. Takeuchi(1950), for the first time, calculated the Love numbers and Shida number based on the distribution of density and elastic parameters (i.e. rigidity and shear modulus) within the earth using the most realistic values in those days, and obtained the values of 0.587-0.610, 0.281-290 and 0.068-0.082 for h, k and l, respectively.

The Love and Shida numbers are a function of the degree of the tidal forces. For the case of the spherical and non-rotating earth model, the vertical deformation (v) and the additional potential change (w) are expressed as

$$\mathrm{v} = \textstyle\sum_{n=2}^{\infty} h_n \mathrm{V}_n / g(r) \tag{17}$$

and

$$\mathrm{w} = \textstyle\sum_{n=2}^{\infty} k_n \mathrm{V}_n, \tag{18}$$

where h_n and k_n are the n-th degree Love numbers, $g(r)$ is the earth's gravity which is a function of the distance r from the center of the earth. The primary gravity tide is given by (7). While, the secondary effects correctly consist of: 1) the radial displacement, 2) the vertical gradient of the additional potential and 3) the acceleration of the observation point due to the tidal deformation. The last effect are usually called an 'inertial correction' in the analysis of the gravity tide.

On the earth's surface, the above three effects are represented as follows.

$$\Delta g_v = (\partial g(r)/\partial r)\mathrm{v} = (-2g_0/r_0)\textstyle\sum_{n=2}^{\infty} h_n \mathrm{V}_n/g_0, \tag{19}$$

$$\Delta g_w = (1/r_0)\textstyle\sum_{n=2}^{\infty}(n+1)k_n \mathrm{V}_n, \tag{20}$$

and

$$\Delta g_I = -\omega^2 \mathrm{v}. \tag{21}$$

The potential theory tells us that the change of w in (18) due to the internal origin has the form of $(r_0/r)^{n+1}P_n^m(\cos z)$ at the surface. Where ω is the angular velocity of the tidal constituent in consideration. In the largest case of the effect, the magnitude for the semidiurnal tide is about 1×10^{-2} in ratio to the inertial correction of Δg_I to Δg_v. Therefore, this term is usually neglected in the analysis, but it cannot be ignored in such delicate discussion of the free core resonance mentioned below. When we neglect the inertial correction, the tidal gravity changes (downward positive) is summarized as

$$\Delta g = \textstyle\sum_{n=2}^{\infty}(-\partial \mathrm{V}_n/\partial r) + \Delta g_v + \Delta g_w$$

$$= \textstyle\sum_{n=2}^{\infty}(1 + \frac{2h_n}{n} + \frac{n+1}{n}k_n)(-\partial \mathrm{V}_n/\partial r) \qquad (22).$$

The coefficient of $(-\partial V_n/\partial r)$ consisting of the combination of Love numbers is the gravimetric tidal factor, and this frequently is called '$\delta-$factor'. The observed $\delta-$factor is also defined as the ratio of the observed tide to the theoretical one on the rigid earth, and its value is compared with the theoretical $\delta-$factor to discuss the response of the deformable earth to the tidal force. The tide on an elastic earth is called 'body tide' or 'solid tide' and is distinguished from the tide on the rigid earth or the tide on an anelastic earth having the dissipative process. The observed gravity tide usually does not coincide with Δg due to the modification by several effects such as the effects of the oceans, air pressure changes, the rotation of the earth and so on.

When the rotation of the earth is taken into account, the tides show large differences from those on the non-rotating earth (i.e. differences between the static tides and dynamic ones). There appear two different features. First, the body tides do have a strong frequency dependency especially in the diurnal tidal band, and even the Δg_I term shows an week frequency dependency in the static case. This frequency dependency is due to the effect of the dynamics of the earth's core, namely, the free core resonance (FCR) which will be described in the subsection 1.2.3.. Second, the $\delta-$factor has also a latitude dependency.

Sasao, Okubo and Saito (1980) established the analytical formulas to describe the effect of FCR on the nutation and tides of the earth by extending the theory of nutation of Molodensky (1961) in more general form. Later, based on the pure numerical method, namely, the eigenmode expansion used in the theory of earth's free oscillations developed by Smith (1974), Wahr(1981) computed the tides on the elliptical, rotating, elastic and oceanless earth model and gave the tables of the frequency dependent Love and Shida numbers for the three earth models of: (1) 1066A by Gilbert and Dziewonki (1975), (2) PEM-C by Dziewonski et al. (1975), (3) C2 by Anderson and Hart (1976). Wahr's computation results are widely used in both the nutation and tide studies as a standard model to be compared with the observation. Wahr's (1981) tables give the values computed based on the formulas written in the geocentric coordinate system. However, Dehant (1987) pointed out that Wahr's Love and Shida numbers should be modified, in order to directly compare with the observed gravity tides which give the gravity change along the local vertical as described in the section 2.2.

Another difference between the static tides and the dynamic ones is the latitude dependency of the δ-factor. In case of the dynamic tides, the δ-factor does not take a constant value, but it shows a latitude dependency. **Figure 6** shows two kinds of δ-factors which were estimated using the table of Love numbers given by Wahr(1981) and the Love numbers modified by Dehant(1987), respectively. The two waves of K_1 and O_1 show in the figure. These are the values for the 1066A earth model. As seen in the figure, the latitude dependency of the tidal factors becomes smaller when Dehant's modification is taken into account. It is to be noted that the difference between these two theories is large at the high latitudes. On the other hand, there are neither frequency dependency nor the latitude dependency in the case of the tides on the spherically stratified and non-rotating earth model. In this case, the value of 1.158 for the 1066A model is obtained as $\delta-$factor of the 2nd degree. This value was estimated using the computer program developed by Saito (1967).

Even though the difference between the two theories by Wahr(1981) and Dehant(1987) is small at 1-2 % or less, it is important in the study of the earth tide to discriminate this from the observation. This is the reason why we needed to calibrate the gravimeter at the accuracy better than 0.5 %.

2.3.2. Free Core Resonance (FCR)

It is theoretically well known that, in addition to the Chandler free wobble of the period of about 430 sidereal days (s.d.), the earth has also a rotational eigenmode called "Free Core Nutation" (FCN). This phenomenon has been theoretically studied by many researchers, for example, Toomer, 1974, Sasao et al., 1980 and Wahr, 1981. A mechanical coupling exists between the mantle and core, namely, 'inertial coupling'. This mechanical coupling may be caused by the following three effects: (1) the misalignment between the rotation axis of the mantle and that of the core due to the tidal force acting on the bulge of the non-spherical earth, (2) the elliptical shape of the core-mantle boundary (CMB) and (3) the dynamical pressure acting to the CMB due to the rotational motion of the fluid core. Due to the misalignment between the rotation axis of the mantle and that of the core, the inertia of the core (i.e. caused by (3)) resists the change in the rotation of the surrounding mantle. This is the origin of the inertial coupling.

The FCN is a free wobble (a rotational eigenmode), which is excited by the pressure torque acting through the CMB by the inertial coupling. The period of this mode is theoretically estimated to be 460.8 s.d. in the inertial frame. This is the rotational period of the mantle figure axis measured in space. For an observer on the rotating earth, the period is observed as slightly less than one sidereal day corresponding to the frequency of 1.00217 cycle/s.d. (= 1+1/468.8 cycle/s.d.). For this reason, the FCN is also called the "Nearly Diurnal Free Wobble" (NDFW). Due to the existence of the FCN, the earth tides exhibits the resonance at the frequencies close to the FCR which lies at the diurnal frequency band. This phenomenon is "Free Core Resonance' (FCR), and its period is mainly governed by the strength of the inertial coupling, which is a function of the dynamical ellipticity of the CMB and the rotational speed of the fluid core.

The earth exhibits the dissipative nature due, for example, to the anelasticity of the mantle. In addition to this, there exist other dissipative processes at the CMB which are related to the FCR. They are the magnetic coupling, the viscus coupling and the topographic coupling. The strength of damping of the FCR, as well as the period, depends on dissipative process. The strength of these coupling is governed by the viscosity of the upper fluid core, both the spheroidal and toroidal magnetic fields intersecting the CMB, the magnetic permeability and the topography of the CMB. Due to the dissipative processes, the phase of the observed tide is modified and above all the out-of-phase component appears in the observed forced nutations (for example, Sasao and Sato, 1994). The observation of FCR parameters, namely, the eigen period, Q-value and strength of the resonance is important in geophysics, because they may provide us with a constraint for the upper and/or lower bound of the physical parameters mentioned above.

Sato (1991) analyzed the strain data obtained from the three components of extensometers at Esashi, and obtained the values of 1.00231±0.00006 cycle per sidereal day and 5,200±2, 500 for the eigen frequency and the quality factor Q of FCR, respectively. Later, by stacking the data obtained from the three SGs in Japan, Sato et al. (1994) obtained 1.00229±0.00007, 6,000 (3,240 to ∞), -4.62±0.28 × 10^{-4} and 0.01±0.17 × 10^{-4} for the frequency in cycle per sidereal day, Q-value, real part of the resonance strength and its imaginary, respectively. It is doubtless that the effect of FCR has been detected both the strain and gravity measurements. As seen in their computation results, however, it is also true that the estimation accuracy of the ocean tide effects directly affects on the accuracy of the estimated parameters of FCR. This is the reasons why we need to improve the estimation accuracy of the effects of the ocean tides and the sea surface height variations.

When the dissipative processes of the earth are taken into account, the δ-factor becomes a complex number. Thus it shows theoretically that a phase lag from the input tidal force is at the order of 0.1° or less in the case of the gravity tides. Therefore, in order to study the dissipative effects of the mantle anelasticity and the FCR from the observation, we need to suppress the phase lag of the instrumental and environmental origins to the magnitude smaller than the theoretically expected phase lag. The phase shift due to the mechanical response of the L & R gravimeter will be discussed in Chapter 6.

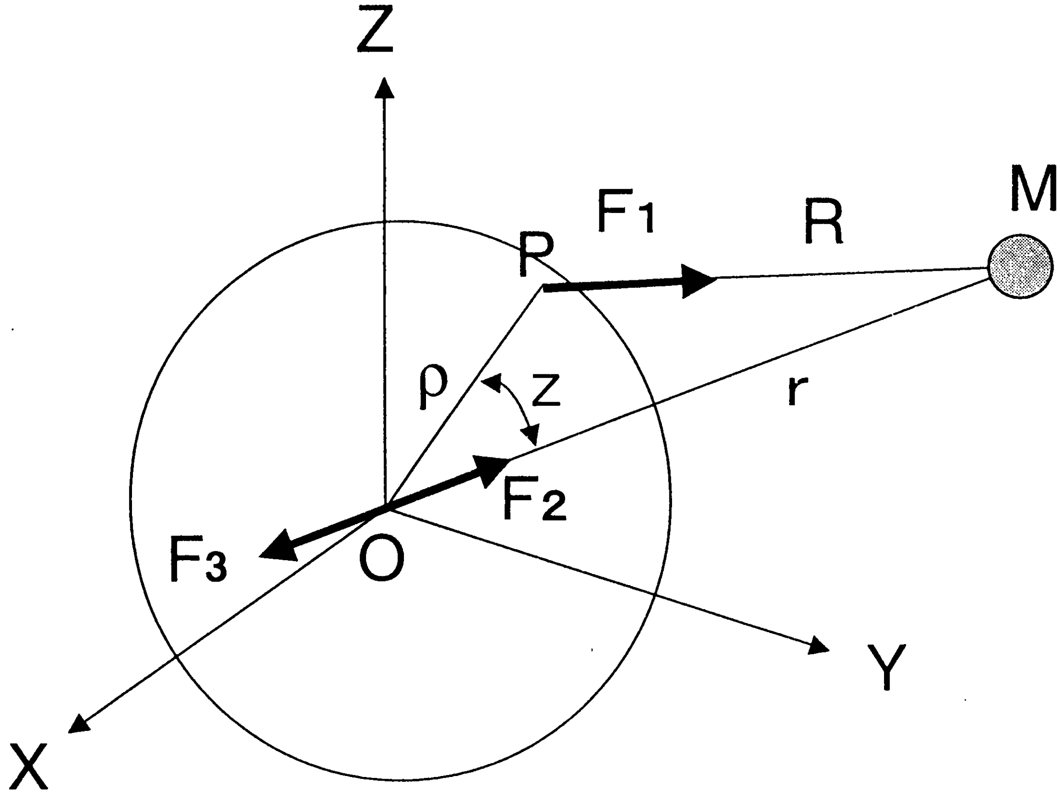

Fig. 2. Forces applied to the particle mass of the Earth. F1 and F2 show the forces by a celestial body M, and F3 is the centrifugal force due to the orbital motion of the Earth.

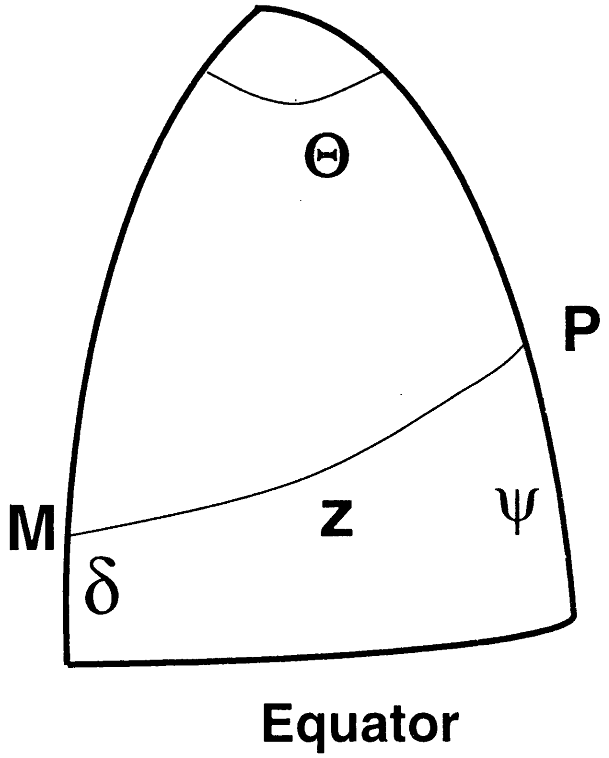

Fig. 3. Celestial spherical triangle to represent the position of the celestial body. This shows the relation between the position of the celestial body (M) and an observation point on the Earth (P), which is illustrated with the equatorial coordinate system. The definitions for other notations are given in the text.

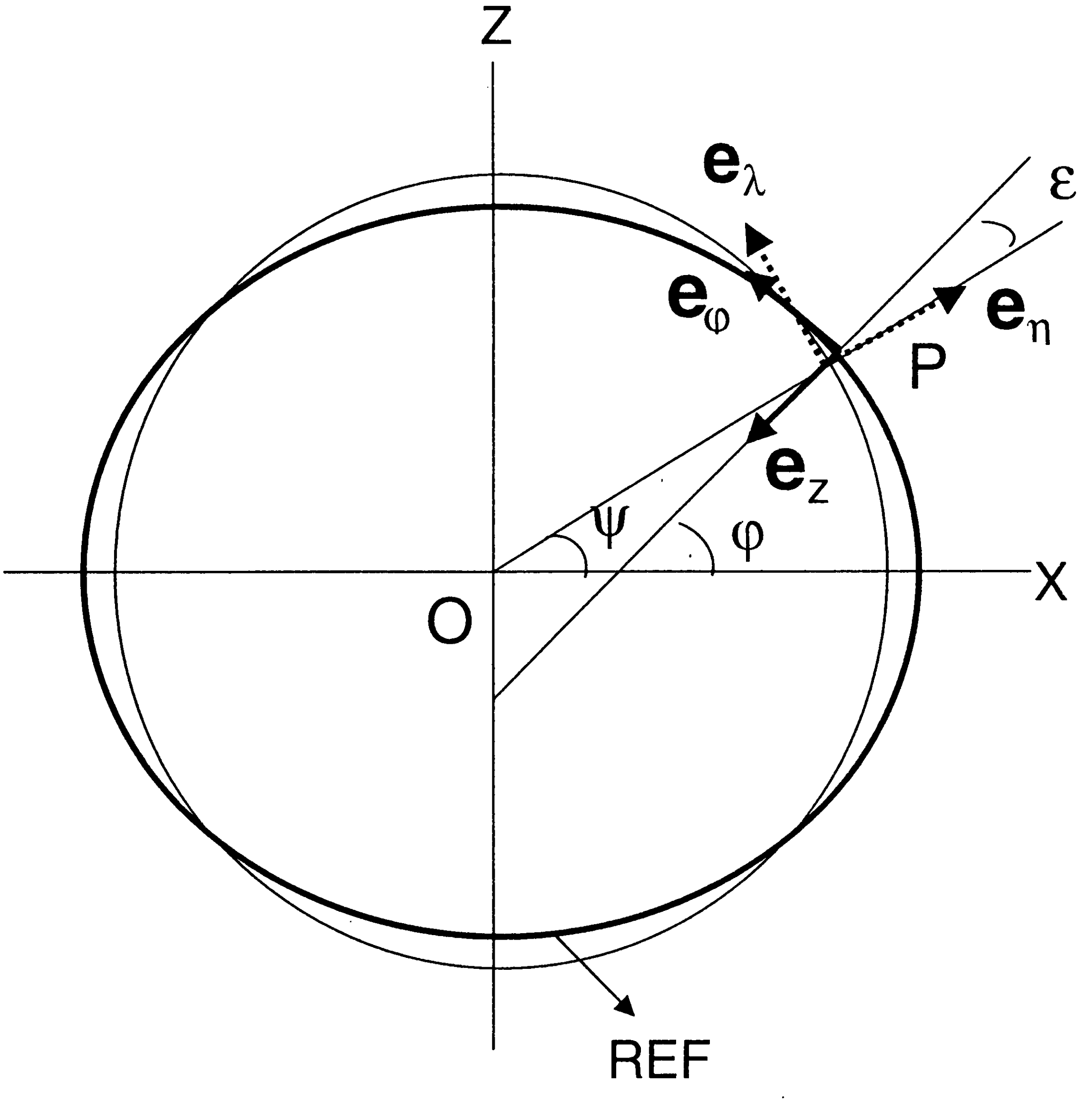

Fig. 4. Relation between the geocentric latitude ψ and the geographic latitude φ. Where REF shows the surface of reference ellipsoid. Other notations are given in the text.

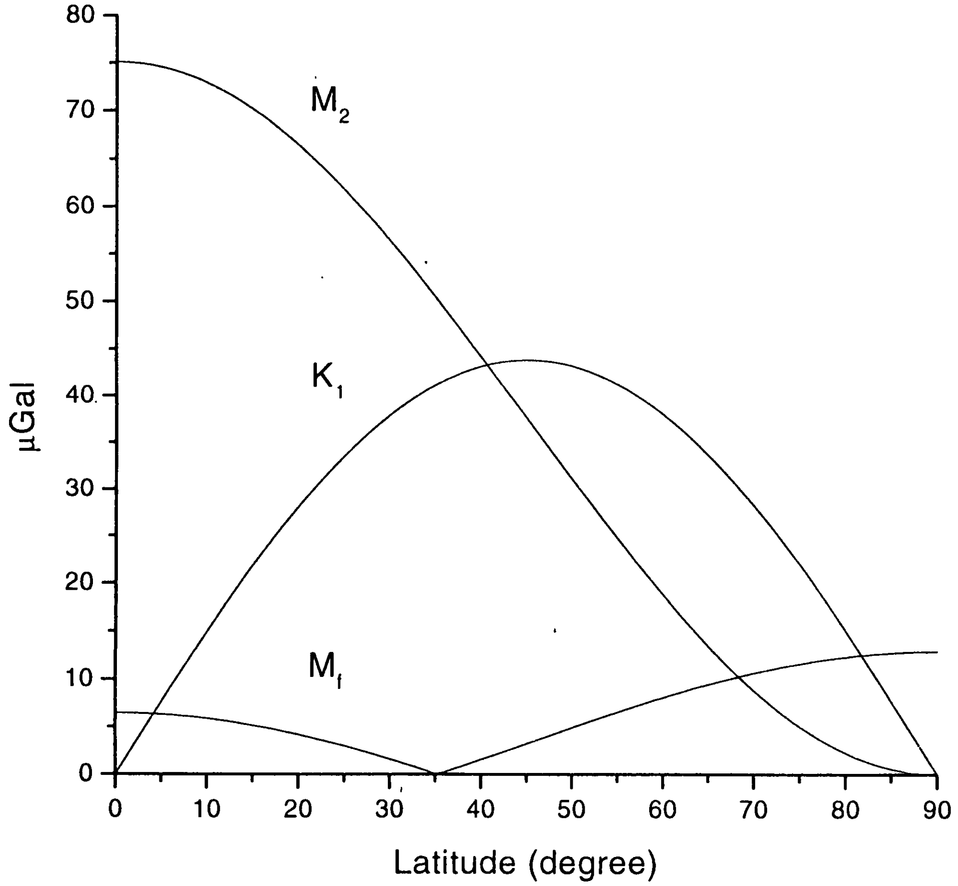

Fig. 5. Latitude dependency of the amplitude of tidal gravity changes. Three constituents of Mf, K1 and M2 are displayed as the main waves in the zonal, tesseral and sectorial tidal species, respectively.
The pattern of the amplitude distribution of each wave is symeric about the equator.

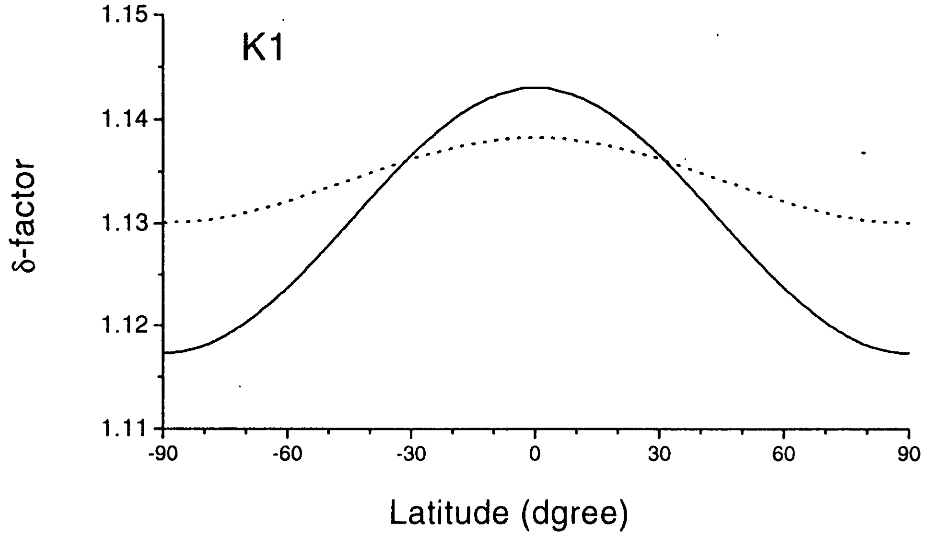

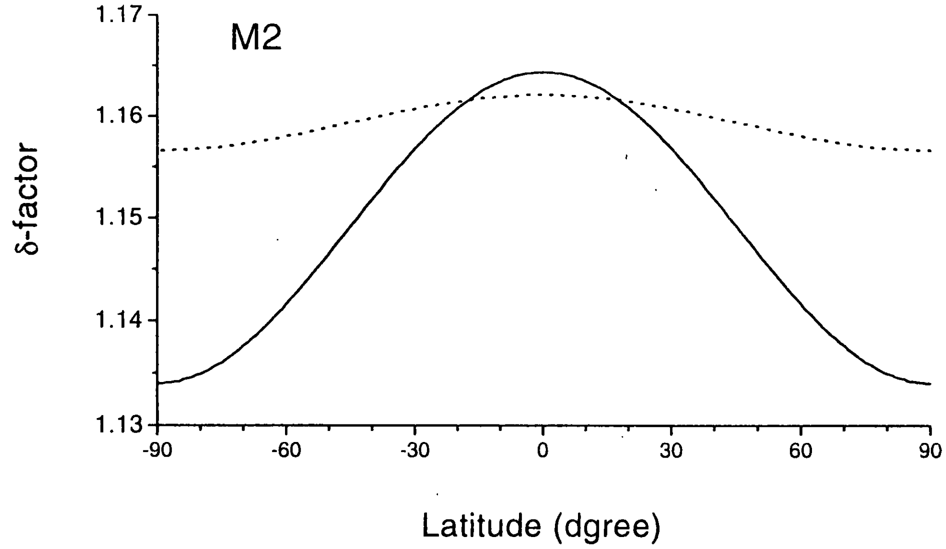

Fig. 6. Latitude dependency of δ-factors for the K1 and M2 waves. These figures show the results for the elliptical, rotating earth computed by Wahr's theory (1981, solid curve) and by Dehant's theory (1987, dotted curve).

Chapter 3.
Effect of the Oceans on the Gravity Observation

The ocean tides produce substantial effects on the observed tidal measurements. In the case of the ground tilt, the secondary effect of the ocean tides shows the amplitude of two times larger than that of the primary effect of the body tides at an observation site close to the sea. In the case of the gravity tides, the ocean tidal effect is also a major source which makes discrepancy between the observed and the theoretically expected tides on the elastic earth. The ocean tides affect on the gravity observation through two different manners, namely, the direct attraction and the deformation of the earth due to the loading of the ocean mass. Occasionally, these two phenomena are collectively called 'ocean loading'.

3.1. Load Green's Function

In order to consider the distribution of surface loading mass, we use $\rho_s(\theta, \lambda)$ of a constant density σ represented as

$$\rho_s(\theta, \lambda) = \sigma \sum_{n=0}^{\infty} P_n(\cos \Theta_L), \qquad (23)$$

where θ and λ are the co-latitude and the east longitude of the loading mass, and Θ_L is 'loading distance' which corresponds to the angular distance between the loading point at (θ, λ) and the observing point at (θ', λ') on the earth's surface. Θ_L is expressed by similar equation as (4) using the angles (θ, λ) and (θ', λ'):

$$\cos \Theta_L = \cos \theta \cos \theta' + \sin \theta \sin \theta' \cos(\lambda - \lambda') \qquad (24).$$

The loading deformation and the additional potential change due to $\rho_s(\theta, \lambda)$ are expressed using the non-dimensional 'load Love numbers' h_n', k_n' and l_n'. These have the similar meanings as the Love and Shida numbers, but they are define on the pressurized surface of the earth. Displacement induced by the oceans are given by

$$\mathrm{v} = (1/g_0)\sum_{n=0}^{\infty} h_n' \mathrm{V}_n' \qquad \text{in vertical,} \tag{25}$$

$$\mathrm{u}_\theta = (1/g_0)\sum_{n=0}^{\infty} l_n' \partial \mathrm{V}_n'/\partial\theta \qquad \text{in } \theta\text{-direction,} \tag{26}$$

$$\mathrm{u}_\lambda = (1/g_0)\sum_{n=0}^{\infty} (l_n'/\sin\theta)\partial \mathrm{V}_n'/\partial\lambda \qquad \text{in } \lambda\text{-direction.} \tag{27}$$

On the other hand, the potential change induced by the oceans is expressed by

$$\mathrm{w} = \sum_{n=0}^{\infty} k_n' \mathrm{V}_n', \tag{28}$$

where V_n' is the gravitation potential induced by $\rho_s(\theta, \lambda)$ and it is represented as

$$\mathrm{V}_n' = 4\pi\sigma \mathrm{GR} \sum_{n=0}^{\infty} P_n(\cos\Theta_L)/(2n+1) \qquad (29).$$

Here, R stands for the earth's radius. The values of load Love numbers for the given earth model are obtained by solving the similar system of the equations for the body tides described in the subsection 1.1.3.. However, different from the case of the body tides, they are solved using the boundary conditions for the stressed surface by the ocean mass.

The gravity changes due to the ocean loading $\rho_s(\theta, \lambda)$ can be expressed as

$$\Delta g' = -1/\mathrm{R}\sum_{n=0}^{\infty}\{n+2h_n'-(n+1)k_n'\}\ \mathrm{V}_n' \qquad (30).$$

By introducing a function given by

$$G(\Theta) = \mathrm{G}/\mathrm{R}^2\sum_{n=0}^{\infty}\{n+2h_n'-(n+1)k_n'\}\ P_n(\cos\Theta) \qquad (31),$$

the effect of ocean loading can be computed by carrying out a convolution integral of the form

$$\Delta g' = (1/\mathrm{R}^2)\int_0^{2\pi}\int_0^{\pi}\rho_0 H(\theta,\lambda)G(\Theta)\sin(\theta)d\theta d\lambda\ . \qquad (32)$$

over the whole oceans on the globe, where ρ_0 and $H(\theta,\lambda)$ are the ocean density and the tidal height, respectively.

$G(\Theta)$ given in (31) is 'load Green's function' which represents the effect of the loading by a point mass. This consists of the two parts, namely the attraction and the loading. By applying a formulae of the Legendre sums to the first term in (31), the effect of the direct attraction due to the point mass of a unit mass ($\rho_0 = 1.0$) is given in the form

$$G(\Theta) = -(\mathrm{G}/\mathrm{R}^2)/(4\sin(\Theta/2)) \qquad (33).$$

This is 'Newtonian part' of the load Green's function.

In general, the load Green's function has a nature which is sensitive to the earth's inside structure at the depth equal to the loading distance. On the other hand, the spatial wave length of the ocean tides is much smaller than that of body tides and the magnitude of the loading effect on the observed gravity is inversely proportional to the loading distance. Therefore, the effect of loading tide is much sensitive to the shallow structure of the earth than that of the body tides. This is a reason why we are needed to compute the Green's function including the very higher order terms in order to represent the loading effect correctly. Farrelle(1972) computed the load Love numbers up to the degree 10,000 of the surface spherical function based on the Gutenberg-Bullen earth model. He estimated the effect of the upper mantle structure on the magnitude of ocean loading, and gave a table of the Green's function. His table is widely used in the study of the tides. In this paper, we computed a similar table with Farrell's one but for the 1066A earth model for the sake of comparison. The values of Green's function were computed by means of the computer program given by Okubo (1983) which is based on the Saito's (1967) one.

3.2. A Computer program GOTIC

The ocean loading effects have been estimated using a computer program "GOTIC' (Global Ocean Tide Correction) which was developed by Sato and Hanada (1984). The program is capable computing the loading effects of 5 components, namely the vertical and horizontal displacements, gravity, tilt and strain. An algorithm to compute the vertical deflection was added later. To carry out the convolution integral of the Green's function, three tools are necessary to be input. They are the ocean tide model and topographic digital map to represent correctly the topography around the observation site. The original version of GOTIC adopted the two Green's functions for the Gutenberg-Bullen earth model by Farrell and the 1066A earth model computed by us, the Schwiderski's(1980) ocean tide model, and two kinds of digital topographic maps representing the worldwide distribution of lands and seas. The mesh sizes are designed to be 1° × 1° for the first-order mesh and $5' \times 7.5'$ for the second-order mesh in the direction of the co-latitude and the longitude, respectively.

Farrell (1973) introduced a disk factor into the convolution process in order to take account of the effect of a finite area of the ocean mesh enclosing the observation site. In stead of this method, GOTIC estimates the contributions from the adjacent ocean (30° × 30° region centered at the site) by integrating the load Green's function, which was approximated by a quadratic function, with the rectangular ocean layer mass. As for distant oceans outside the above region, the integration is carried out by simply taking the convolution of the load Green's function with a point mass centered at each ocean mesh of 1° × 1°. The value of 1.025 kg m^{-3} is adopted as the sea water density throughout the whole oceans.

GOTIC have been revised several times so that it can incorporate upgraded digital maps, new ocean tide models, which became available after 1980 when the time Schwideski's model was opened. Further revision was also made to take account of the effect of the ocean mass conservation pointed out by Agnew (1983) and to estimate the effect of anelasticity of the earth.

Chapter 4.
Superconducting Gravimeter and Its Setting up at Syowa Station

4.1. Superconducting gravimeter

A superconducting gravimeter (SG) is a kind of relative gravimeters, which uses a magnetic force induced by the superconducting current as the force to support the proof mass instead of a metal spring of conventional gravimeters such as the LaCoste-Romberg gravimeter. The proof mass used in the SG is a spherical shell of 1 inch in diameter, which is made of a superconducting material Nib. The solenoid coils producing the magnetic field are also made of Nib.

The sensing unit consisted of the proof mass, coils and capacitance position transducer is in the cryogenic environment of 4.5 °K by using the liquid helium. The proof mass is levitated by the magnetic repulsion force generated by the Meisner effect appearing at the superconducting state. In an actual SG, two coils, namely, the upper coil and the lower coil, are equipped so that we can adjust the strength of the gradient of the magnetic force as a levitation force. The gradient can be changed by adjusting the ratio of superconducting current of the lower coil to that of the upper coil. When the gradient is weakened, the sum force making the two coils is also weakened and the period of the pendulum system is elongated. Consequently, the sensitivity of the SG becomes high.

In general, the capacitive transducer shows a strong non-linearity in its output signals as a function of the position of the proof mass measured from the electrodes. In order to reduce this non-linearity, the feedback force is applied to the mass so that the mass is kept its position at the center between the two electrodes, and the SG is as well. In the SG, the feedback is realized by adjusting the current flowing in the third coil (the feedback coil) equipped in the sensing unit.

The environment of a cryogenic low temperature gives the following two advantages to the gravity sensing unit of the SG; (1) decreasing the long-term instrumental drift due to thermal effect and creep of metallic material used in the sensor part and (2) diminishing the thermal noise of the electronics used in the sensor. Thus, the superconducting gravimeter shows very high long-term stability compared with the conventional gravimeter using a metal spring. This is mainly due to the stability of the superconducting current itself which flows under the condition of zero resistance at the superconducting state (Prothero, 1967 and Spratt, 1981). Due to these advantages, the SG has a potential to detect such small gravity signals as less than 1 nGal in magnitude or the long-term gravity signals with the period of longer than one year (Goodkind, 1999). However, a disadvantage in the SG is the weakness in horizontal restriction of the superconducting sphere. The displacements of the sphere in the horizontal direction is restricted only by the horizontal magnetic force that is produced by the same field used to levitate the proof mass. Therefore, the mass is not so strongly restricted as compared with the conventional gravimeter or vertical accelerometer. This weakness of constraining the horizontal direction, namely, a freedom in the horizontal direction, may yield a noise at the high frequency band as seen in **Fig.** 10 of Chapter 5.

The apparent gravity value observed by the gravimeter is changed by tilting of the gravimeter in any directions. Because the vertical direction of the sensor attached to the gravimeter frame is not always coincident with the direction of the changes in gravity, namely, the direction of the local vertical. This inconsistency in the directions makes a cosine error in the observed gravity signals. In the first order, this error is proportional to the square of the difference in angle of the two directions. In order to reduce this error as possible as small, the SG is equipped with a feedback system called the thermal leveler to compensate the ground tilts. This system consists of the X-Y tilt-meters and the leveler having the X-Y actuators thermally expanded or shrunk with the heaters. The leveler compensates the misalignment in the respective vertical directions caused by the ground tilts by adjusting the length of the two actuators with the electric current applying to the heaters. The magnitude of the heater current is adjusted using the tilt signals detected by the X-Y tilt-meters equipped inside the SG. The time constant of the leveler is about 2 minutes, so this system could not compensate the tilt motion and/or horizontal acceleration at the period shorter than the time constant.

The actual SG consists of the five components; 1) a liquid helium dewar, 2) the gravity sensing unit installed in the dewar, 3) the thermal leveler, 4) the cryogenic system consisting of a refrigerator (a cold head) and a compressor to operate the cold head, and 5) the electronics to control the gravimeter and leveler. The SG set up at Syowa Station is shown in **Photo** 2.

4.2. Outline of Syowa Station as an Integrated Geodetic Observation Site

Figure 7 shows the geographical position of Syowa Station, 69.0°S in latitude and 39.0°E in longitude. It is well established that changes in the height of the water table in soil or sedimentary layers affect the observed gravity (Delcourt, 1968, Richter et al. 1995a and Mukai et al., 1999, for example). The irregular drift associated with this effect may disturb the observed long-period signals. In addition, since the ground water change generally shows a seasonal variation, it probably disturbs the annual gravity variation. In 1980, seismic explosion experiments were made in the Ongul Islands region. The experiments revealed surface exposure of basement rocks with P-wave velocity of 6.1 $\mathrm{km}^1\mathrm{s}^{-1}$, confirming non-existence of sedimentary layers from geological reconnaissance (Ito et al.,1984). Their experimental results obviously indicate that there is no sediment layer at Syowa Station which can reserve a ground water. As a consequent, we expect that there is no groundwater effect at Syowa Station. This means that Syowa Station is a favorable observation site to monitor the long-period tides and the secular gravity changes related to the post-glacial rebound of the ground and/or sea-level variations.

Usually the sea surrounding Ongul Islands is covered with sea ice throughout the year. Thus the ground noise level in the frequency range of 0.1–2 Hz due to the ocean waves is small. However, the packed sea ices in Lutzo-Holm Bay, where the observation site is located, are sometimes blown away for 1-2 month, then the ground noise attains 10-30 mkine (1-3x10-5 m/s) in the frequency range of 0.1-2 Hz due to the ocean waves striking Ongul Islands. Since the dominant frequencies of the ocean waves overlap those of the SG mode signals, free oscillations of the earth and/or core modes observed during high ocean waves may be contaminated by harmonics of these high ground noises.

As schematically illustrated in **Fig.** 7, Syowa Station is now innovated as an observatory for global geodesy in Antarctica [Shibuya, 1993]. Because the gravity variations are influenced by variations of nearby atmospheric and ocean water masses, precise monitoring of surface synoptic data and ocean tide data are indispensable. It is to be noted that these observations have been continued for over 30 years at the Meteorological Laboratory (ML) and the Tide Observation Hut (TOH), respectively. For example, monitoring of the sea level has been carried out using a pressure-transducer water level meter, and a part of the data was analyzed by Odamaki and Kuramoto (1989). We integrated the tidal parameters obtained by them into our computation of the ocean tide effect as will be discussed later.

There may also be an unknown gravity change related with the variation in the earth's geomagnetic field in local and/or global scale. The monitoring of the magnetic field has been continued at the Geomagnetic Variometer Hut

(GVH) also for over 30 years. In January, 1990, the distance measurements with VLBI (Very Long Baseline Interferometer) technique were carried out at Syowa Station connecting with the two stations of Kashima, Japan and Tidbinbilla, Australia [Takahashi et al., 1997]. Now the observations with VLBI and GPS are continuing as one of the observation projects of JARE. The permanent observation with 'Turbo Rogue receiver' , as part of the International GPS Service for Geodynamics (IGS) network, was started from JARE-36 program (from February 1995). There is also a DORIS beacon site near the Earth Science Laboratory (ESL) with successful transmission of one year data (from February 1993). The details of the geodetic observations made at Syowa Station are introduced in the paper by Shibuya (1993). These observations associated with the SG observation should give us interesting information to implement the SG observation in the future.

4.3. Gravimeter Room

The SG was installed in the Gravity Observation Hut (GOH of **Fig.** 7 and **Photo** 1). A concrete pier to support the SG dewar (see **Photo** 2) was constructed in February 1991 by JARE-31 at the hut. There is another pier registered as an observation point of the International Absolute Gravity Base station Network (IAGBN, Boedecker and Fritzer, 1986) and absolute gravity measurements were already conducted using the three different kinds of absolute gravimeters (Nakagawa et al., 1994).

The SG dewar is hung from the thermal leveler placed on a concrete pier in the GOH. In order to suppress possible high frequency noises, which are mainly due to vibration of the hut-wall during blizzards, the base of the pier is detached from the floor of the hut. Thus, ground noises from vibration of the hut under high-winds are designed to be suppressed. As a result, the ground noise is in the range of 10 μkein (1-2x10-7 m/s) under calm weather conditions. However, the ground noise attains 1-3 mkein (1-3x10-5 m/s) in the frequency range of 20-30 Hz during blizzards. This caused an insignificant effect on tidal gravity observations as shown in later in the analysis. Because most of the noises at this frequency band are excluded both by the analog filters (time constant of 50 s) equipped on the SG and by the digital filter (cut-off period of 180 s) applied to the raw data in analysis procedures.

Another problem of the SG data at Syowa Station originated from a strong effect due to the operation of liquefier in the gravity room. The operation to make liquid helium and of transferring it into the gravimeter dewar is done about twice a year. Usually the operation is continued for about 2 weeks and this causes a large step-like change or long-interruption of the gravity data. hence there is a possibility that the observed semiannual and annual gravity changes are contaminated by the effect of this operation. We will discuss this effect in the later sessions.

4.4. Setting up the SG

Due to difficulty in accessing to Syowa Station, we needed to install a helium liquefier in order to continue the observation. The liquid helium (L/H) is produced from gaseous helium of high quality called the grade of six nine. Installation of a nitrogen liquefier is also required to precool the SG dewar to liquid nitrogen (LN2) temperature (70 degree K), because direct cooling of the gravimeter dewar with LHe from the room temperature (300 degree K) means total evaporation.

Including the above preparation of the liquefiers, the installation procedure of the SG consists of the following 11 steps:

(1) install a thermal leveler for tilt compensation and hang the SG dewar on the leveler placed on the pier;

(2) produce 70 liters of LN2 and 100 liters of LHe;

(3) transfer LN2 to the SG dewar;

(4) completely discharge LN2 from the SG dewar after pre-cooling;

(5) pre-cool the gravity sensing unit (GSU) with LN2;

(6) transfer LHe to the SG dewar;

(7) insert GSU into the SG dewar and demagnetize it in order to avoid to trap a external electromagnetic flux on to superconducting sphere (SS) as a proof mass;

(8) levitate the superconducting sphere;

(9) adjust the SS position by iterative adjusting the two superconducting currents (in the upper and lower superconducting coils) which produce the magnetic force balancing the gravity force applied to the SS;

(10) set the GSU to a tilt-insensitive position with the micrometers of the leveler so that the effect of ground tilting on the gravity measurement is minimized;

(11) make a fine tilt tuning of the leveler to realize the final tilt-insensitive position.

An operational difficulty that we first met to was safely transport of the cryogenic dewars to Syowa Station. During our attempt in 1992-year expedition, abnormal evaporation of LHe from the SG dewar occurred at the step (7) and subsequent steps had to be given up. From the inspection by the manufacturer and the author, it was found that the abnormal LHe evaporation resulted from a so-called "cold leak". The size of micro-cracks as the origin of the leakage was estimated as being smaller than the size of LN2 but larger than that of LHe. This is the reason why the leakage at Syowa Station has occurred at the step of filling up LHe not at filling up LN2. When LHe leaks into the vacuum space of the SG dewar through the molecular size defect on the inside wall of the dewar, the specification for thermal isolation of the dewar is rapidly decreased. This was the origin of the abnormal evaporation at the installation in 1992.

Although an exact cause of the defect was hardly identified, material fatigue during transportation was suspected. The angles of rolling and pitching of the icebreaker "Shirase" during 40-day' cruse (from Tokyo via Fremantle, Australia to Syowa Station) respectively attained ±35° and ±10° with an acceleration of ±0.4 G (1G=9.8 ms^{-2}) for vertical and horizontal directions in the period range of 1-20 s. On the other hand, three component vibration measurements on Shirase's helicopter S-61A showed the maximum vertical acceleration of ±0.8 G (18 Hz predominant frequency) at the hovering stage (30s duration) for landing, while it is usually less than ±0.2G during 30 minutes flight from Shirase to Syowa Station. The vibrations acted on the SG dewar during the transportation by the helicopter (a few km in distance at the moment in 1992) may also be a cause to make the cold leak.

Thus based on the experiences in 1992, we prepared a special dewar (type: RD-143 HD) which has much harder mechanical strength than the previous dewar RD-200 after some discussions with the manufacture. In order to reduce the pendulum motion of the inside vacuum vessels with respect to the outmost vessel at the neck part as a fulcrum, the inside vessels were fixed at the top flange of the outmost vessel by using a long cylinder which has a diameter of just fitting the inner diameter of the gravimeter neck and has the same length with the distance between the top of the neck and the bottom of the innermost vessel. **Figure** 8 schematically shows the design of the SG dewar and the cylinder used to protect the inside vessels from their swing motion. Moreover a special transportation mounts using shock absorbers (Barry Cupmounts; NC-2040) was made to mount the SG dewar and it was pulled on a sledge by an over-snow vehicle from the anchoring site of "Shirase" to a place 500 m distant from GOH, without relaying on a heli-borne transportation.

Thus the SG016 was successfully installed and the continuous observation started on March 22, 1993. Since that time, the observation with the SG has been continued under the framework of JARE. The gravimeter room and the observational environments are shown in **Photo** 1 and 2, respectively. In **Photo** 1, the right side building is the gravimeter room and we can see the dome of the multi purpose 11-m antenna on the left side. The instruments shown in **Photo** 2 are, from the left: the chart recorder (top) and data logger (bottom) to monitor environmental variations; the two gravimeter electronics (GEP2 for the control of the SG (top) and DPS-3 heater pulsar to adjust the superconducting currents (bottom); a He gas cylinder for maintenance; the gravimeter dewar RD-143HD (blue one) which is hung from the thermal leveler (black one put on the top of the concrete pier; the cryogenic vessel of the helium liquefier (bright one) and its controller (yellow one); part of the nitrogen liquefier. The data acquisition system is installed at the opposite side of these instruments (this side of **Photo** 2).

4.5. Data Acquisition System

Figure 9 illustrates the data acquisition system. Output signals from the SG are separated into low/high frequency components by a TIDE/MODE filter. This has the same frequency characteristics as those used in the network IDA (International Deployment of Accelerometers, Agnew et al., 1986), where TIDE filter is a low pass filter with a cut-off period of Tc = 50 s (-3 dB point) and with a slope of -36 dB/oct. Analog outputs through these filters and isolation amplifiers are multiplexed by a scanner at sampling intervals of 2 s, then through an analog-to-digital (A/D) convertor of 7.5 digits, the output signals are recorded on a hard disk. The least significant digit of the obtained TIDE data corresponds to an apparent gravity change of 0.0006 μGal.

The clock of the digitized data series is automatically synchronized to UTC (Coordinated Universal Time) within 1 ms by a timing pulse from a GPS receiver. The observed gravity signals are affected by atmospheric pressure changes, and their effect frequently exceeds 20 μGal. In order to correct for this effect, air-pressure transducer to a resolution and precision of 0.1 hPa was installed in the GOH and parallel data acquisition is made with the same sampling interval as that for the gravity data.

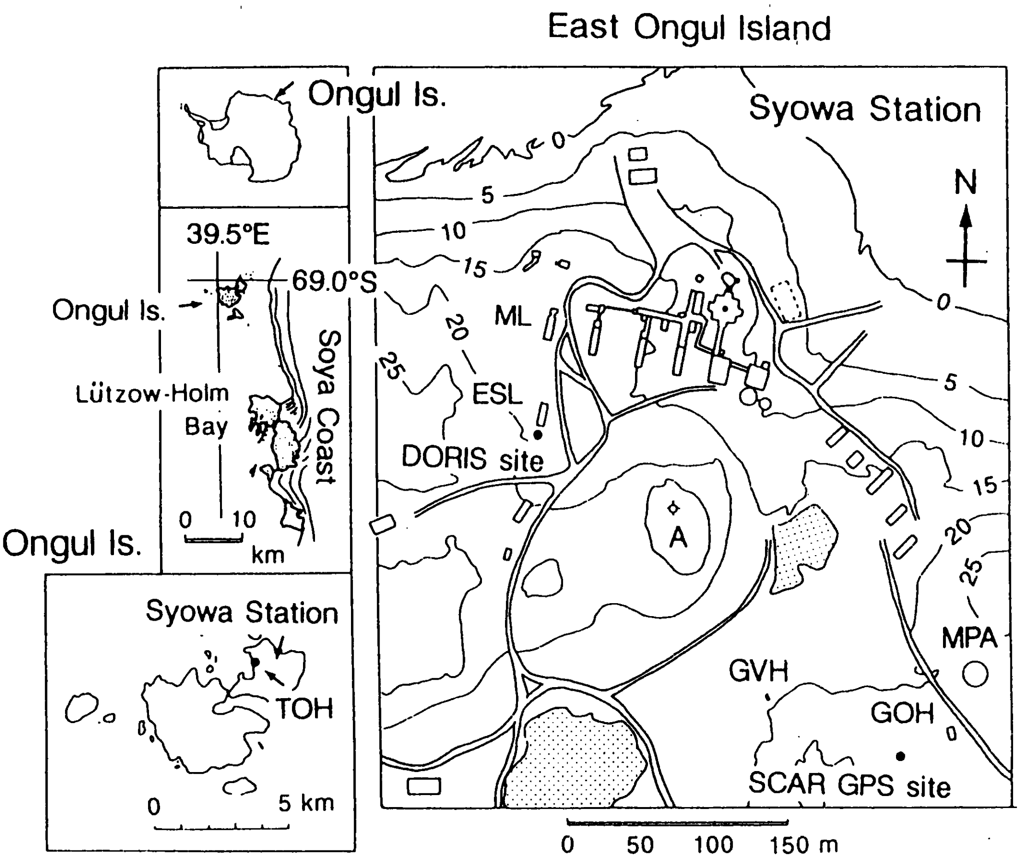

Fig. 7. Geographical location of Syowa Station and geophysical facilities in the station. Several facilities related to the SG observation are available in the site as shown in the figure of the right hand side. The SG observation is carried out at GOH (Gravity Observation Hut). The tidal observation with the LaCoste & Romberg gravimeter G477 was carried out at SV (Seismogram Vault) in 1987. SV is located at about 150 m south-west of the GOH in distance (out of this figure). As the related facilities, the followings are shown; ESL: Earth Science Laboratory, GVH: Geomagnetic Variometer Hut; ML: Meteorological Laboratory, MPA: Multi Purpose Antenna, and TOH: Tide Observation Hut..

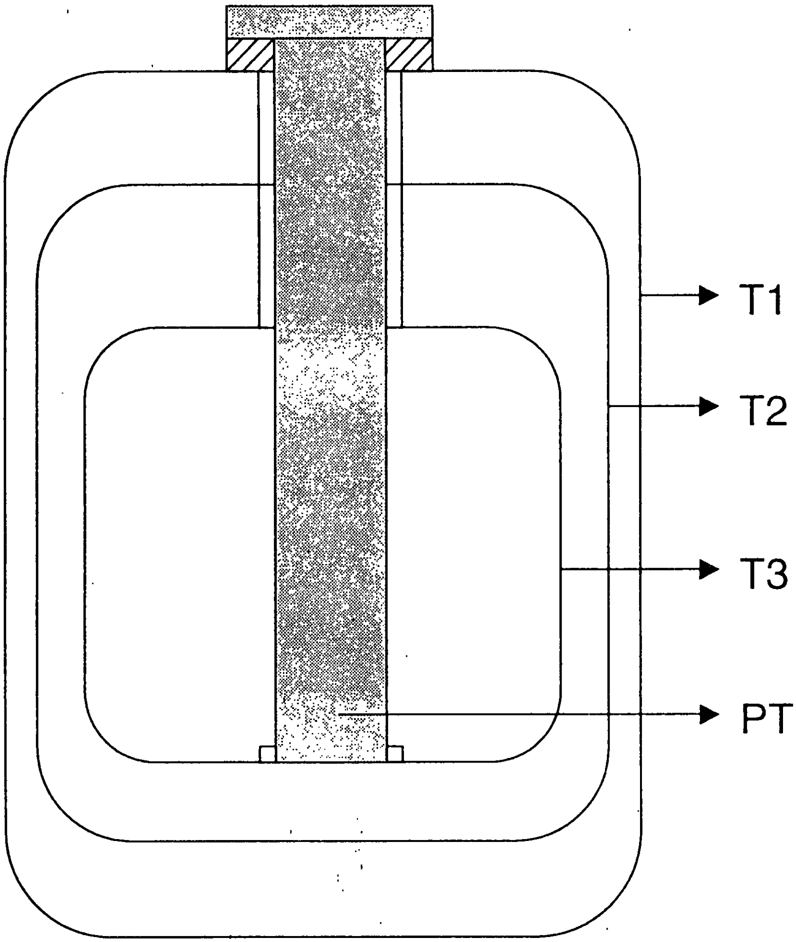

Fig. 8. Inside structure of the liquid helium dewar of RD-143HD dewar. T1 and T2 are the outer and inner tanks, respectively, and the space between the two tanks is being kept to vacuum. T3 is the tank to reserve liquid helium of 143 liters. PT shows a cylinder used to protect the inside tanks from the large pitching and rolling motions of the ice-breaker Shirase during the transportation. In order to limit the relative motion of the tanks as possible as small, the clearance between the cylinder and the neck part of the tank was designed within 2 mm in the magnitude of gap.

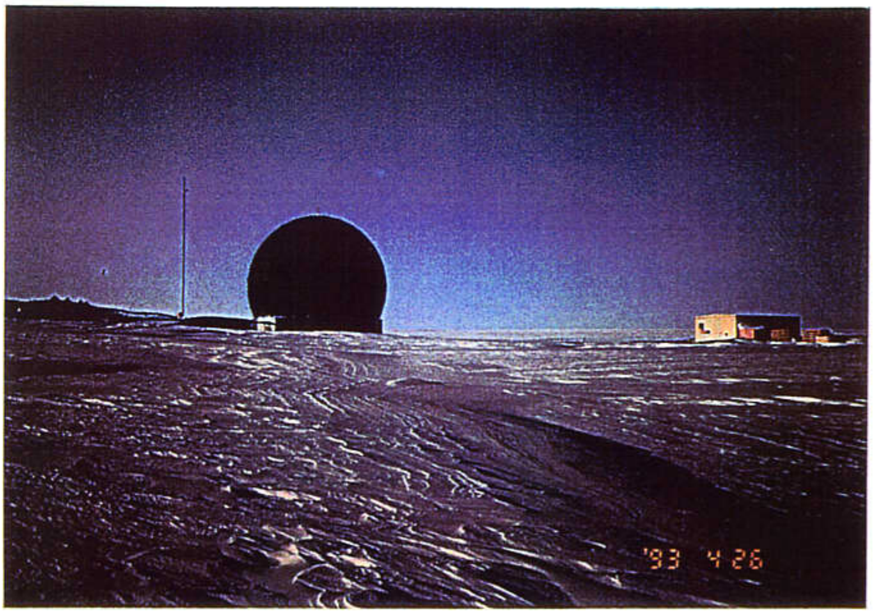

Photo 1. Gravity Observation Hut (GOH) at Syowa Station. Two of GOH (right) and the dome of the multi purpose antenna (left, MPA in Fig. 7) can be seen in this photo.

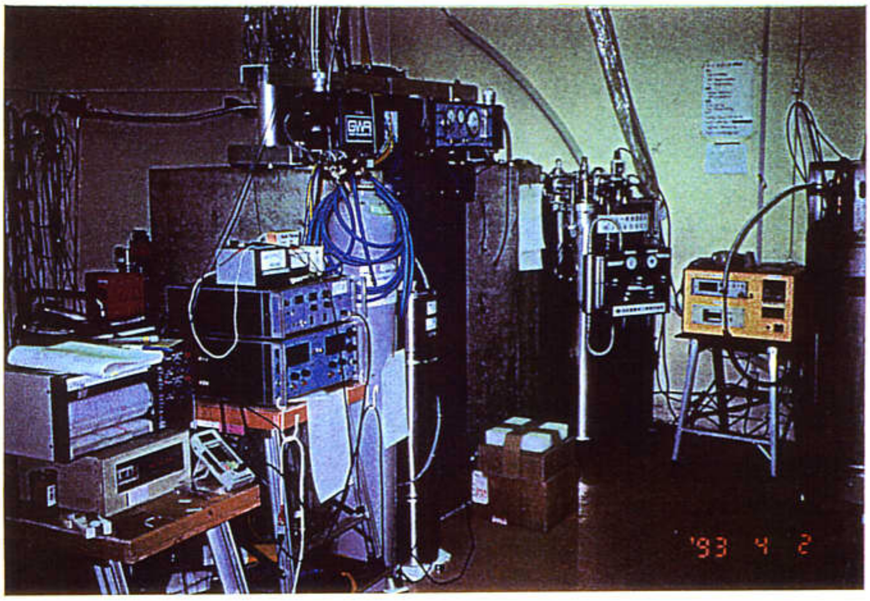

Photo 2. SG#016 and other observation instruments set at Syowa Station. From the left: a data logger and 2-pen chart recorder to monitor environmental variations ; gravimeter electronics (GEP2 for the control of the SG and DPS-3 heater pulsar to adjust the superconducting currents ; He gas cylinder ; the liquid helium dewar RD-143HD (blue one) of the SG. The dewar is hung from the thermal leveler set on the concrete pier. ; the cryogenic vessel of the helium liquefier (left) and its controller (right) ; the nitrogen liquefier can be seen at the most right. The data acquisition system is installed at the opposite side of these instruments (i.e. this side of this photo).

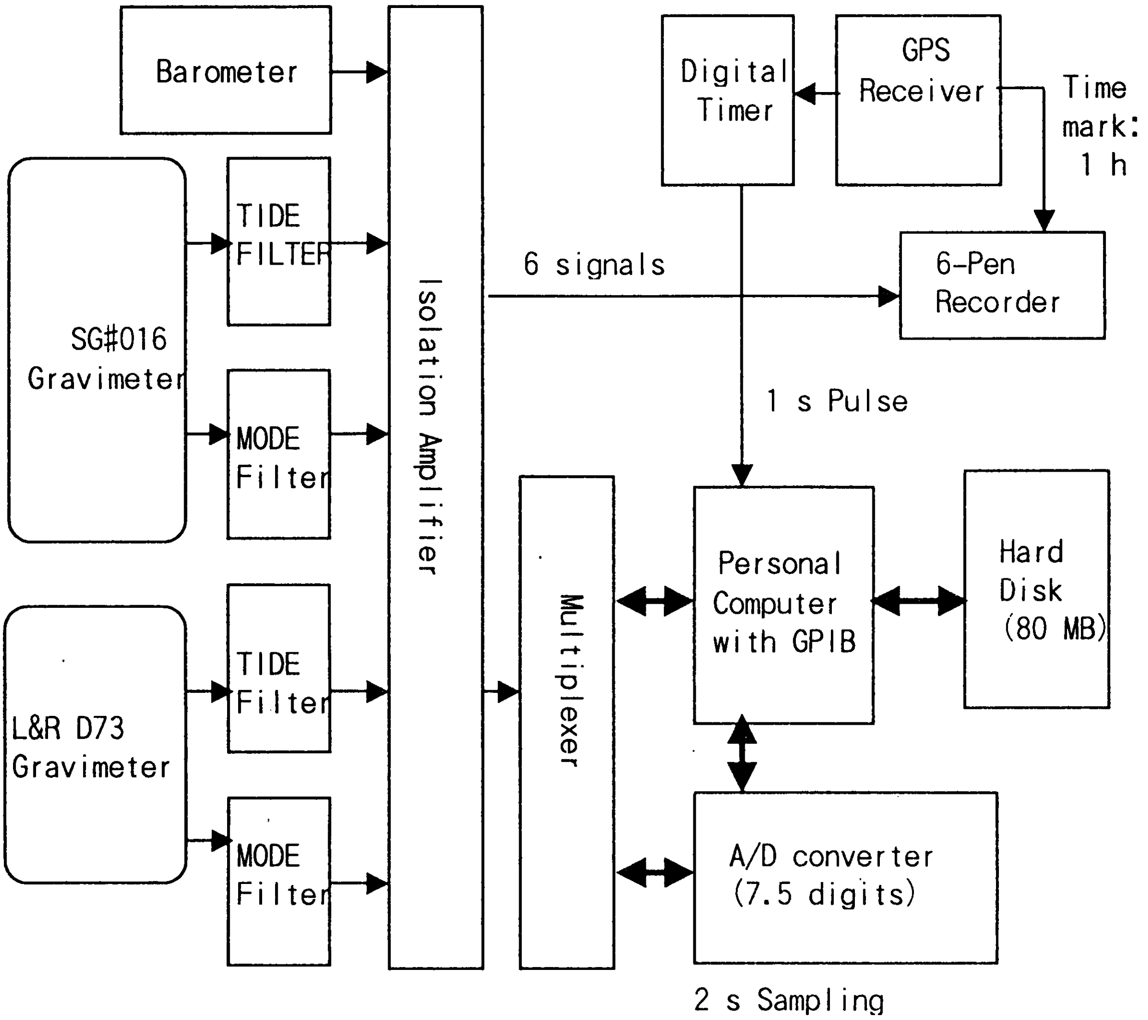

Fig. 9. Data acquisition system set at Syowa Station. This system has been used till January 1999. There appears two kinds arrows: thin one-side arrow shows the flow the signals and the thick two-sides arrow shows that the instruments are linked with the PC through the GP-IB line.

Chapter 5.
Preliminary Data Processing and Tidal Analysis Method

5.1. Preliminary Data Processing

Figure 10 shows an example of MODE signal and its amplitude spectrum which was obtained in a quiet day at Syowa Station. As seen in **Fig.** 10, a sharp peak appears at the frequency of about 5.6 mHz (i.e. about 180 s in period). This peak is caused by the eigen mode of motion of the superconducting sphere itself (for example, Prothero 1967) which was excited by external disturbances mainly due to such high frequency ground vibrations and could not be compensated by the thermal leveler having the time constant of about 2 minutes. The TIDE filter has the similar frequency characteristics with that of the MODE filter at the frequency band higher than 50 s. In order to reduce the effect of the high frequency noises on the tidal analysis, a digital low-pass filter was applied to the original two-second data and resampled them at the interval of every 1 min. The digital filter used here has the characteristics of the cut-off period of 240 s and -14 dB gain at the period of 180 s,

Figure 11 shows the 1-minute TIDE data (top) obtained from the SG at Syowa Station during the observation periods of JARE 34 and JARE 35, namely, from March 22, 1993 to January 27, 1995. As shown in the figure, usually the SG records include the spike-like noise and step-like changes (offset) caused by several reasons. They are, for example, the lock-off of the feed-back system of the thermal leveler due to strong mechanical shocks accompanied with refilling of liquid helium, exchange of the cold head and the large earthquakes. Different from Japan Islands located in an active tectonic region, as it rarely occurs local earthquakes at Syowa Station, these step-like changes are not considered to be associated with natural earthquakes. Main sources of the step are the mechanical shocks accompanying with the operation of the liquid helium liquefier made at the observation room twice a year and also the electric shocks by the power failure. For example, a large step was seen at around 460,000 minutes in **Fig.** 11 (in February 4, 1994). This step occurred by the power failure, and it was corrected in August 2, 1994 (i.e. at around 720,000 minutes) by adjusting the value of superconducting current using the heater pulsar, when the operation for refilling of liquid helium was done. Judging from the difference in magnitude between the two steps, it is considered that the step of about -2.5 V, corresponding to about +140 μGals in gravity value, occurred during the operation. In addition, there is a possibility that the sensitivity of the SG was changed due to this adjustment of the superconducting current. We will mention about this in the section 6.3.

The magnitude of the steps in the original 1-minute data was estimated, based on the 1-minute data for which both the tidal and the air pressure change were subtracted. We predicted the tidal variations using the δ-factors and phases obtained from the preliminary tidal analysis by the BAYTAP-G program (details of this computer program will be introduced in the next section). While, the pressure effect was computed using the mean pressure coefficient at Syowa Station (i.e. -0.37 μ/hPa $\doteqdot$ -6.6$\times 10^{-3}$ Volt/hPa as represented by the output signal with the unit of Volt). With use these data, it is easier to discriminate the step from the large and rapid signal changes due to the effects of tides and/or pressure changes. Consequently, it is expected that the estimation accuracy of the magnitude of steps increases, and it is also expected to avoid misjudging of the signals as an artificial step. The magnitude of steps was estimated from the daily medians or the successive differences of the 1-min data. The results for the step-corrections are shown in the bottom of **Fig.** 11. This figure shows the residuals after correcting for the tides and pressure changes. The 1-hour data resampled from the corrected 1-minute data were used for the tidal analysis.

5.2. Tidal Analysis Program BAYTAP-G and -L

The tidal analyses were carried out using an analysis program called 'BAYTAP'. BAYTAP is the abbreviation of 'BAYesian Tidal Analysis Program'. This computer code was originally developed by Ishiguro et al. (1981) and was completed as 'BAYTAP-G' for the tidal analysis program by Tamura et al. (1991). There are two versions of BAYTAP. One is BAYTAP-G for the analysis of short-period tides. The other is 'BAYTAP-L.' for the analysis of long-period tides. The tidal potentials used in BAYTAP-L are different from those used of short-period waves. Thus the potentials for the periods of 1/3 days to 1 day are considered in BAYTAP-G, while those of long-period ones (4-5 days to 365 days) are considered in BAYTAP-L. However, the optimization method of unknown parameters with an Akaike's Bayesian Information Criterion (ABIC; Akaike, 1980) and decomposition scheme in the BAYTAP-L processing are essentially the same as those of BAYTAP-G.

BAYTAP-G decomposes the original data y_i into four components, namely, the tide T_i , the response R_i, the trend d_i and the irregular noise e_i, by fitting to the following model:

$$\begin{aligned} y_i &= T_i + R_i + d_i + e_i \\ &= \sum_{m=1}^{M} a_m \sum_{n=1}^{N_m} a^*_{nm} \cos(\varpi_{nm} t_i + \phi^*_{nm} + \phi_m) + \sum_{k=0}^{K} b_k x(t_i - t_{i-k}) + d_i + e_i \end{aligned} \qquad (34)$$

The unknown parameters to be estimated are the tidal factor a_m and phase ϕ_m for the $m'th$ tidal group, the response coefficients b_k for the associated data $x(t_i - t_{i-k})$ and the trend d_i at each data point. While the known parameters are: ϖ_{nm} the angular frequency of the $n'th$ wave in the $m'th$ tidal group, and

a^*_{nm} and ϕ^*_{nm} the theoretical amplitude and phase of the tidal wave of angular frequency ϖ_{nm}, respectively. e_i is the residual irregular noise. The air pressure data obtained at the observation site is incorporated as the associated data. As explained by Tamura et al.(1991), BAYTAP-G does not postulate an explicit time function for the trend model, such as a polynomial, but only defines its linearity or smoothness by assuming an integrated random walk model for the trend. Hence, in the BAYTAP processing, we take our standing point is that we do not know nor assume *a priori* the explicit time function for a trend. Therefore, we expect that the decomposed trend component faithfully represents the long-term gravity variations consisting of the long-period tides, the polar motion effects and the instrumental drift.

The integrated random walk model is represented by

$$y_i - 2y_{i-1} + y_{i-2} = u_i \tag{35}$$

where y_i, y_{i-1} and y_{i-2} are the successive three data in a data set, and u_i denotes the white noise sequence with zero mean. The degree of linearity of the trend term is adjusted by a weight D (i.e. the parameter v^2 in Tamura et al.,1991). This is defined as a hyperparameter (Akaike, 1974) in a "analyzed least squares method' as BAYTAP processing. In general, there is a tendency that the fluctuation of the trend term is controlled to be smaller by setting a larger hyperparameter D and *viceversa*. We will mention this point more in detail in Chapter 7 where the analysis for the long-period tides.

We expect that more than 85 to 90 % of the air pressure effect will be absorbed into the response term decomposed by BAYTAP-G, except for the case of large and rapid pressure changes. Because the major part of air pressure effects is direct attraction of air mass from the surrounding area of a few hundreds kilo meters in diameter, the response term approximated using the pressure at the observation site will well represent the pressure changes in this area, especially the changes in a synoptic scale which causes the major pressure effect. Moreover, for the loading effect, the effect of air mass on the ocean surface is largely compensated by the IB (Inverted Barometer) response of the ocean. This compensation effect is dominant at the observation close to sea coast such as Syowa Station. This has already been confirmed by Sato et al. (1990). They compared the time series data of the observed pressure effect at Esashi obtained by BAYTAP-Analysis and those estimated from the global pressure data assembled by the Japan Metrological Agency, provided at a sampling interval of 6 hours. The study by Mukai et al. (1995) based on pressure data which are more precise in spatial resolution than those used in the study by Sato et al. (1990) also shows the similar results.

In this thesis, we adopt a sign convention for the gravity data such that an increase (downward acceleration) is positive. Although BAYTAP-G and -L define the lag of the observed gravity tide against the tidal potential as negative phase, we changed its sign definition in order to have consistency with the definition of the global ocean tide models. For the δ-factor, BAYTAP estimates the value by referring to the tidal force which is normal to the elliptical rigid earth.

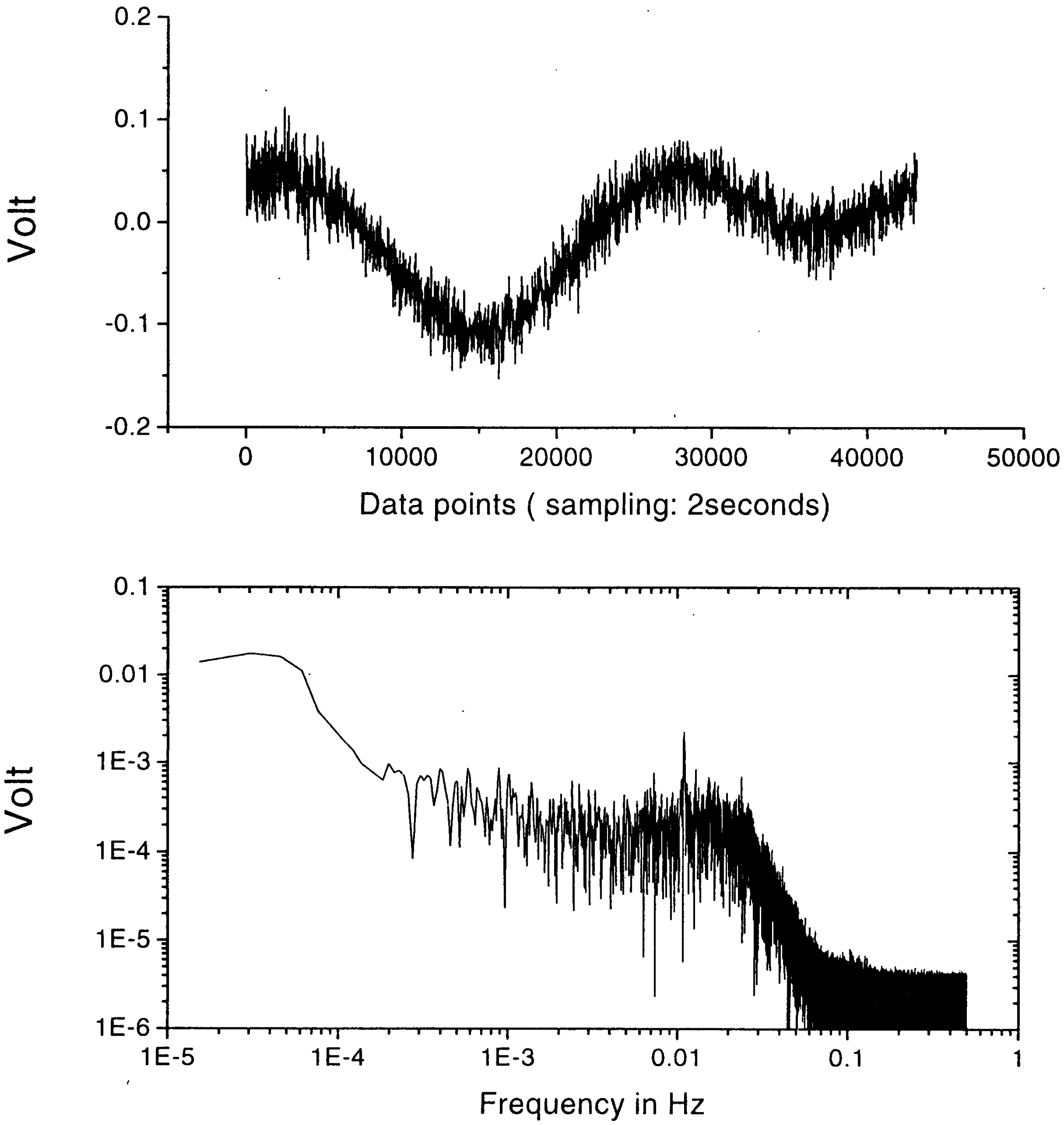

Fig.10. MODE signal obtained from SG#016 at Syowa Station and its spectrum. Top shows the 2-s MODE data of 1 day in length, which were obtained 24 hours from 00:00:00 UTC of December 26, 1993. Bottom shows the FFT amplitude spectrum of that data. The scale factor of the MODE signal is about 2.3 μGal/V. Therefore, it is estimated from this figure that the noise level at Syowa Station is of about 0.86 nGal, for example, at the frequency band around 2 mHz in quiet day.

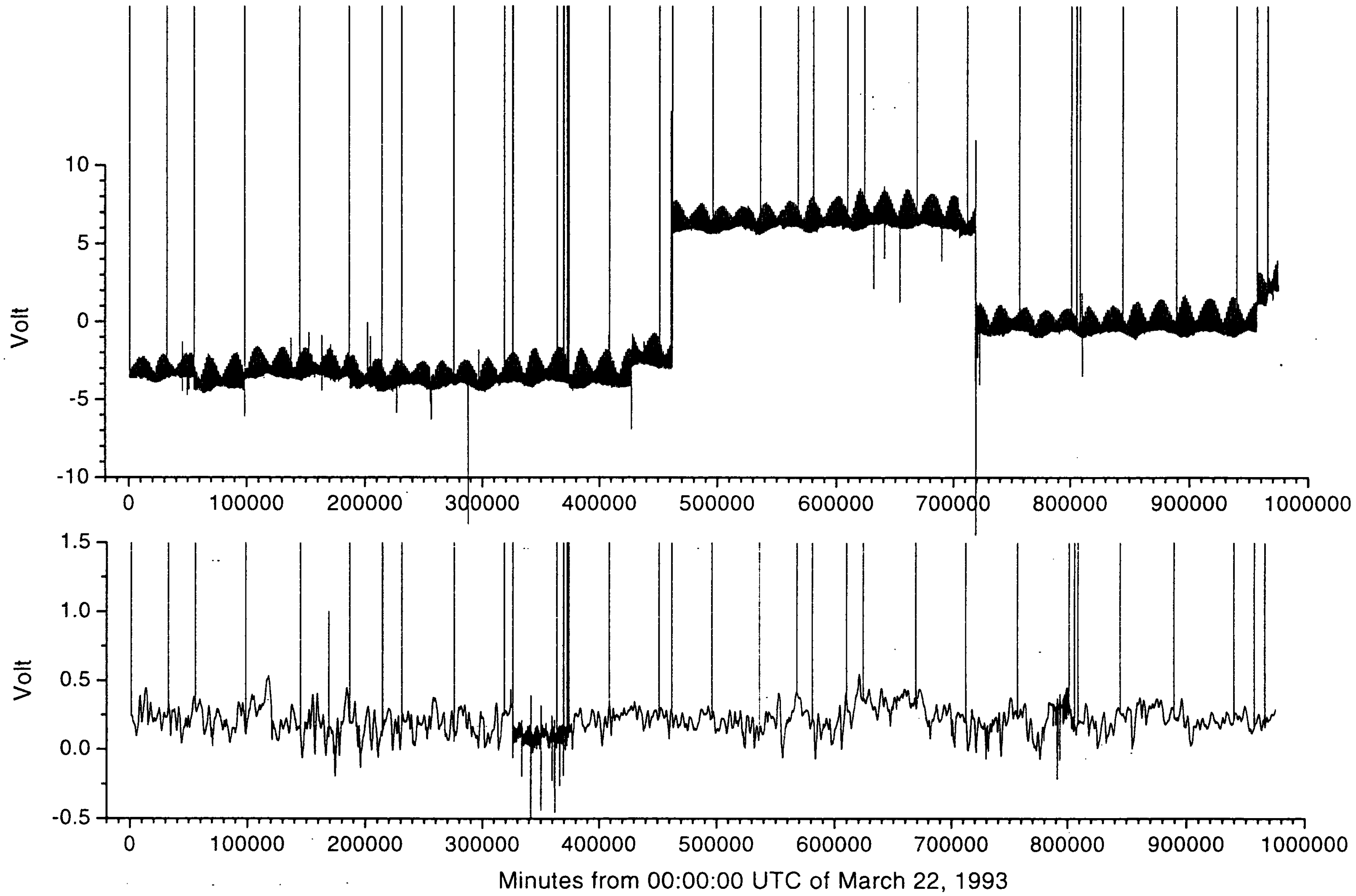

Fig.11. Correction for the step-like changes of the original 1-min data. Top: original 1-min data obtained from the SG at Syowa Station. Bottom: residuals of the 1-min data corrected for the step-like changes. The magnitude of step-like changes were estimated based on the 1-min data which were subtracted both effects of the tides and air pressure changes from the original data.

Chapter 6.
Short-Period Tides

6.1. Introduction

The precise determination of both the parameters of FCR and the latitude dependency of $\delta-$factor is an important target of the tidal gravity observation. As described in the subsections 2.3.1 and 2.3.2, the observation accuracies of better than 1 % in amplitude and 0.1° in phase are required for this purpose. On the other hand, the gravity observation is affected by the ocean tides, and the estimated FCR parameters are sensitive to the treatment of the ocean tide correction. As given in the result by Ogawa et al. (1991), a large discrepancy is shown in between the observation and theoretical tides. We suspect that this discrepancy may stem from inaccurate treatment of the ocean tide effects. This is one of the motivations that we reestimate the ocean tide effects at Syowa Station.

Tidal observations of gravity tides at Syowa Station have been carried out several times with different types of gravimeters, and the results of tidal analyses are given by Ogawa et al. (1991), Kanao and Sato (1995) and Sato et al. (1995a). Ogawa et al. (1991) analyzed three-month data obtained in 1987 with the LaCoste-Romberg (L & R) gravimeter G477 which was installed at the seismic vault (SV in Figure 7), and concluded that the observed semidiurnal ($M_2$and S_2) δ-factors corrected for the ocean tide effects estimated using the Schwiderski (1980) model (hereafter referred to as the SCH model), were 10 - 14 % larger than the theoretical values by Wahr (1981). As for diurnal waves (O_1, P_1 and K_1), there were no significant differences between the observation and the theory. Kanao and Sato(1995) confirmed the conclusions by Ogawa et al. (1991) based on the analysis results for one-year data obtained with the L&R gravimeter D73 installed at the Gravity Observation Hut (GOH in Fig. 7) and the he ocean tide corrections estimated by Ogawa et al.(1991). In March 22 of 1993, the observation with a superconducting gravimeter (SG016) started in the GOH. The obtained tidal factors obtained from the first one-year data of the SG016 (Sato et al., 1995a) support the previous analysis results.

As a standard model, the SCH model has been widely used for the correction for the ocean tide effects. However, the SCH model is considered as not so accurate in the southern hemisphere where there are few observations to constrain the model. Matsumoto et al. (1995) recently developed the global ocean tide model (hereafter referred to as the MAT model) using the TOPEX/POSEIDON (T/P) altimeter data, and compared their 0.5°× 0.5° grid data with a data set called 'ST104' for the globally distributed tide gauges. It was shown that the MAT model is more consistent with 'ST104' than the SCH model for any of the eight (M2, K1, O1, S2, P1, N2, K2 and Q1) waves. We, therefore, reestimated the ocean tide effects at Syowa Station using this new model in cooperating the revised digital topographic maps which are much more accurate than those used in the computation by Ogawa et al. (1991).

6.2. Instrumental Phase Lag of the LaCoste & Romberg Gravimeter

The LaCoste & Romberg Gravimeter (L & R gravimeter) is usually equipped with an electronic beam position indicator (CPI card) to improve reading accuracy. Before the feedback method proposed by Harrison and Sato (1984), this instrument has been widely used to the tidal observation by directly recording the output from the CPI card without a feedback (hereafter referred to as "deflection mode"). A serious problem of the deflection mode is the large phase lag which appears in the observed tides mainly due to the hysteresis of the metal spring called a "zero-length spring". This hysteresis effect on the tidal observation was first clearly recognized by test observations made by Sato (1977), and was later reconfirmed by the simultaneous observation carried out in 1997 using five L & R gravimeters (Tsubokawa et al., 1997). As described by Sato(1977), the magnitude of the obtained phase lag depends directly on the mechanical sensitivity of the gravimeter (i.e. ratio of the magnitude in deflection of the pendulum beam to the change in the force applying to the proof mass). The mechanical sensitivity itself depends on a setting angle called an 'offset angle' (see **Fig.** 12). According to the measurement by Sato (1977), the hysteresis effect on the observed tides reaches to about 1° at the periods of the diurnal and semidiurnal tides. Such large phase delaying could not be explained by the usual theory of the pendulum with a linear friction.

When the gravimeter is set at a high sensitivity, the spring is much stretched by the same magnitude of gravity change compared with the gravimeter set at a low sensitivity. Thus the hysteresis effect becomes larger by setting the sensitivity higher. To the same extent, it means that the sensitivity of the gravimeter always changes by tilting of the ground. Usually a building is tilted by about 1-2 seconds of arc in peak to peak amplitude due to the thermal expansion and also of the contraction of the building wall and ground by heating of Sun in day time and by cooling in night, respectively. Therefore, it is highly possible that the observed tides, especially diurnal ones, are violated by this thermal effect, when we use the gravimeter with the deflection mode. However, Harrison and Sato (1984) showed that most of the problems mentioned above can be solved by modifying the gravimeter to a feedback mode. In the feedback mode, the spring is not stretched by the tidal force as long as its magnitude does not exceed the dynamic range of the feedback force. Therefore, the problem on the hysteresis due to stretching of the spring dose not appear or becomes negligible small in the practical observation. The method of implementation of the feedback mode, as well as its efficiency, is explained in the paper by Harriosn and Sato (1984).

In order to avoid possible problems in the deflection mode, two L & R gravimeters used at Syowa Station (G477 and D73) were modified to the feedback mode at Mizusawa before sending out to Antarctica.

6.3. Scale Factor of the SG

The scale factor, namely the conversion coefficient from the voltage output to the gravity change in μGal, of the SG of Syowa Station was determined by comparing the amplitude of the M_2 wave obtained by the SG with that obtained by L & R D73 gravimeter which is installed beside the SG. As the scale factor of the L & R D73 gravimeter, we adopted here the value obtained by Kanao and Sato(1995), which was determined based on the data obtained during one year from 1993 to 1994. Generally, the scaling error of the D73 gravimeter directly results in the amplitude uncertainty of the SG records. However, as a result of monthly calibration procedures of the D73 gravimeter, it was provided that the scale factor of D73 showed 1 % uncertainty throughout the observation period. Based on this comparison, we obtained the values of -57.965 μGal/Volt for the scale factor of the SG, and this scale factor is used throughout this thesis.

An error source in determining the scale factor is the error of the reading dial of the D73 gravimeter. Calibration of the scale factor of the D73 gravimeter is made by measuring the output voltage generated by rotating the reading dial. By rotating the reading dial, position of the proof mass is shifted in vertical direction through the gear system and the double reduction lever system, and the output voltage of the gravimeter is proportional to the rotation of the reading dial. In an ideal system, the change in the vertical motion of the proof mass, namely, the output voltage, is proportional to the given rotation of the reading dial. In practice, however, there exist departures from this ideal situation mainly due to the periodic errors caused from the imperfection of the gear system, namely, the error due to eccentricity of the screws. This error is called 'periodic error' or 'circular error' (Harrison and LaCoste, 1978). On the analogy of the measurements with the G-type gravimeter (Harrison and Sato, 1984), the short-period circular error for the D73 gravimeter is considered to be 0.1 % at worst, when the rotation of the reading dial to calibration is carried out within the range of the feedback voltages (i.e. about 3000 μGal). Because the circular error of the D-type gravimeters was improved to one tenth of the G-type gravimeter (Valliant, 1991). On the basis of the above reasons, an accuracy within 1 % amplitude calibration is believed to be maintained for the SG. However, it is to be noted that we do not have the data concerning the long-period circular error of the D73 gravimeter.

As described in the section 4.1, the sensitivity of the SG depends on the gradient of the supporting magnetic field (Prothero and Goodkind, 1968). Another possible change of the SG scale factor took place when adjustment of the superconducting current was made on August 2 in 1994. The balancing position of the superconducting sphere was largely shifted by the power failure occurred in February 1994, and the sphere position was re-centered on August 2 in 1994. In order to examine the change of the scale factor due to this adjustment, we compared the M_2 amplitudes of the two data subsets, that is, (a) February 23 - July 31, 1994 and (b) August 3 of 1994 - January 31, 1995. The results are 13.497±0.005 μGal for the former and 13.503±0.005 μGal for the later. The difference was only at 0.006 μGal. Thus the adjustment made in August, 1994 gave rise to an uncertainty of less than 0.1 % of the SG scale factor.

Simultaneous observations with an absolute gravimeter FG5 was carried out by GSI (Geographical Survey Institute) from January 20 to February 11 in 1995. Instrumental condition of the FG5 was not the best due to an unexpected accident. Nevertheless a comparison with the SG data was done by Aoyama et al. (1997). In order to avoid the possible degradation of the accuracy of the determination of the scale factor by including bad data, the whole data were divided into three periods taking account of instrumental condition of the FG5.

Also bad data of known origins were rejected. The derived is -57.499±0.312 μGal/Volt as an averaged of the estimates of the three periods of data spans.

As described above, two calibration factors obtained by the L & R D73 gravimeter and the FG5, respectively, are consistent within the error of 0.8 % and the SG scale factor was stable at 0.1 % level against to adjustment of the superconducting current. Further, the amplitudes of M_2 wave obtained from different data spans are also consistent within the error of 0.1 %. These facts clearly show that the SG of Syowa Station is calibrated at the accuracy better than 1 %. Therefore, it is expected to calibrate the SG scale factor more accurately using the absolute gravimeter data covering longer period than that of the experience in 1995.

6.4. Tidal Parameters Obtained from the SG

The data used in the tidal analysis covers 677 days from March 22, 1993 to January 27, 1995. The parameters of the short-period tides were estimated by means of the BAYTAP-G (see in Chapter 5). The 1-hour data corrected for the steps are shown in **Fig.**13A. The four components decomposed from this data by BAYTAP-G are shown in **Fig.** 13B, C, D and E, which, respectively, shows the decomposed tidal component, the response term to the local air pressure changes, the trend component and residuals as the irregular part. As seen in **Fig.** 13D (trend component), the SG at Syowa Station clearly observed the long-period tides, such as the Mf and Mm waves. It is also shown from the linear drift that an apparent decrease of 30 to 40 μGal took place during two years.

When instantaneous air mass attraction and load deformation by the air-pressure changes is assumed, the associated admittance is obtained to be 0.371±0.003 μGal/hPa as an average over two years. Without correction of air-pressure effect, root mean square (rms) noise in each tidal constituent became twice as large in amplitude. The responses to air-pressure variations (**Fig.** 13C) generally have amplitudes of 20 μGal with short-period (shorter than 1 day) characteristics. However, as described in the section 5.2, we expect that more than 80 % of the atmospheric effects may be decomposed with the adoption of in-situ barometric data. As seen in **Fig.** 13E, magnitude of irregular noise series changes with time. At an earlier observation epoch, the software bug (sign-bit error) in the data acquisition program contributes to rise the noise level. The spike-like noises are mainly caused from earthquakes and maintenance works. However, random nature of these noises had actually no significant effect on the estimation of the parameters of the short-period tides.

The obtained tidal parameters of the four main waves are shown in **Table** 3. For comparison, the tidal amplitudes, phases and δ-factors obtained by Ogawa et al. (1991) and by Kanao and Sato(1995) are also shown in this table. All these values were estimated by using BAYTAP-G, in which the effect of the local air pressure variations was taken into account. As described in the previous session, both the G477 and D73 gravimeters were improved with the feedback method. Hence, it is considered that the results obtained by the L&R gravimeters are free from the error due to instrumental phase delay.

It is to be noted that the observation period for the L&R G477 gravimeter is shorter than those of other gravimeters, and further that the environmental conditions at the SV (quality of the observation pier and temperature stability) are not good compared with those at the GOH. Due to these reasons, as seen in **Table** 3, the errors of the δ-factors obtained by the L&R G477 are about 10 times as large as those of the SG016. Nevertheless, **Table** 3 shows that the amplitudes observed with three different types of gravimeters during three different epochs are consistent with one other within the discrepancy of 1.8 % for all waves. The scale factor of the SG016 was determined by adjusting its M2 amplitude to that observed with the L&R D73 gravimeter (see the section 6.3.).

Hence, it is natural that the M2 amplitudes of both gravimeters take almost the same values in **Table** 3. Further, it is significant that both D73 and SG016 observations are also consistent within the difference of 0.1 % in the amplitudes of other waves. It is also ascertained that the scale factor of the L&R D73 gravimeter itself was stable within 1 % uncertainty throughout the observation period (Kanao and Sato, 1995). Therefore, the differences of 10-14 % in the semidiurnal δ-factors between the observation and the theory (Ogawa et al., 1991) is not considered to be caused by uncertainty of observations. Among the three observations compared here, data span of SG016 is longest, namely, two years, showing the smallest observation errors. We, therefore, use the results of the SG016 for the purpose of comparison with the theoretical values.

Table 3. Comparison of the tidal parameters at Syowa Station obtained with three different gravimeters during three different observation periods

		G477			D73			SG016	
wave	amp.	phase	δ-factor	amp.	phase	δ-factor	amp.	phase	δ-factor
O1	23.92	−0.60	1.345	26.33	−0.62	1.2637	26.357	−0.69	1.2670
	±0.08	±0.17	±0.004	±0.03	±0.06	±0.0013	±0.009	±0.02	±0.0004
K1	34.55	0.39	1.180	34.99	−0.22	1.1960	35.039	−0.07	1.1974
	±0.13	±0.21	±0.004	±0.02	±0.04	±0.0008	±0.007	±0.01	±0.0003
M2	13.24	−0.20	1.371	13.46	−0.67	1.3946	13.474	−0.61	1.3954
	±0.02	±0.10	±0.002	±0.01	±0.03	±0.0008	±0.002	±0.01	±0.0002
S2	6.59	0.20	1.468	6.71	1.29	1.4946	6.714	1.38	1.4945
	±0.04	±0.33	±0.088	±0.01	±0.06	±0.0016	±0.002	±0.02	±0.0005

Note for **Table** 3: (1) The observation period and reference: 1987.04.01-1987.06.01 for G477 (Ogawa et al., 1991); 1992.02.17-1993.01.27 for D73 (Kanao and Sato, 1995); 1993.03.22-1995.01.27 for SG016. (2) Units of amp. (amplitude) and phase are given in μGal and degree, respectively. (3) Phase shows the difference between the observation and the local potential.

6.5. Ocean Tide Correction

The ocean tide effects were estimated by means of the program GOTIC explained in the section 3.2. GOTIC usually prepares two kinds of digital topographic maps to represent the global distribution of lands and seas, which we call the first-order and the second-order meshes. The mesh sizes are 1° × 1° and 5" × 7.5" in the directions of the co-latitude and the longitude, respectively. However, as Syowa Station is very close to the shoreline of East Ongul Islands (see **Fig.** 7), other two meshes of smaller scale were prepared to represent sea-land distribution around Ongul Islands more in detail. They are the third-order mesh (30" × 45") and the fourth-order mesh (7.5" × 15"). **Figure** 14 shows the modeled coastal topography of East Ongul Islands with the fourth-order meshes. The number in each mesh of the figure expresses the fraction of land area in tens of percentages. 9 means that the mesh is completely occupied with land, while 0 with ocean. The topography to the extent of 150" × 315" centered at the observation site was modeled with the fourth-order meshes. The surrounding regions of 40' × 60' and 30° × 30° were represented with the third-order meshes and with the second-order meshes, respectively. For all other remaining areas, the first-order meshes were used.

The MAT model by Matsumoto et al. (1995) was generated by assimilating the T/P altimeter data with a hydrodynamic equation. As the T/P data do not cover the polar regions outside of ±66° in latitude, they extrapolated the tidal amplitudes and phases by means of hydrodynamic interpolation method. The amplitudes and phases directly obtained from the T/P data after applying a response method were used as the boundary conditions. Although the original MAT model is given with the grid interval of 0.5° × 0.5°, in order to make comparison with the Schwiderski's model (SCH model), we reduced the grid spacing of the MAT model to 1° × 1° intervals, by simply averaging four values given in the 0.5°×0.5° grid system over each 1°×1° mesh area. Both the SCH and the MAT model were modified to satisfy the condition of the conservation of ocean-mass, by subtracting uniformly the unconserved ocean-mass approximated with a sheet mass from the mass of each ocean mesh (Agnew, 1983).

Due to small diameter of East Ongul Island (e.g. about 2 km) , the estimation of the ocean tide effects is sensitive to the location of the observation site (shown with the mark of 'S' in **Fig.** 14). We adopted the coordinates of 69° 00' 22.5"S and 39° 35' 10.0"E at the GOH in accordance with the Bessel geodetic system. The Green's function for the 1066A earth model (Gilbert and Dziewonski, 1975) was used in the convolution integration.

6.6. Results and Discussions

The computation results are listed in **Table** 4. For the comparison with the estimates by Ogawa et al. (1991), namely, Case 1, we give in Case 2 the results estimated only using the first- and second-order meshes and ignoring the ocean-mass conservation. In this case, East Ongul Island is wholly included in one element of the second-order mesh. Case 3 is the results obtained by using the SCH model, but the 3rd- and 4th-meshes were used in the computation. In Case 4, the MAT model was used in stead of the SCH model. In both the two cases of Case 3 and 4, the ocean mass of the models was forced it to conserved.

The computation results shown in **Table** 4 may be summarized as follows.
(1) The ocean effects of Case 2, which were estimated using the SCH model and only using the two kinds of the first- and second-order meshes, are consistent with those by Ogawa et al. (1991). The differences between the two estimates are only 0.04 μGal in amplitude and 0.2° in phase; the discrepancy may be due to slightly different station coordinates adopted in the two computations.
(2) As compared Case 2 with Case 3, both were obtained from the same ocean model (the SCH model), we see that inaccurate topographic effect appears more

on amplitudes rather than on phases, and the amplitudes estimated without finer third- or fourth- order meshes are likely to be 30-50 % underestimated for both the diurnal and semidiurnal waves.

(3) When four kinds of meshed oceans are included as representing detailed topography, the amplitudes estimated with the MAT model (Case 4) are larger by 0.2 μGal than those with the SCH model (Case 3) concerning all of the listed four waves. When compared with the diurnal waves, the phases of semidiurnal waves seem to be affected more by the less accurate SCH model. As a reason of this, we may point out that the variation in spatial distributions of amplitude and phase of the semidiurnal waves are more complex than those of the diurnal waves. Compared with the diurnal tides, the wave lengths of the semidiurnal waves are short. This may contribute the difference in the complexity of the spatial distributions.

Table 4. Comparison of the estimated ocean tide effects.

Case	1		2		3		4	
model	SCH		SCH		SCH		MAT	
mass	non		non		yes		yes	
meshes	1st-2nd		1st-2nd		1st-4th		1st-4th	
wave	amp.	phase	amp.	phase	amp.	phase	amp.	phase
O1	1.89	346.11	1.85	346.05	2.41	346.99	2.63	346.99
K1	1.39	354.42	1.37	353.31	1.88	352.19	2.08	358.11
M2	1.37	333.50	1.35	333.37	2.04	339.61	2.35	349.59
S2	1.00	352.33	0.98	352.09	1.55	352.87	1.72	358.59

Note for **Table 4**:

SCH and MAT mean the ocean models by Schwiderski (1980) and Matsumoto et al. (1995), respectively. The units of amp. (amplitude) and phase are the same as those in **Table**.3. The phases were converted to the values refereed to the local meridian at the observation site (lag positive). 'mass' shows the treatment of the total mass of the ocean models: 'non' means the mass is not conserved and 'yes' means that it was forced to conserve.

As seen in **Fig.** 6 of Chapter 2, the theoretical δ-factor shows a latitude dependency. We have compared the observed tidal factors with the two theoretical values by Wahr's (1981) and by Dehant's (1987), which take account of the core dynamics induced by the effect of earth's rotation. The results are shown in **Table** 5. As for diurnal tides (O1 and K1), the observed δ-factors corrected with the MAT model (Case 4) agree within the difference of 0.5 % from the theoretical factors, while those corrected with the SCH model (Case 3) are systematically larger by about 1 %. On the other hand, as for the semidiurnal tides (M2 and S2), the δ-factors corrected with the SCH model are larger by about 4 % than those corrected with the MAT model. It is noted that the δ-factors corrected with the MAT model are consistent with the theoretical values within the difference of 2 % concerning any of the two theoretical models and any of the four waves compared here. Since the amplitudes of the observed semidiurnal waves are only half of the diurnal waves (see **Table** 3) but on the contrary the magnitudes of the ocean tide effects are almost the same for both waves (see **Table** 4), it is considered that the semidiurnal δ-factors are likely to be more strongly affected by an inaccurate ocean tide modeling than those for the diurnal waves.

Table 5. Comparisons between the observed δ-factors and theoretical ones.

	Observation		Wahr's theory		Dehant's theory	
Wave	δ-factor	Phase	δ-factor	Phase	δ-factor	Phase
O_1	1.144	0.66	1.143	0.0	1.152	0.0
K_1	1.127	0.04	1.122	0.0	1.131	0.0
M_2	1.157	1.41	1.136	0.0	1.157	0.0
S_2	1.111	2.34	1.136	0.0	1.157	0.0

As seen in **Table** 5, the discrepancy between the observation and the theory are complex to be correctly interpret, as its magnitude differs from the wave to wave. However, if we take an average of the two waves of each tidal specie, we obtain the values of 1.135, 1.133 and 1.142 for the diurnal specie with respect to the observation, Wahr's theory and the Dehant's theory, repetitively. Likewise, the values for the semidiurnal specie are of 1.134, 1.136 and 1.157. The discrepancies between our values and the Wahr's theory are about 0.2 % for both the diurnal and the semidiurnal tides and those with the Dehant's are about 0.6 % and 2 % for the diurnal and the semidiurnal tide, respectively. This implies that the Wahr's theory is more consistent than the Dehant's theory with respect to the observed δ-factor. However, in order to make a definitive conclusion, it is still needed to increase the accuracy of the scale factor of SG016, which has an uncertainty of 0.8 % as discussed in the section 6.2. This is also desired to discuss precisely the FCR parameters from the observation.

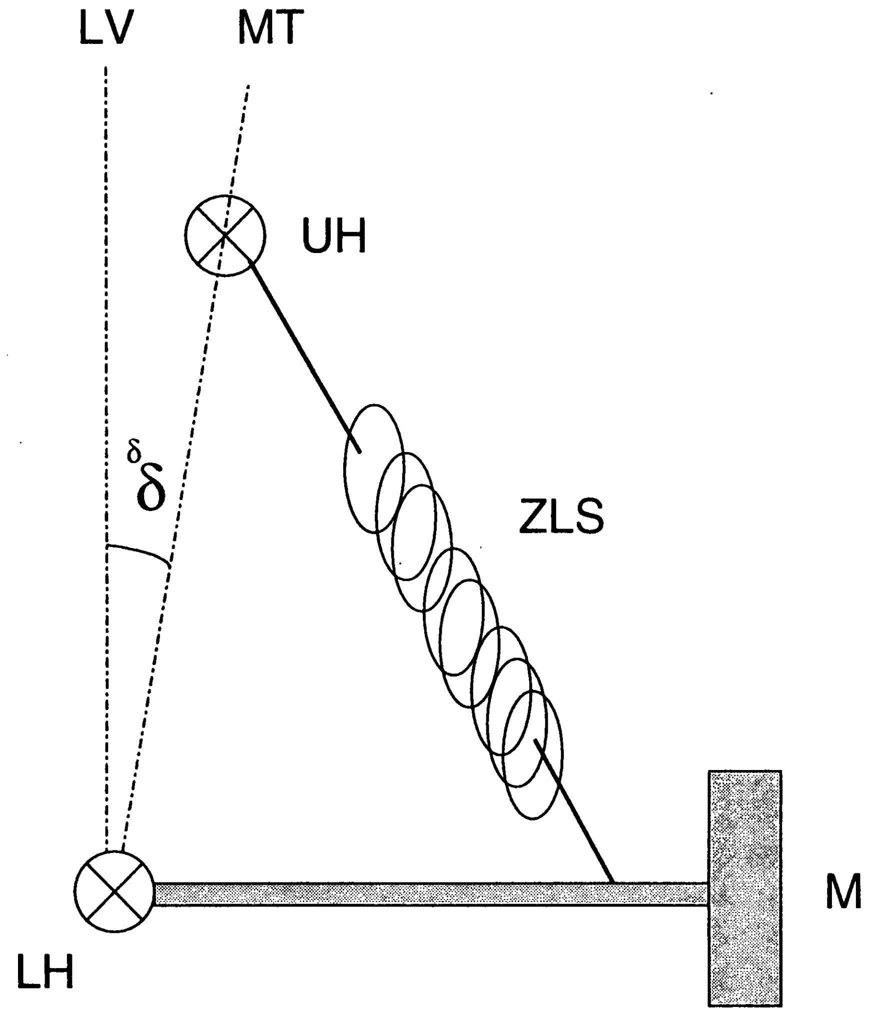

Fig. 12. Offset angle. This schematically shows the suspension system of LaCoste & Romberg gravimeter using a zero-length spring (ZLS). UH and LH are the upper and lower hinges of the gravimeter beam, and M shows the proof mass. LV shows the direction of the local vertical. The angle δ between the two lines of LH-LV and LH-MT is called the offset angle. By changing the angle δ by tilting the gravimeter case using foot screws, we can adjust the sensitivity of the gravimeter. When δ is set to zero, the sensitivity becomes infinity in an ideal gravimeter.

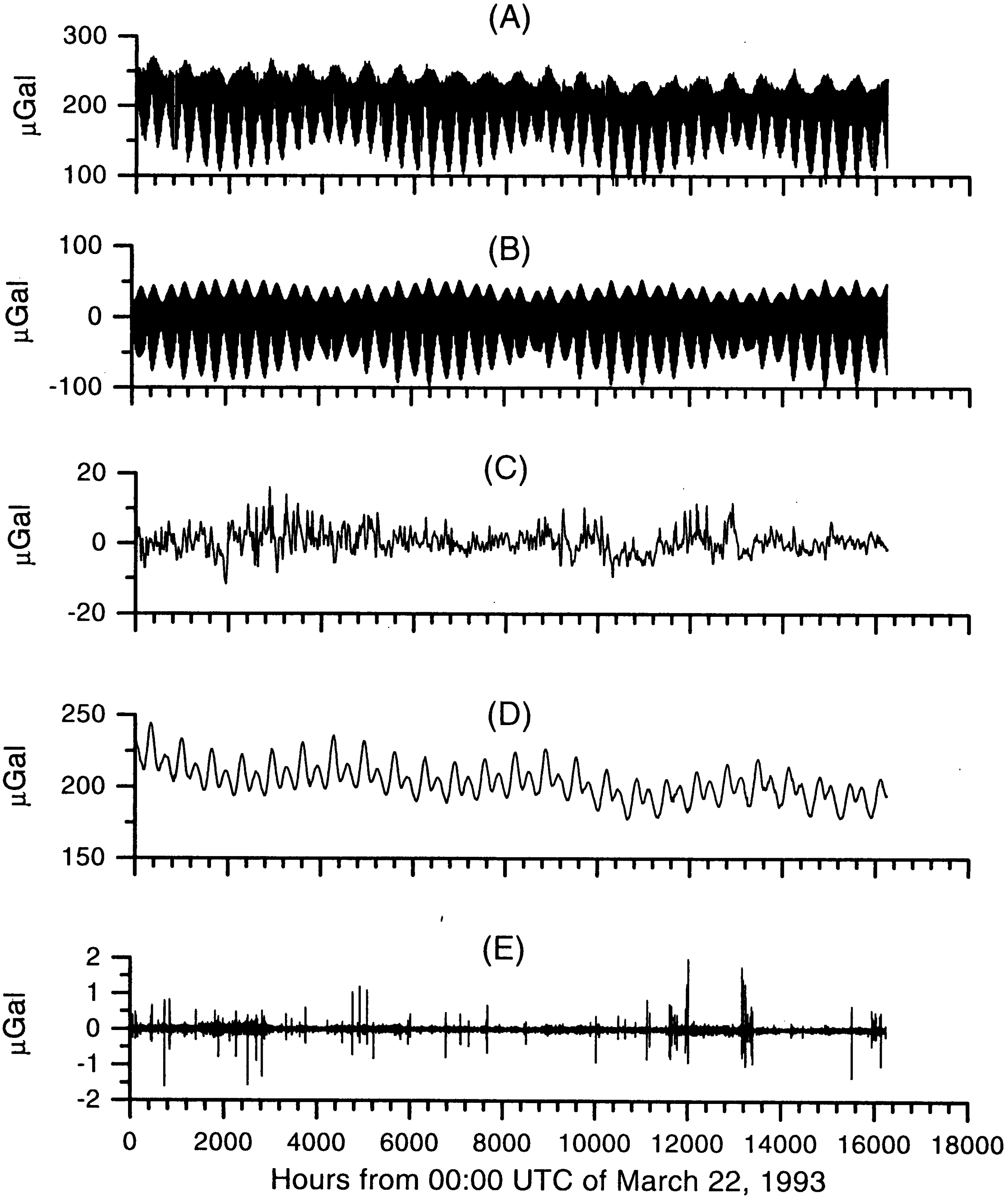

Fig.13. Results for the decomposition by BAYTAP-G. From the top: (A) 1-hour data corrected for the steps, (B) decomposed short-period tidal component, (C) response to the local air pressure changes, (D)trend component, and (E) residuals as an irregular part. The data of about two years (March 22, 1993 to January 27, 1995) were used for the analysis.

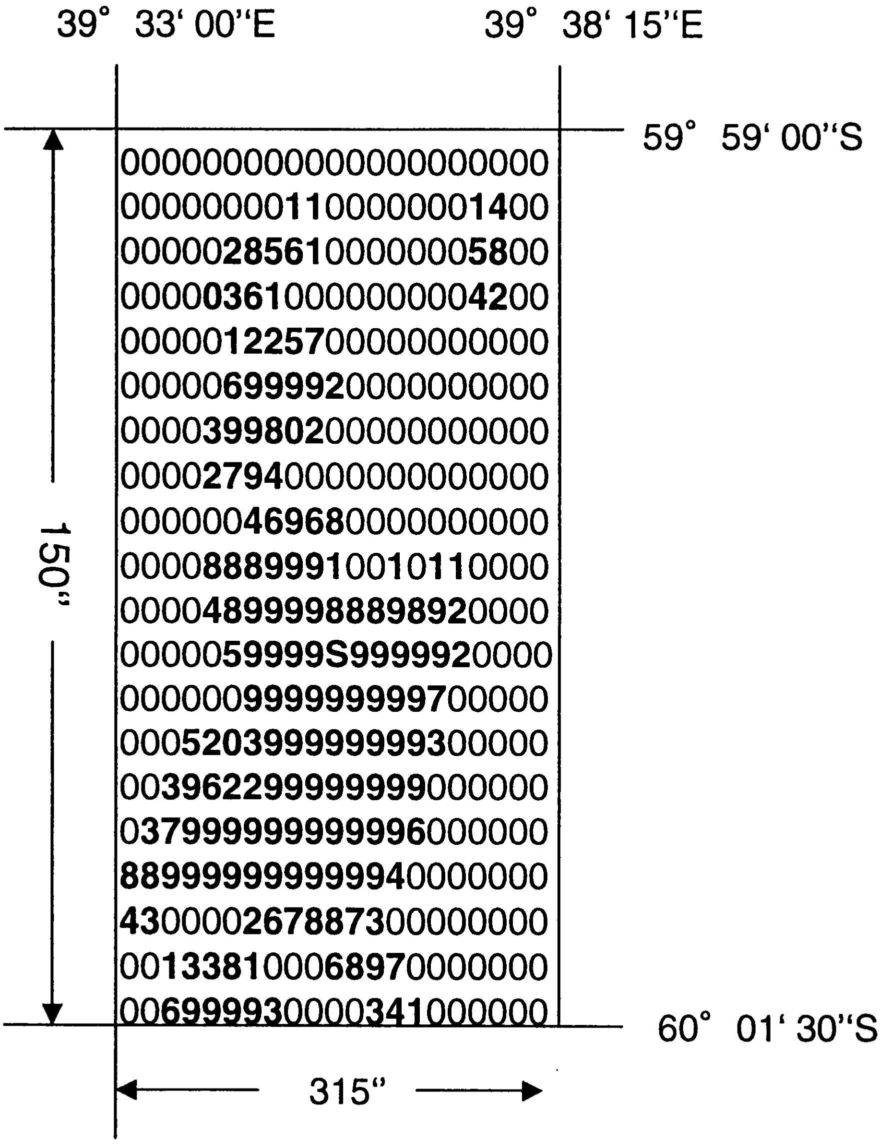

```
000000000000000000000
000000001100000001400
000002856100000005800
000003610000000004200
000001225700000000000
000006999920000000000
000039980200000000000
000027940000000000000
000000469680000000000
000088899910010110000
000048999988898920000
0000059999S9999920000
000000999999999700000
000520399999999300000
003962299999999000000
037999999999996000000
889999999999940000000
430000267887300000000
001338100068970000000
006999930000341000000
```

Fig.14. Coastal topography of East Ongul Island represented with the 4th order meshes. The position of the gravity observation hut (GOH in Fig.7) is indicated with the mark 'S' at the central part of this figure. The area of the land in each mesh is represented with the number from 0 to 9. Here, 0 means that it is an ocean mesh. The number calculated with a formulae of (9-this number)/9.0 was took into consideration for the actual convolution integral as a weight representing the contribution from each mesh.

CHAPTER 7.
Long-Period Tides

In this chapter, we deal with the long-period tides mainly based on the paper by Sato et a. (1997) titled 'Long-period tides observed with a superconducting gravimeter at Syowa Station, Antarctica, and their implication to global ocean tide modeling'.

7.1. Introduction

The observation of long-period tides is believed to give us a good constraint to study of an anelastic behavior of the earth at the low-frequency band. For example, Chao et al. (1995) analyzed the zonal tide signals in the length of day (LOD) data during 13 years, and concluded that the non-equilibrium ocean tide model with an anelastic mantle explains the observation results better than the equilibrium ocean tide model with a pure elastic mantle. On the other hand, gravity signals in the long-period tides are small in amplitude at mid-latitudes, and this makes it difficult to detect the signals clearly. Although there exists a number of SG observation sites at mid-latitudes, sufficient amount of results have not been obtained yet. Taking advantages that the amplitude of long-period tides become the largest at both poles, long-term observations with a L & R ET gravimeter have been continuing at the Antarctic Amundsen-Scott station (90° S), (Rydelek and Knopoff, 1982). Recently, Zurn et al. (1995) reviewed the gravity studies at the South Pole, and summarized that the observed phase lags of long-period tides showed remarkably large discrepancy from the theoretical prediction deduced by the elastic model of Wahr (1981) and Schwiderski's (1980) ocean tide model.

We analyze here the long-period tides using the SG data obtained at Syowa Station. For the long-period tides, we can stress the following three advantageous points to conduct the SG observation at Syowa Station: (1) As seen in **Fig.** 5 of Chapter 2, compared with the observation made at the mid latitudes, the amplitude of the long-period tide at the high latitude is larger and its magnitude obviously exceeds the detection capability of the SG (about 0.001 μGal). For example, the amplitude of Mf wave exceeds 10 μGal. (2) The instrumental drift of the SG is as small as 10-20 μGal/year (see **Fig.** 13). (3) Syowa Station is not affected by the ground water problem as described in Chapter 4. On the other hand, a disadvantageous point of this site is that, as the diameter of East Ongul Island is as small as 2 km, the SG site is very close to the shoreline. Therefore, the ocean tide effects on the SG observation are fairly large. We, therefore, improved our computation of the ocean tide effects by incorporating the tidal parameters obtained by Odamaki and Kuramoto (1989) estimated from the pressure-transducer water level meter set at the Tide Observation Hut (at TOH shown in **Fig.** 7) in the convolution integral.

7.2. Trend Component Decomposed by BAYTAP-G

The data accumulated during 677 days data from March 22, 1993 to January 27, 1995 were used for the analysis of long-period tides. These ate the same data set used for the analysis of short-period tides. From these data, we resampled at the interval of one day from the trend component (see **Fig.** 13D). As shown in **Fig.** 13D, the trend component consists mainly of the long-period tides and the exponential drift. We observe that the trend term was superposed by seasonal variations. However, exact estimation of their $\delta-$factors must await longer observations. **Figure15** shows the FFT amplitude spectrum of the trend component. We clearly observe the sharp peaks corresponding to the Mf and Mm waves as indicated with the mark and the arrow. **Figure** 15 also suggests that the background noises are at the level of less than 0.1 μGal at the frequency band covering both the Mf and Mm waves, and the long-period tide was detected with a signal-to-noise ratio better than 100 in magnitude. From the trend component used here, the effects of air mass attraction/load deformation was clearly subtracted based on the local air pressure data as described in Chapter 5. The admittance of the local pressure changes was estimated as 0.371±0.003 μGal/hPa as an average of two years, based on the one-hour data, assuming a non phase lag between the gravity and pressure data.

7.3. Observed Long-Period Tides

For analyzing the long-period tides, the 1-hour series of the trend component shown in **Fig.** 13D was resampled at intervals of 24 h (every 00h UT). Then we estimated the amplitudes and phases of 10 constituents (Mf, Mm, Ssa, Msm, etc.) using the BAYTAP-L program.

As explained in the section 5.2 regarding the BAYTAP processing, the trend (drift) component is determined by assuming its smoothness and a random walk model (see the equation (35)). The degree of smoothness is controlled by a hyperparameter D and the optimal value of D of the given data is determined on the basis of an information criterion called ABIC. In this processing, we have experienced a tendency that the degree of fluctuation of the trend term is controlled to a smaller order by setting a lager hyperparameter D and *vice versa.* Since the equation (35) involves only three adjacent terms, it is suspected that the constraining condition depending on D (in other word, separation of the long-period tides from the instrumental and secular drifts) may become too weak when the decomposition is carried out with the 1-hour sampling data. This is the reason why we used the data resampled at the 24 h interval. We thus first examined dependency of the least-squares solution on the value of D. **Table** 6 shows migration of the Mf amplitude, the phase difference and their associated uncertainties, together with the associated ABIC value by taking the value of D as a parameter. As seen in **Table** 6, the minimum ABIC is obtained at D = 8.0 indicated by an asterisk. This value is remarkably larger than the usual D value (around 1.0) derived in the analysis of short-period tides using a 1-hour data.

Table 6. dependence of the Mf wave amplitude, phase difference and the associated error, taking the value of hyperparameter D as a parameter

D	ABIC	S.D. μGal	Amplitude μGal	Phase deg., lag positive
0.10	-334.24	0.0734	11.623±0.223	-0.21±1.10
0.22	-379.27	0.1421	11.629±0.201	-0.16±0.99
0.48	-464.15	0.2278	11.631±0.149	-0.15±0.73
1.00	-527.33	0.3055	11.634±0.098	-0.13±0.48
2.20	-563.74	0.3764	11.638±0.059	-0.12±0.29
4.80	-589.60	0.4292	11.641±0.040	-0.12±0.20
* 8.00	-593.17	0.4590	11.642±0.035	-0.12±0.17
10.00	-590.02	0.4718	11.642±0.034	-0.12±0.17
22.00	-559.96	0.5169	11.644±0.034	-0.11±0.17
48.00	-503.28	0.5647	11.648±0.037	-0.09±0.18
100.00	-417.67	0.6201	11.651±0.041	-0.05±0.20
220.00	-300.95	0.6910	11.652±0.045	0.00±0.22
480.00	-173.55	0.7705	11.652±0.050	0.04±0.25

Table 7 shows the obtained amplitudes, phase differences and the δ-factors of the 10 long-period waves at the adopted value of D = 8.0. Due to the effects of time epoch selection of resampling interval, there are some uncertainties in the estimation of long-period tides and a trade-off between the long-period tides and the trend terms as mentioned the above. We will discuss these in the sections 7.5.1 and 7.5.2.

Rydelek and Knopoff (1982) obtained 1.1589±0.0017 as Mf δ-factor and 0.40°±0.08° as the associated phase at the South Pole from the six years data. As for northern latitudes, Richter (1985) obtained 1.148±0.020 and 0.2°±1.0°, respectively, at Bad Homburg (50.2285° N) from the superconducting gravimeter data of three years. On the other hand, Melchior et al. (1996) obtained 1.1449±0.0045 and 0.006°±0.223° at Brussels (50.23° N; almost the same latitude as Bad Homburg) from the SG data of 12 years. It is essential to apply precise ocean tide correction for the analysis of Mf tide. Zurn et al. (1995) and Melchior et al. (1996) suggest that the oceanic correction is imperfect when the Schwiderski (1980) model was integrated.

Table 7. Long-period tides estimated by BAYTAP-L

24 h Sampling	δ-factor	Amplitude μGal	Phase degree
Ssa	1.0835±0.3514	5.323±1.697	-8.06±18.69
Msm	1.2467±0.0734	1.307±0.077	-9.38±3.38
Mm	1.1205±0.0106	6.143±0.058	0.33±0.54
Msf	1.1200±0.0332	1.018±0.030	2.24±1.69
Mf	1.1218±0.034	11.642±0.035	-0.12±0.17
Mstm	1.0396±0.0709	0.392±0.027	-7.80±3.89
Mtm	1.0973±0.0155	2.180±0.031	-1.58±0.81
Msqm	1.1507±0.0923	0.365±0.029	-1.86±4.61
Mqm	1.1462±0.1087	0.301±0.029	-14.95±5.43
4-5 days	1.0998±0.2793	0.084±0.021	-20.50±14.58
			S.D.=0.459 μGal
19 h sampling			
Mm	1.1194±0.013	6.137±0.075	0.29±0.70
Mf	1.1206±0.0035	11.629±0.036	-0.08±0.18
			S.D.=0.443 μGal

7.4. Ocean Tide Correction

The GOTIC program described in the section 1.3.2 was applied to calculate the effects of the ocean tide on gravity. As the same reason for computing the ocean tide effect on the short-period tides, in addition to the first and second order mesh maps, we incorporated the third order mesh (30"×45") and the fourth order mesh (7.5"×15") in GOTIC to represent sea-land distribution in detail. For comparison, five global ocean tide models were prepared for our calculation of the ocean tide effects. They are (1) equilibrium ocean tide model, (2) Schwiderski (1980) model, (3) Dickman (1989) model, (4) CSR model which was given by Eanes (1995), and (5) Desai & Wahr (1995) model. The equilibrium ocean tide model was generated by using the Love numbers for the 1066A standard earth model (Gilbert and Dziewonski, 1975) given by Wahr (1981). Here we neglected the effects of both deformation of ocean bottom due to tide loading, and self–attraction of ocean mass.

Schwiderski (1980) model is based on the Laplace's tidal equations and numerical integration based on a grid system (1°×1°), using the observed tide gauge data as boundary conditions. This model is widely used in the tidal study as a standard ocean model. Dickman (1989) model is also based on the Laplace's tidal equations, but it was generated by a least squares fitting procedure after solving the matrix equations which consist of the tide and boundary constraining conditions developed with spherical harmonic functions. Although the original Dickman (1989) model is specified by the coefficients of spherical harmonics up to the degree of 15 for the untrancated dynamic solution, we converted them for comparison into the same grid system (1°× 1°) as that of Schwiderski (1980) model. Both the models of CSR (Eanes, 1995) and Desai & Wahr (1995) are based on the TOPEX/POSEIDON satellite altimeter data. The CSR model was computed by the similar way as that of Ma et al. (1994). Since these two models do not cover polar regions outside ±66° latitudes, extension to whole oceans was made using the Schwiderski model. Hereafter we call the above (modified) models as EQO, SCH, DKM, CSR+SCH and D&W+SCH models, respectively. In order to avoid possible computation error due to unconserved mass in the global ocean tide model, we slightly modified EQO, SCH and DKM models by approximating the unconserved mass in each model using a sheet mass of uniform thickness throughout the whole oceans, then by subtracting the sheet height uniformly from the tidal height of each ocean grid.

Although the original CSR and D&W models were extended to the polar regions with the SCH model, we also have considered this mass conservation correction to the CSR+SCH and D&W+SCH models.

Odamaki and Kuramoto (1989) analyzed the sea level variation data obtained by the bottom pressure gauge installed at East Ongul Island (see Fig. 7). They obtained the amplitude and the local phase lag of the Mf wave as 0.0268 m and 196.0° and those of the Mf wave as 0.0166 m and 195.2°, respectively. Sato et al. (1995b) confirmed that the direct measurement of the sea–ice displacement using the level staff stood over the bottom–pressure gauge was consistent with the data obtained by the gauge within 5 % difference in amplitude. Since East Ongul Island is located very close to the northern edge of the first–order mesh point (0.007° difference in co-latitude, see Figure 5), the corresponding global ocean model data together with the northern adjacent mesh data, was replaced by the observed values above.

Table 8(a) shows the final computation results of the ocean tide effect of the Mf and Mm waves using the five global ocean models, which were computed by incorporating the fourth–order mesh map, correction for the mass conservation, and modification with an in-situ observed ocean tides at Syowa Station. The Green's function for the 1066A earth model was used in the computations. When the original model was used in place of the in-situ observed parameters, the scatter of the amplitudes among the five ocean models became larger by 0.01 μGal. This definitely indicates effectiveness of inclusion of observed ocean tide at Syowa Station. The phases estimated from the EQO model are not exactly zero because we replaced part of the model with the observed values. The error budget of our estimates of the ocean tide effects will be discussed in the section 7.5.3, and the results given in **Table** 8(a) will be discussed in the section 7.5.4.

Table 8. Comparison of the estimated ocean tide effects using the five different models.

(a)

	Mf		Mm	
model	Amplitude	Phase	Amplitude	Phase
EQO	0.432±0.033	182.17±4.49	0.237±0.019	178.23±4.60
SCH	0.389±0.027	198.35±3.69	0.239±0.025	182.99±5.97
DKM	0.493±0.012	182.35±1.40	0.268±0.010	178.19±2.14
ENS+SCH	0.403±0.013	200.92±1.15	0.235±0.010	181.70±2.44
D&W+SCH	0.446±0.009	200.90±1.16	0.239±0.031	176.60±7.42

(b)

	first	second	third	fourth
M2	14.1 %	53.5 %	17.0%	15.4 %
O1	22.0	48.3	15.6	14.1
Mf	42.6	37.1	10.8	9.5
Mm	43.3	36.3	10.9	9.5

Note for **Table** 8: (a) Computation results for the Mf and Mm waves. (b) Percentage contribution of the ocean tide effects from each of the four ocean areas represented with the first-, second-, third- and fourth- order meshes.

7.5. Discussions

7.5.1 Effect of Sampling Epoch

The results given in **Table** 7 were obtained from the data sampled every 24 hours at the epoch of 00 UT. It may be necessary to see differences in the analysis results among other 23 subsets according to the shift of sampling epoch by 1 hour. The differences of the amplitude and the associated phase difference were ±0.015 μGal and ±0.08° (the Mf wave), while ±0.009 μGal and ±0.13° (the Mm wave), respectively. It is noted that the associated uncertainty of each wave for the 23 subsets are almost the same as those of the corresponding parameters in **Table** 7. These results indicate no significant dependency of the analysis results on the difference in the analysis epoch.

In order to investigate the effect of aliasing, similar analyses were tested using several data sets resampled at different sampling intervals. As an example, the results for the Mf and Mm waves obtained from the data resampled at every 19 hours are summarized in the lower column of **Table** 7. We can conclude that no significant change when compared to the results of 24-hour sampling case. As described in the section 4.3, the scale factor of SG at Syowa Station has been calibrated with L & R gravimeter D73 and an absolute gravimeter FG5. From these calibrations, the scale factor was able to be determined at the accuracy of better than 1 %, therefore, the absolute accuracy of the δ- factors in **Table** 7 is considered to be estimated at the similar accuracy. This value is about two times larger than the one expected from the formal error estimated from the 1-σ error of the residuals (irregular term decomposed by BAYTAP-L).

7.5.2. Trade-Off Among the Tidal Parameters, Drift and Irregular Noise

As described in the section 7.3, we examined the dependence of estimates, namely, the Mf amplitude, the phase difference and their associated errors, the resultant ABIC value, and the total rms residuals (S.D.), on the hyperparameter D that constrains the smoothness of the trend component in the BAYTAP–L analyses (see **Table** 6). The results given in **Table** 6 may be summarized as follows; (1) The rms errors of both the estimated Mf amplitude and the phase difference show systematic tendency to decrease with increasing D value, (2) On the contrary to (1), S.D. as the total rms residual increases with increasing D value, and (3) The Mf amplitude itself becomes monotonously larger with increasing D value, while the associated phase difference shifts from larger lead toward zero within rather wide range of the assumed D values.

These suggest that some trade-off among the long-period tides, instrumental drifts and irregular noises is inevitable when we use in the decomposition method of BAYTAP algorithm. Especially when D is too small, irregular noises (short-period variations) may contaminate the trend and tide components. This is the reason why errors of the amplitude and the phase increase with small D. On the contrary, when D becomes too large, the linearity constraint becomes too strong. As a result, the Mf amplitude is overestimated due to subsequent exclusion of long-period nature from the instrumental drifts. Also occurred in this case is increase of S.D. due to decrease of the degree of model fitting, even though rms errors of the estimated tidal amplitude and phase decrease apparently. As seen in **Table** 6, when each of the estimated parameters of amplitude, phase and their errors and S.D. takes just their intermediate values, ABIC becomes minimum. This suggests that the minimum ABIC criterion works well in the analysis for the long-period tides, likewise the analysis for the short-period tides.

7.5.3. Error Budget in the Estimation of Ocean Tide Effects

Taking the SCH model as a case study, we describe the sensitivity of the estimates of the ocean tide effects with respect to the following three points: (1) different adoption of elastic earth model, (2) roughness of digital topography representation around Syowa Station, and (3) the condition of the ocean-mass conservation. As for (1), we compared two results obtained using the two different Green's functions, namely, those for the 1066A earth model and the Gutenberg-Bullen standard earth model (Alterman et al., 1961) by Farrell (1972), however, the difference was small as 0.003 μGal at most in the case of the long-period tides. This is due mainly to the following two reasons; 1) the wave length is long, and 2) as a nature of Green's function, the loading effect from the mass at some loading distance reflects the earth's elastic structure at the depth corresponding to that loading distance. Because the major differences in the structure between two earth models of 1066A and Gutenberg-Bullen are in the upper most parts less than a few tens km in depth.

With regards to (2), we compute percentage contributions of ocean tide effect from the four groups of the meshed oceans (**Table** 8(b)). From this, we see dominant contributions (80 %) from distant oceans (first- and second-order meshed oceans). This is different from the cases of the short-period tides where the distant oceans have relatively less prominent contributions (68–70 %). When we replaced the fourth-order meshed areas totally with the third-order meshed oceans, the resultant increase of ocean tide effects was about 0.032 μGal for the Mf wave and 0.019 μGal for the Mm wave respectively. When the location of the observation site GOH (star mark in Figure 5) was shifted artificially to the center of the fourth-order mesh next to the north-east direction of the original position, i.e. putting the site GOH close to a sea shore by about 230 m, the amplitude of the ocean tide effects increased by 0.047 μGal for the Mf wave and 0.022 μGal for the Mm wave, respectively. Therefore, inclusion of the fourth-order meshes is indispensable to estimate the ocean tide effects at Syowa Station at an accuracy better than a few 0.01 μGal.

In the case of the SCH model, the amplitude and phase of the unconserved sheet mass correspond to 9.3×10^{-4} m and 5.1° for the Mf wave, and the neglect of this correction results in underestimate of 0.038 μGal. As for the Mm wave, they are 2.4×10^{-3} m in amplitude and 58.6° in phase, and the neglect of them also result in underestimate of 0.039 μGal. Although the magnitude of the unconserved mass correction varies from model to model, similar tendencies were obtained within the ranges of 0.003–0.05 μGal and 0.3°– 6.7° for the Mf wave, while of 0.003–0.03 μGal and 0.2°– 35.4° for the Mm wave, respectively.

Although an accurate estimate of the overall error in the computation of the ocean tide effect is rather difficult, from the tests mentioned in the above, we assumed here that the following three factors contribute to the overall amplitude error. For the case of the SCH model, they are (1) 0.003 μGal error due to different (uncertain) load Green's function, (2) 10 % influence due to missfitting of the land–sea topography around Ongul Islands, that is respectively 0.005 μGal and 0.002 μGal for the Mf wave and the Mm wave, and (3) 50 % influence from inaccurate treatment of the unconserved mass correction, that is 0.019 μGal for the Mf wave and 0.02 μGal for the Mm wave. Thus the total error results in 0.003 + 0.005 + 0.019 = 0.027 μGal for the Mf wave and 0.003 + 0.002 + 0.020 = 0.025 μGal for the Mm wave. Moreover, we assumed that the phase error may result in 100 % from the combination of the above three error contributions. For explanation, uncertainty diagram is shown in **Fig.**16. The errors of the amplitudes and phases shown in **Table** 8(a) were estimated in this way. If we accept the errors shown in **Table** 8(a), then the error of our estimates is about 10 % in amplitude at most for both the Mf and Mm waves. It is noted that, among the three error sources, the difference in the treatment of the total ocean mass is a main cause for the computation error, and it introduces the error of the similar order of magnitude as that caused by the difference in the global ocean models used for the computation.

7.5.4. Comparison of the Observation with the Theory

When the tidal gravity coefficients for the 1066A earth model given by Wahr (1981) are adopted, we obtain the value of 1.157 as the elastic δ- factor for the Mf and Mm waves at the latitude of Syowa Station (69.0° S). While we obtain the value of 1.159 from those given by Dehant and Ducarme (1987) for the same earth model. The difference between the two estimates are mainly due to the difference in definition of the tidal forces, i.e. the radial derivative of the mean spherical tidal potential is used in Wahr (1981), while the force along the normal to the elliptical earth is used in Dehant and Ducarme (1987). For the effect of mantle anelasticity, Wahr and Bergen (1986) theoretically estimated its effects on Love numbers h and k, and gave the range of correction terms dh and dk in their **Table** 3, where dh and dk are complex numbers. When we substitute their upper and lower limits of dh and dk to the correction equation $3dk/2 + dh$, and apply to the elastic δ- factor of 1.157, we obtain the δ- factors in the range of 1.158 - 1.161 covering both the Mf and Mm periods. The theoretically expected phase delay is very small as the degree of 0.005° – 0.04° (delay positive) at the same periods. Dehant and Zschau (1989) also estimated the effects of mantle anelasticity on the tidal factor and phase. Using their coefficients for the case of elliptical rotating earth gives the values of 1.159 and 0.01°.

By correcting the ocean tide effect (**Table** 8(a)) on the observed amplitude and phase (**Table** 7), and by taking the ratio of the corrected amplitude to the tidal amplitude on the rigid earth, we obtained the δ- factor and phase which can be directly compared with the theoretical value for the body tide. Using the amplitudes and the δ- factors obtained by BAYTAP (see **Table** 7) gives 10.378 μGal and 5.482 μGal as the tidal forces for the Mf and Mm waves, which are normal to the elliptical rigid earth at the latitude of Syowa Station. The δ- factors and phases corrected for the ocean tide effects are shown in **Table** 9. Where the associated errors were calculated by considering both the observational errors (**Table** 7) and the errors in the estimation of ocean tide effects (**Table** 8(a)), and no errors were assumed in the rigid tide. As seen in **Table** 9, due to the differences in the five ocean models used for the corrections, the corrected δ- factors vary within the ranges of 1.157 to 1.169 for the Mf wave and 1.163 to 1.169 for the Mm waves. However, if we take the average of the five ocean models, then we obtain 1.162±0.023 and 1.165±0.014 for the Mf and Mm waves, respectively. It is noted that both mean δ- factors prefer the δ- factors for the anelastic earth rather than the elastic values, even though the errors of the observed δ- factors are still large to tightly constrain the effects of mantle anelasticity.

Table 9. δ-factors and phases for the Mf and Mm waves corrected for the ocean tide effect.

	Mf		Mm	
model	δ-factor	Phase(o)	δ-factor	Phase(o)
EQO	1.163±0.008	-0.04±0.23	1.164±0.010	0.25±0.55
SCH	1.157±0.044	0.47±0.20	1.164±0.017	0.43±0.57
DKM	1.169±0.004	-0.02±0.17	1.169±0.008	0.24±0.53
CSR+SCH	1.158±0.016	0.57±0.17	1.163±0.008	0.38±0.53
D&W+SCH	1.162±0.018	0.64±0.17	1.164±0.021	0.19±0.59

Among the five models compared here, for both the waves of Mf and Mm, the DKM model gives the δ- factors which are noticeably larger than those expected from the elastic and anelastic tide models, on contrary this, the SCH model gives the smallest Mf δ- factor. Both the models of CSR+SCH and D&W+SCH, which were extended into the polar regions outside of ±66° latitudes by using the SCH model, show the similar tendencies as those obtained from the SCH model, but the δ- factors corrected with these combined models give the intermediate values in magnitude as compared with the other models. The DKM model not only shows a very close agreement in the δ- factors between the two waves of Mf and Mm but also shows the smallest associated uncertainty in the δ-factors. Moreover the phases corrected with the this model are very similar with those with the EQO model. As the reasons for this similarity, we may point out the low spatial resolution of the DKM model. Since the DKM model was computed using the low degree spherical harmonic functions (up to 15 degrees), this model is considered as relatively insensitive to local or regional changes in the topography and ocean depth compared with other three models of SCH, CSR and D&W. The original Dickman's harmonic coefficients, which were used here to generate the grid data, have been already forced to conserve the ocean mass. This is the reason why the errors of the δ- factors and phases corrected with the DKM model are smallest among the five ocean models compared here.

Recently Matsumoto et al. (1995) assimilated the TOPEX/POSEIDON altimeter-derived tide data into a hydrodynamic interpolation method, and generated a global ocean tide model for the diurnal and semidiurnal waves including the polar regions. As described in the previous chapter, we reexamined the short-period ocean tide effects at Syowa Station using this new model, and obtained the ocean-tide corrected δ- factors of 1.144 (O1 wave) and 1.157 (M2 wave). The discrepancy from the Wahr (1981) theory reduced drastically to 0.5 % (O1 wave) and 2.0 % (M2 wave), as compared with the previous 1-2 % (O1 wave) and 10 % (M2 wave) larger values with the correction using the SCH model (see Ogawa et al., 1991). The results for the short-period tides and the large difference in the Mf δ-factor suggest that, as compared with the accuracy in the mid latitude regions, the SCH model is not so accurate in the southern hemisphere or in the oceans at the high latitudes where there are few observations to constraint the model.

Finally, it is noted that the Mm phases of the ocean tide effects are close to 180° and show remarkably less dependence on global ocean modeling as compared with those for the Mf wave (see **Table** 8(a)); thus the range of the corrected phases are 0.24° to 0.43° for the Mm wave, while those for the Mf wave -0.02° to 0.49° (see **Table** 9). The similar tendency is also seen in the comparison of the δ- factors; thus 1.157 to 1.169 for the Mf wave, while 1.163 to 1.169 for the Mm wave. These characteristics suggest that the Mm ocean tide of longer-period is much close to an equilibrium state than the Mf tide of relatively shorter-period, and the associated ocean tide correction shows less dependency on the difference in the ocean modeling. Therefore, although the amplitude of gravity tide for the Mm wave is about one-half of the Mf wave at Syowa Station, there is a possibility that the Mm wave gives a tighter constraint condition for the mantle anelasticity rather than the Mf wave when the analysis with much longer observation data than that used here is available.

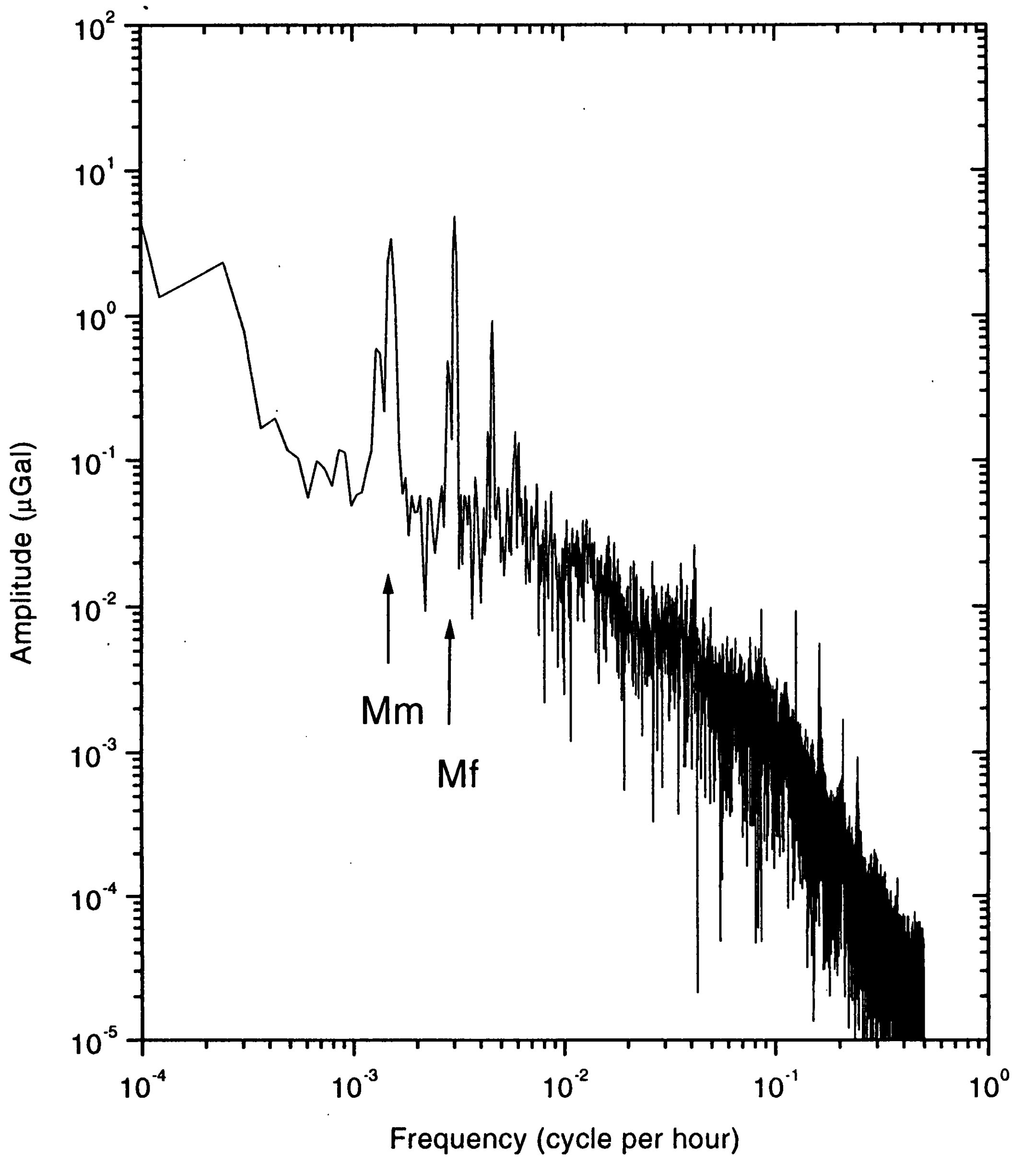

Fig.15. Amplitude spectrum of the trend component shown in Fig.13D. The spectrum peaks corresponding to Mf and Mm waves are clearly observed at the positions indicated with the arrows and symbols, respectively.

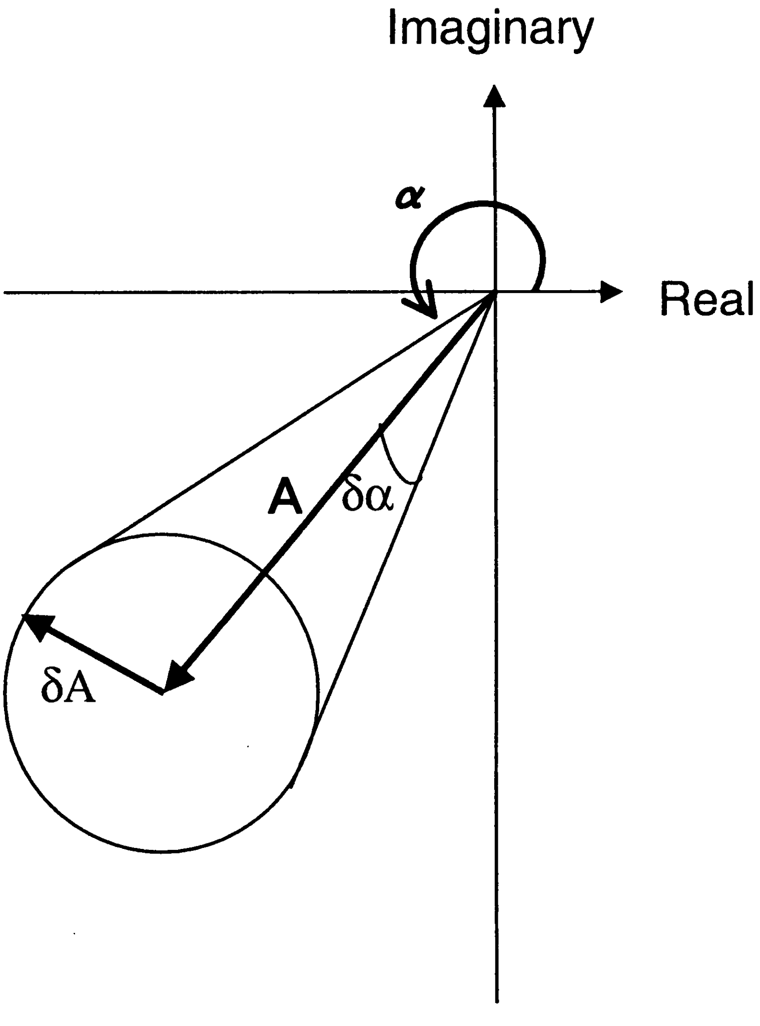

Fig. 16. Assumed error range in the estimation of the ocean tide effects. Where A and α show the amplitude and phase of the ocean tide effects, and δA and δα show their errors, respectively. We assumed the error circle (360 deg.) of the amplitude error of δA results in the phase uncertinty of δα. In the case of the Mf wave of the SHW model, A, δA and δα are 0.389 μGal, 198.35 and 3.69 deg, respectively.

Chapter 8.
Polar Motion Effect and Annual Gravity Changes

This chapter describes the polar motion effect on gravity observations and the annual changes including its effect based on the two papers by Sato et al.(1997) and Sato et al. (2000).

8.1. Introduction

The development in the space geodetic observation techniques such as VLBI (Very Long Baseline Interferometer) and GPS (Global Positioning System) makes possible to observe the temporal changes of EOP (Earth Orientation Parameters) with an accuracy of 1 mas (1 mas =1 milli arc second) or better. The variations in EOP, either changes in the position of the rotation axis (polar motion) or spin rate of the earth (Length of Day, LOD) cause a perturbation of gravity through changes in the centrifugal force. If we can observe the earth's response to EOP changes at a similar relative accuracy, they give us very important and accurate information about the nature of earth's interior in a frequency band much lower than the seismic and short-period tidal bands and the knowledge about a mechanical interaction between the earth's fluid parts and solid parts. Since there are only few kinds of observational data which are available to measure the earth's response at these lower frequencies, the gravity observation is one of the useful candidates. If we assume the values of 0.6 and 0.085 as Love numbers h and k, respectively, we can expect a change in the surface gravity of about 15 μGal at the most. This is an enough magnitude to be detected with a conventional spring gravimeter. However, mainly due to the unpredictable large long-term drift of conventional spring gravimeters, such long period gravity variation as the polar motion effect has not been successfully observed. Recently, the observation results for the polar motion effect by SGs have been reported, for example, the observation at Bad Homburg in Germany (Richter, 1990) and that at Kakioka, Japan (Seama et al., 1993).

A preliminary analysis for the polar motion effect using the two years data (March, 1993-January, 1995) obtained from the SG at Syowa Station have already been conducted by Sato et al. (1997). They obtained the amplitude factor (δ-factor) of 1.198±0.035 and a time lag about 20 days against to the gravity changes predicted from the IERS (International Earth Rotation Service) polar motion data. However, the length of the SG data used in the their analysis was too short to safely separate the two dominant periodic components in the polar motion, i.e. annual (12 months) and Chandler (14 months) periods. Recently, Loyer et al. (1999) analyzed the 8-year SG time series obtained from Strasbourg in France, and estimated the amplitude factor and phase of gravity changes at the Chandler period. Since the parameters estimated by them are dependent on the number of waves considered in the analysis, they obtained phases distributed within a range of 9° to 22°, corresponding to a delay of 10 to 27 days in the time domain. If we take the mean value simply averaged over their table (**Table** 1. by Loyer et al. 1999), we obtain 18.0°±7.2° (21.8 days). Comparing with the phase lag expected from theoretical estimates based on the anelasticity of the earth (Wahr and Bergen,1986 and Dehant and Zau, 1989), the observed phase lag is too large to be the effect of mantle anelasticity.

There are several possible sources which may produce the phase lag, including atmospheric loading, water table changes and the ocean dynamics. Among them, the effect of sea surface height (SSH) variations may be a major contribution on the phase lag. As the first step in our study for the earth's gravity response to the polar motion, the effect on the annual component at the actual SG observation sites was evaluated. Since the annual component of the polar motion is a forced motion, we consider that the effect on the annual component will be much simpler and better determined than that of the Chandler component which is a rotational free motion of the earth. However, the SSH variations should also cause gravity effects at other frequencies to the same extent. In order to see the spatial and temporal characteristics of the SSH data used here and the estimated gravity effects at the long-periods, we also examine the SSH and its gravity effects in a more general way by means of a method called 'PCA' (Principal Component Analysis, Preisendorfer and Mobely, 1988).

In the following sections, we begin by describing the problems on the analysis for polar motion effects following those which were discussed by Sato et al. (1997). Next, we reanalyzed the data obtained from the SG at Syowa Station by using an analysis model which was modified so that the experience in the previous study was taken into account. For this analysis, we used the data much longer than those used in the previous study by Sato et al. (1997), and compare with those obtained other two SG sites of Esashi, Japan and Canberra, Australia. Finally, we discuss the SG data focussing on the relation between the observed and predicted annual gravity changes.

The gravity data employed were obtained from the SGs at three of the six sites of the GGP-Japan Network which is a SG observation network being developed by Japanese SG group: from the north, three of Esashi, Matsushiro and Kyoto in Japan, Bandung, Indonesia, Canberra in Australia, and Syowa Station, Antarctica (Sato et al., 1999, Quite recently, a seventh station was established at Ny-Alesund in Svalbard Islands, Norway). The sites used in this study are the three of Esashi, Canberra and Syowa Station. From the strain measurement with the quartz tube extensometers carried out at Esashi, it is known that the observed secular ground motion at there shows very low coherency with the rail fall (Sato et al., 1980). At Canberra, the SG observation is made at the basement of a building that is very close to the top of Mt. Stromlo (790 m in altitude) and the soil layer at there is very thin (less than a few meters). As described in the section 4.2, it is known that there is no sediment layer around Syowa Station, which can reserve a ground water. Moreover, all of the SGs at the three sites are installed on the piers set directory on massive base rock. From these reasons, the effect of the water table on the gravity observations made at these three sites is expected to be small, although it needs to make sure the actual effect of the water table in detail.

8.2 Polar Motion Effect

8.2.1. Computation of the Polar Motion Effects

Loyer et al. (1999) gives a formula to estimate the gravity change taking into account both effects of the polar motion and LOD based on the faithful definition for the changes in the EOP. At the level of accuracy required for this study (0.1 μGals), the effects of LOD changes can be safely neglected because they are about 2 orders of magnitude smaller than that of the polar motion. With this approximation, the gravity change Δg on the earth's surface due to the EOP changes may be written to first-order as

$$\Delta g = \delta \Omega^2 a \sin 2\theta (x \cos \lambda - y \sin \lambda) \tag{36}$$

(Kaneko et al., 1974 and Wahr, 1985, for example). Where $\delta = 1 + h - \frac{3}{2}k$ is the gravimetric factor containing the second-order Love numbers h and k. Ω is the mean angular velocity of the earth, a is the radius of the earth, and θ and λ are the co-latitude and east longitude of the observation site, respectively. x and y are the time variations in the Celestial Ephemeris Pole relative to the International Reference Pole. Using equation (6.2) and assuming the delta factor to be 1.155, a nominal value given by Wahr (1981), we estimated a time series for Δg from the daily EOP data. We used here the 'EOPC04' EOP data provided by IERS.

Figure 17 shows the gravity changes at Syowa Station which were computed from the IERS data for the period of about 16 years from January, 1983 to May,

1999. As seen in the top figure of **Fig.**17, the amplitude is about 7 μGals in Peak-to-Peak at the most for the 16 years. The bottom figure of **Fig.**17 shows the FFT amplitude spectrum computed from this data. We observe the largest amplitude at the frequency of about 0.00229 cpd (i.e. 436 days in the period). This peak corresponds to the Chandler component. Beside this peak, we observe the peak of the annual component. From the figure, we see that the Chandler motion is the most dominant spectrum peak in the polar motion effect and it has an amplitude about two times larger than that of the annual component. We see also in the figure that the amplitude of the semiannual component is small compared with these two major components, i.e. about 10 % of the annual component in magnitude.

8.2.2. Temporal Variation in the Polar Motion Effect

The IERS data used in the computation results shown in **Fig.** 17 were obtained from such modern observation techniques as VLBI and GPS. When we use the data obtained before 1983 including the optical instruments into the analysis, the peaks become much broad ones and the obtained Chandler period changes in time. In the analysis using the much longer gravity data, the change in the period directly affects the reliability of the results obtained by the analysis models given in the equations (37) and (38), which are assumed a constant period for each of all periodic components. Therefore, prior to the reanalysis of the polar motion effect, we have examined the temporal variation of the semi-annual , annual and Chandler components. Especially we are interested in the temporal stability of the Chandler period. For the test, the time series data for Δg generated by the equation (36) were fitted to an analysis model consisting of 5 terms, a constant, linear trend, and the three periodic terms of the annual, semiannual and Chandler components.

The temporal changes of the periodic terms were examined by fitting 6 year segments of the data set and by successively shifting the analysis epoch by one year. The optimum Chandler period for each 6-year data set was selected to minimize the RMS error for the residuals within those obtained from 100 iterations which were carried out by changing the Chandler period within the range of 410 days and 450 days. **Figure**18 is an example of the results for the 6-year analysis using the EOP data from 1993 to 1998. This figure shows the changes of the standard deviations of residuals as the function of the Chandler period assumed in the fitting process. We see that the minimum value is attained at around 435-436 days close to a nominal vale known as the Chandler period.

Figure 19 shows the temporal variations in the polar motion effect computed using the EOP data of the 33 years from 1962 to 1999. A, B and C show the variation in the period, amplitude and phase of Chandler component, D and E show those in the amplitude and phase of annual component, and F is the variation of SD (Standard Deviation) of the residuals obtained from each successive 6-year analysis. As noted in the home page of IERS web site, the accuracy of the observed EOPs was greatly improved after 1983 mainly due to the improvement in the space geodetic observation techniques. From **Fig.** 19, we also recognize that large changes in the Chandler period (**Fig.**19A) and the phase (**Fig.**19C) for the analysis periods before 1983 are substantially reduced after 1983. These strongly suggest that the temporal changes in the Chandler component observed with the optical instruments are mainly caused by some local effects such as due to meteorological disturbances. We see in **Fig.** 19A that the Chandler period is stable within the range 433.0 days to 437.1 days over the 16 year period from 1983 to 1999, especially, in the recent period for which we discuss the polar motion effect on the gravity observation. 435.4±1.3 days was the mean value averaged over the 16 years. We adopted here this value as the Chandler period to be used in the fitting process described in the later section.

8.3. Results Obtained in The Previous Analysis

8.3.1. Analysis Model and Results

The model used in the previous analysis by Sato et al. (1997) is

$$\begin{aligned} y(t) &= b_0 + b_1 t + b_2 \exp(-t/\tau) \\ &\quad + b_3 \sin(\varpi_1 t) + b_4 \cos(\varpi_1 t) + b_5 \sin(\varpi_2 t) + b_6 \cos(\varpi_2 t) \\ &\quad + b_7 P(t + \tau_p) + e(t) \qquad (37), \end{aligned}$$

where $y(t)$ is the time series data of the trend component decomposed from the original data by means of BAYTAP-G and -L, so that they mainly consist of the time variation components having a period longer than the monthly tide; t and τ are the time in days and a time constant of the exponential decay of $y(t)$; ϖ_1 and ϖ_2 are the angular frequencies of the annual and semiannual components (here the periods of Sa and Ssa tidal waves, respectively); $P(t + \tau_p)$ represents the gravity changes due to the polar motion effect, which were predicted from the IERS (International Earth Rotation Service) polar motion data by assuming the amplitude factor of 1.0. τ_p is a variable which was introduced to represent a time lag or time advance of the gravity changes to the polar motion effect predicted from the IERS data; $e(t)$ is an observational error. The unknown parameters of (6.2) are the ten of $b_0, b_1, b_2, b_3, b_4, b_5, b_6, b_7$, τ,and τ_p. There were estimated by means of a non-linear least squares method, the Levenberg-Marquardt method (Press et al., 1989).

The results for iteration depend on not only the initial values used in the iterations but also the assumed τ_p value. Therefore, we first searched the optimum initial parameter values for the given analysis data by changing τ_p. From the pilot analyses, we found that the standard deviation of the residuals (SD) decreases when τ_p takes a value close to -20 days. Here the minus sign of τ_p means a lagging of the observed gravity against to the polar motion effect predicted from the IERS polar motion data. Next, we examined the change of SDs by changing τ_p within the wide range between -70 days and 50 days and without estimating the 9 parameters of b_0 to b_7 and τ in (6.2), i.e. by fixing them to the values obtained by the iteration with $\tau_p = -20$ days. This is because the iteration have failed when τ_p exceeds -30 days or +40 days, if all parameters were treated as free parameters. **Figure** 20 shows the behavior of SDs by changing τ_p values. This figure shows that the minimum SD is attained at around $\tau_p = -20$ days. Final results for the iteration with $\tau_p = -20$ days are listed in **Table11** as Case A. We obtained 1.198±0.035 as δ-factor of the polar motion effect. This value is slightly larger than the theoretically anticipated gravimetric factor for an elastic earth model (i.e. 1.16).

8.3.2. Interference Problem

To separate safely the annual component from the Chandler component, we would need a data length of at least 6 years. Moreover, the observed data include not only the annual component due to the effect of the polar motion but also those caused by other origins such as the solid and ocean tides, the seasonal variations in the ocean height, the change in the level of ground water and so on. However, since the available gravity data does not clear this condition in the data length, in the analysis by Sato et al. (1997), we were forced to fit the observed SG data to the time series data for polar motion effect which were not separated the three main effects of the semi-annual and Chandler components.

In order to see the effect of interference between the annual components and Chandler component of the polar motion, a test was carried out by comparing the analysis results using the two data sets which are different in the treatment of the polar motion data. The first case (Case A) is the similar as the actual analysis, thus the polar motion effect $P(t + \tau_p)$ generated by (6.1) includes the three effects of the semi-annual, annual and Chandler components. Other one (Case B) is a method which first the data set for the polar motion effect was generated by using a long time series of EOP data which has sufficient data length to separate the annual and Chandler component (i.e. nine years in length), and the annual and semiannual components are then removed from this data by means of the usual least squares method. Obtained residual time series is expected as mainly consisting of the Chandler component. The δ-factor of 1.0 was assumed to generated the polar motion effect for both the cases of A and B. Finally, this predicted Chandler time series was fitted to the observed gravity data. This method is the similar as that suggested by Richter(1990).

Table 10 compares the results obtained with the two methods, where Case A and Case B show the results by the method in Section 8.3.1 and those by the method in this section, respectively. In **Table** 10, first it is noted that the two different methods give δ-factors quite similar to each other, i.e. 1.198±0.035 for Case A and 1.230±0.037 for Case B. For the semiannual component, there is not significant difference between the two cases of A and B. It may contribution the following three on this small difference in δ-factors: (1) the smallness in the semiannual amplitude of the polar motion effect, (2) the relatively large amplitude of semiannual tide and (3) goodness in separation between the semiannual and annual component and between it and the Chandler component. While, for the annual amplitudes, there is significant difference between the two cases, as compared with their formal errors of 0.1 μGals. The difference is at 2.34 μGals in magnitude. If we simply take the sum of the annual amplitude for Case A (i.e. 2.06 μGals) and that of the subtracted polar motion effect (i.e. 1.16×1.13 μGals = 1.31 μGals), then we obtain the value of 3.37 μGals. Comparing this with the annual amplitude for Case B (i.e. 4.40 μGals), the difference is reduced to at a level of 1 μGal. But this difference clearly suggests that there still remains the effect of the interference between the annual and Chandler components. On the other hand, the amplitude of the Chandler component is estimated as 3.97 μGals (i.e. 1.23×3.23 μGals). If a half of the difference of

1 μGal shown in the above equally contributes to the estimation of both the Chandler and annual components, then it gives an error of about 15 % in the estimation of δ-factor. If so, both formal errors of the annual amplitude and δ-factor shown in **Table** 10 may be underestimated.

The interference problem was also examined based on the simulation data. The simulation data were generated with the equation (6.2). The random errors within the range of ± 1.5 μGals were added to the simulated data, which are the similar magnitude as those of the observation (see **Fig.** 13). The polar motion effect was computed from the actual IERS polar motion data by respectively assuming 1.16 and 0.0 as δ-factor and the time lag τ_p, respectively. Two data sets were prepared for comparison: one is a data set of 677 days in length (Set A) and the other of 3164 days (Set B). Set A has the same data length as that of the observed SG data, while Set B has enough data length to separate the Chandler motion from the annual component. The analysis results are listed in **Table** 11 for the three components of semi-annual, annual and polar motion effect with their true (given) values. The results shown in **Table** 11 suggest that all results for the iterations give the minimum SD at around $\tau_p = 0$ days in both simulation data sets, as expected from the given τ_p-value. **Table** 11 suggests also that, even though the data length of Set A is short as 677 days, the analysis results for Set A are not so meaningless a result as compared with those for Set B of 3164 days in length, and the results obtained from the actual SG data, too.

Table 10. Comparison of the parameters obtained by two different analysis methods

Term		Case A	Case B	Unit
epoch		March 22, 1997	March 22, 1997	
data length		677	677	days
τ_p		-20	-20	days
Constant		218.04±0.16	213.60±0.10	μGal
Linear		-0.0331±0.0002	-0.0337±0.10	μGal/day
Semi-annual	real	5.17±0.06	5.02±0.06	μGal
	imaginary	0.48±0.06	0.69±0.06	μGal
Annual	real	1.77±0.01	4.08±0.13	μGal
	imaginary	-1.06±0.06	-1.88±0.06	μGal
Exponential	amplitude	10.42±0.16	11.06±0.56	μGal
	$1/\tau$	-0.072±0.006	-0.066±0.006	1/day
	δ-factor	1.198±0.035	1.230±0.037	
SD of the residuals		0.679	0.672	μGal

Table 11. Results for the analysis using the simulation data.

Term		True	Set A	Set B	Unit
data length			677	3164	days
Semi-annual	real	5.0	5.00±0.06	4.970±0.025	μGal
	imaginary	0.5	0.68±0.06	0.682±0.025	μGal
Annual	real	1.8	1.78±0.18	1.811±0.026	μGal
	imaginary	-1.0	-0.94±0.15	-0.969±0.027	μGal
Polar motion effect	δ-factor	1.16	1.156±0.038	1.161±0.008	
SD of the residuals			0.264	0.265	μGal

Note: τ_p was fixed to the value of -20 days.

8.3.3. Effect of Step-Like Changes

It can be pointed out that the data of the SG at Syowa Station have a disadvantage on the analysis for long-period components. Because, at there, the He liquefier is operated at the period of about twice a year and many works are carried out at the gravimeter room accompanying with the member change between the old and new wintering parties. Though the disturbances by these works is certain to continue the SG observation at Syowa Station, it is evident that these noises affect on the analysis results for Syowa Station. It is also true that the most of large step-like changes accompanying a long-term after effect have been occurred at the time when the above works are carries out. In order to reduce the effect of steps on the analysis, the correction for steps based on the daily medians have been applied to the original data as described in the section 5.1. However, it is observed a tendency that the accuracy of the step correction is reduced when the step accompanying the long-term after shock. On the other hand, the results obtained with a linearized least-squares method are sensitive to the quality of this correction. Therefore, we tested the effect of the inaccurate step correction using the simulation data sets which were generated by using the same model as (6.2) and by adding one step within the rage of -5 μGal to +5 μGal at just mid data position of each data set of 677days in length.

The analysis was also carried out the similar method as described in the section 6.3.1. The results for this test suggest that the estimated amplitudes change within the range of 4.6 μGals to 5.4 μGals and 1.1 μGals to 3.3 μGals for the semiannual and annual components, respectively, where the true values are 5.025 μGals and 2.059 μGals for the respective components. The behavior of the estimated δ-factor are plotted in **Fig.** 21 as the function of the magnitude of the given steps. We observe a tendency in this figure that δ-factor is underestimated if the analysis data include a step. This may be due to the decreasing in correlation in the statistic structure between the observed data and the assumed model by increasing the magnitude of step-like change that was artificially added. Consequently, the analysis model (6.2) can not represent the data structure. From the test made here, it is estimated an uncertainty of about ±1 μGal in magnitude for the step corrections based on the daily medians. This error in the step correction may make an systematic error of the observed δ-factor for the polar motion effect of about 1 % at least.

8.4. Reanalysis of the Polar Motion Effect

The polar motion effect at Syowa Station was reanalyzed using much longer data in length than those used in the previous analysis. There is a possibility that the scale factor of the SG at Syowa Station changed during the three months from February to April, 1996 (Tamura et al., 1997). The most probable origin of this is the effect of change in an electronic potential caused by connecting the gravimeter electronics to an uninterrupted power supply for a test After the test for the three months, the interrupted power supply was disconnected from the observation system to back it to the previous state. The change in the scale factor is corrected for the data used in the analysis.

Referred to the experiences described in the sections 8.3.2 and 8.3.3, the analysis model (8.2) was revised so that it can reestimate the possible error in the step estimation based on the daily medians and it can simultaneously estimate the phase difference between the gravity data and the IERS data with other parameters. Thus the revised analysis model is

$$\begin{aligned} y(t) &= b_0 + b_1 t + b_2 \exp(-t/\tau) \\ &\quad + b_3 \sin(\varpi_1 t) + b_4 \cos(\varpi_1 t) + b_5 \sin(\varpi_2 t) + b_6 \cos(\varpi_2 t) \\ &\quad + b_7 (P(t) - b_8 \Delta P(t)) + \sum_{k=1}^{n} c_k H(t - t_k) \qquad (38). \end{aligned}$$

The unknown parameters to be estimated are 10+n of b_0, b_1, b_2, b_3, b_4, b_5, b_6,

b_7, b_8, τ and c_1 to c_n.The terms considered in equation (38) and their notations are similar as those for equation (37), but the treatment of two effects of the polar motion and steps are different from (37). Thus, in (38), $P(t)$ is not the time series data for the gravity changes which were generated directly by using equation (8.2) and the IERS polar motion data. Instead of this, the annual and semiannual components have already removed from the gravity changes predicted using the IERS data which have enough data length to separate the two of the annual and Chandler components. The method used to the separation is the same as that described in the section 8.1 Therefore, we believe that this time series consists mainly of the Chandler component. We assumed here also the value of 1.0 as the gravimetric factor δ. b_7 is the gravimetric factor to be estimated from the observation. $\Delta P(t)$ is the first time difference of $P(t)$ which is added to represent a time lag of the observed gravity $y(t)$ against $P(t)$ and b_8 is the coefficient of $\Delta P(t)$. A similar term has been used by Mukai(1999) to analyze SG data obtained at Kyoto, Japan. The last term represented with $H_n(t)$ and b_n is the Heaviside's step function and its amplitude, respectively. The Heaviside step functions were introduced to re-estimate the residual magnitude of the step like changes (offsets) which were not correctly estimated based on the method using the daily medians, which was described in the section 5.1. The fitting was also carrying out by the Levenberg-Marquardt method (Press et al., 1989).

For comparison, we also analyzed the data obtained from other two SGs installed at Esashi and Canberra. The geographical coordinates of the sites are listed in **Table** 12 with the data periods used in this study.

Table 12. The SG data used in this study.

Site	Latitude	Longitude	Altitude	SG	Analysis period (days)
Esashi	39.148°N	141.335°E	393 m	TT#007	1995.01-1999.04 (1337)
Canberra	35.321°S	149.008°E	724 m	CT#031	1997.01-1999.04 (776)
Syowa Station	69.006°S	39.586°E	24 m	TT#016	1993.03-1997.12 (1552)

note: TT and CT show the old type SG and the new compact one, respectively.

Figure 22 shows a comparison of the observed trends and the model values. From the top, they are the results for Esashi, Canberra and Syowa Station. Long interruptions are observed in the trends of Esashi and Syowa Station. These are mainly due to the trouble of observation instruments or the large local earthquakes (i.e. earthquakes within a few hundred kilometers in an epicentral distance and of the magnitude larger than or equal to IV in the seismic intensity listed in the table of Japan Meteorological Agency). The data of these periods were rejected from the analysis data. In general, a large step and long interruptions of the data occurred at these parts, and it is very difficult to correctly estimate the magnitude of this kind of steps from the daily medians. This is the reason why we included the term for step correction into the analysis mode. Although the observed data were affected by several disturbances, we recognize from **Fig.** 22 that the observed gravity changes are well represented by the analysis model given by the formula (38). The annual and semiannual components due to the EOP changes are obtained together with the effects of the tides, SSH variations and other perturbations. **Table** 13 gives the obtained parameters for the annual component with their formal errors which were estimated from the 1-σ error for the residuals. The phases are those referred to 00h UTC of January 1, 2000.

Table 13. The observed annual amplitudes and phases obtained at the three SG sites.

Site	Amplitude (μGals)	Error (μGals)	Phase (degrees)	Error (degrees)	SD (μGals)
Esashi	1.30	±0.11	-2.1	±6.5	1.09
Canberra	1.88	±0.09	-147.8	±7.0	0.32
Syowa Station	0.77	±0.08	31.2	±5.6	0.91

As described in the section 6.3.4, the accuracy of the correction for offsets affects on our results. We have introduced here a Heaviside step function into the analysis model in order to reexamine the magnitude which could not accurately estimated from the method using the differences of the daily medians. This method works well to reduce the error, especially, to improve the effect of such offsets accompanying long interruptions. For example, in the analysis of the data for Syowa Station, we have reestimated the six offsets with a total magnitude exceeding 30 μGals in the original data. Our analysis indicates that, compared with the data corrected for offsets using daily medians, the SD is improved using the step function in the fit by about 15 % (i.e. from ±1.05 μGals to ±0.91 μGals). Of course the ideal way to maintain the sensitivity and calibration of gravity record is by carrying out regular comparison observations with an absolute gravimeter at an accuracy of 1 μGals or better. In order to increase the accuracy of analysis for the annual and Chandler components, it is desirable to carry out such comparison observations twice a year at least.

8.5. Effect of SSH Variations on Gravity

In order to clarify the ocean effect on the gravity observations, the effect of SSH variations was estimated and compared with the observations made at the three sites. The computations were carried out based on the two kinds of SSH data. One is the POCM (Parallel Ocean Climate Model, Stammer et al., 1996). Other one is the TOPEX/POSEIDON altimeter data.

8.5.1. SSH and SST data

We used here a 3.2 year series of the POCM data which corresponds to the TOPEX/POSEIDON (T/P) repeat cycles 2-119 (October 17, 1992 to December 22, 1995). These data were provided by NPS (Naval Post Graduate School of USA). The POCM is a general circulation model for the ocean, and the data used here are from the recent POCM_4B version (Stammer et. al., 1996). This model covers the ocean regions between 0° and ±75° latitude. Although the SSH data from the model are given on a grid with a nominal lateral resolution of 1/4° in both latitude and longitude, we averaged the original data over 1°by 1° grid area. To estimate the steric effect in the SSH variations, we used the SST data which were used to drive the POCM (Tokmakian, 1998). This data was also provided by NPS.

For comparison, we carried out the computation with the T/P data which were also provided by NPS. The data used here are 'filtered T/P data' of 2° by 2° gird, which were smoothed by applying the spatial low-pass filter proposed by Shapiro(1970) in order to reduce stationary small scale sea surface fluctuations mainly related to geoid errors. In addition to the steric effect, the altimeter data are also affected by the sea surface pressure changes. The T/P data has therefore been corrected for the pressure effect using the inverse barometer (IB) hypothesis (Stammer, 1996). For the POCM data, it is not necessary to make any pressure correction because the model has been run assuming the sea surface free from static pressure changes. The sea surface may, however, be affected indirectly by the pressure changes through the wind stress.

8.5.2. Steric Coefficient and the Annual Field

The SSH variations include a signal which is due to the steric effect of the thermal expansion of the water column. This signal does not cause any significant gravity changes. Thus we need to apply a steric correction to estimate the gravity effect of the SSH variations. We estimated the steric coefficient $\alpha_{i,j}$ as a linear regression coefficient between the SSH and the SST by fitting following equation by means of the least squares method:

$$\Delta SSH(\theta_i, \lambda_j, t) = \alpha_{i,j} \Delta SST(\theta_i, \lambda_j, t) \qquad (39),$$

where θ_i and λ_i are co-latitude and longitude of each ocean grid; t is time of each data point; $\Delta SSH(\theta_i, \lambda_j, t)$ and $\Delta SST(\theta_i, \lambda_j, t)$ are the deviation parts of SSH and SST on each grid, obtained by subtracting their mean values.

From the fit based on the POCM SSH data, we have obtained values for $\alpha_{i,j}$ within the range from -1.30 $\times 10^{-2}$ m/°C to 1.58 $\times 10^{-2}$ m/°C. In order to see the characteristics in the spatial distribution of the obtained $\alpha_{i,j}$ values, we averaged them zonally over 10° wide belts across each ocean basin of the Pacific, Atlantic and Indian oceans. The averaged values vary between -0.06$\times 10^{-2}$ m/°C and 1.09$\times 10^{-2}$ m/°C. Low $\alpha_{i,j}$ values (0.2$\times 10^{-2}$ m/°C to 0.3$\times 10^{-2}$ m/°C) were found at high latitudes in both the northern and southern hemispheres. In low latitude regions within ±20°, $\alpha_{i,j}$ shows complex spatial variations and the averaged value ranges from -0.06$\times 10^{-2}$ m/°C to 1.09$\times 10^{-2}$ m/°C. In mid latitudes, ocean regions where strong western currents such as Kuroshio or the Gulf Stream flow also showed a complex spatial distribution of $\alpha_{i,j}$, but its variation was smaller and distributed around a value of 0.6$\times 10^{-2}$ m/°C. For the mid latitudes, the southern hemisphere region of the Pacific ocean showed relatively low mean $\alpha_{i,j}$ values (for example, 0.36$\times 10^{-2}$ m/°C at 40°S), compared with those for the northern hemisphere region (for example, 0.81×10^{-2} m/°C at 40°N), however, this tendency is not so clear in the Atlantic ocean. A similar latitudinal dependency of the mean $\alpha_{i,j}$ values mentioned above was obtained from the analysis using the T/P data except for the high latitude in the northern hemisphere (i.e. a value of about 0.5×10^{-2} m/°C for the T/P data).

The value of steric coefficient clearly varies with the location but as an approximation, we have evaluated an average coefficient $\alpha_{i,j}$ over the central regions of the Pacific and Atlantic oceans. We chose these regions for the following two reasons: (1) a reliable mean steric coefficient could be evaluated from the ocean regions where a high correlation between SST and SSH is observed, and (2) we avoid possible disturbance due to the effect of strong ocean currents. Consequently, we obtained a value of 0.60×10^{-2} m/°C from the POCM SSH data, and 0.52×10^{-2} m/°C from the T/P data. In what follows we adopt a value 0.60×10^{-2} m/°C to correct for the steric effect in both the POCM and T/P SSH data.

The EOFs (Empirical Orthogonal Functions) obtained by PCA (Principal Component Analysis, Preisendorfer and Mobely, 1988) indicate that the annual component is the dominant signal in both the SSH and SST variations. However, these data did not show a simple annual sinusoidal variation in time. Instead, they usually include an overtone of the annual period. Therefore, we evaluated the annual fields of the SSH and SST by applying an analysis model which consists of constant, linear, annual and semiannual terms, to each ocean grid. By considering the semiannual component in the analysis, we expect to reduce the estimation error of the annual component.

8.5.3. EOF of SSH Data

First, the EOFs were evaluated using the data for the steric heights estimated from the SST data and the original POCM SSH data which were not corrected for the steric effect in order to examine the characteristics in the time-spatial variations of these data. The obtained spatial patterns of the principal three modes are given in **Plates** 1 and 2 for the SST data represented with the term of steric height and the original POCM SSH data, respectively. As is to be expected, the most dominant signal in both the SST and SSH was the annual changes, and this signal appears clearly and commonly in the first modes which show a symmetrical spatial variation about the equator (see **Plates** 1a and 2a). For the SST, the temporal variations in the second mode consist of mainly two of the annual and semiannual components, however, the dominant signal in the third mode is a long-term behavior whose period is longer than 1 year. Different from the SST, the dominant period of temporal variations in SSH is 1 year for both the second and third modes. The contributions of the first, second and third modes to the total variations were estimated at 90.4 %, 2.9 % and 2.0 % for the SST and at 28.8 %, 17.9 % and 11.7 % for the SSH, respectively. Different from the SST, the first mode of the SSH has not an overwhelming large magnitude over the second and third modes. From these discrepancies in both the magnitude in contributions and dominant periods between the two data sets, the SSH variations are believed to be partially caused by the thermal effects, although it is evident that the effects of SST on the SSH are very large.

Next, based on the SSH data corrected for the steric effect, we re-evaluated the EOFs. **Plate** 3 shows the spatial distribution of the EOFs computed using the corrected POCM SSH data. From the top, the three principal components of the first, second and third modes are displayed. Among the features observed in the corrected EOFs compared with those shown in **Plate** 2, the notable points are: (1) in the first mode (**Plate** 3a), the strong symmetrical spatial pattern about the equator is moderated especially in the Pacific and Atlantic oceans, (2) in the second mode (**Plate** 3b), a symmetrical oscillation about the equator which is localized in the tropical regions is observed, and (3) in the third mode (**Plate** 3c), the ENSO (El Nino Southern Oscillation) like oscillation clearly appears. For the temporal variations, the periodic signal of 1 year is still a dominant signal of both the first and second modes. However, it is notable that a long-period trend of a bow like shape, which has a positive peak at about 600 days from September 28, 1992 (i.e. at around the mid of May, 1994), is the most dominant signal in the third mode, instead the 1 year period.

From the features mentioned above, we believe our steric correction works well to reduce the thermal steric effect including the SSH.

8.5.4. Calculation of The Gravity Effect

The gravity change due to the effect of SSH variations (i.e. each effect of attraction and loading) can be evaluated by convolving SSH data with a gravity Green's function over the whole ocean area. This computation has been carried out using a modified version of the computer program 'GOTIC'. In order to improve the accuracy of the topographic digital global maps, the 2nd order maps prepared for the original version of GOTIC were replaced with the 5'×5' 'ETOPO5' digital map (National Geophysical Data Center, 1988).

For modeling of SSH variations, it is very difficult to realize the condition for a conservation of the ocean mass rigorously because to do so we need to take into account all of the hydrologic cycle over the oceans such as density profiles and temperature variation in the water column, for example. Therefore, instead of mass conservation, POCM is constrained so that the total volume of the oceans is conserved (Tokumakian, 1998). Following this procedure, we forced both the data of POCM and T/P to conserve their volumes by adjusting the mean SSH height over all ocean grids. Thus we estimated an ocean height which is obtained by averaging the SSH data of each day over the whole ocean grids, and subtracted it uniformly from the SSH data of each grid. Because the original POCM fields have been already conserved their volume, the volume adjustment may be needed not to do any more. But, since the steric field does not conserve its volume, we applied the correction for unconserved volume to the POCM data, too. Different from the case of the modeling of ocean tides, the magnitude of the correction value can vary every day. Last, the value of 1.025×10^{-3} kg/m^3 was adopted for sea water density throughout the whole ocean.

8.6. Results and Discussions

8.6.1. Spatial Distribution of Steric Coefficient and Annual SSH Variations

Figure 23 compares the latitudinal variations in the annual amplitude of the POCM SSH and SST averaged over latitude belts of 1° width. From **Fig.** 23, we can see some of the characteristics in the spatial distribution of $\alpha_{i,j}$ described in the section 8.6.2. Thus, this figure clearly shows the low coherence in the low latitude zones and the high coherence in the mid latitude zones. Moreover, it suggests that the high SSH amplitude in the region around 10°N to 20°N may not be due to the effect of SST, because the annual amplitude of SST at there is very small compared with other latitude zones.

Plate 4 shows the spatial distributions of the annual amplitude and annual phase evaluated from the POCM SSH data. Three kinds of the amplitude and phase fields are displayed in **Plate** 4. From the top, they are for the original SSH, the steric component and the SSH corrected for the steric effect, respectively. The amplitude and phase fields are displayed in **Plates** 4a, 4c and 4e and in **Plates** 2b and 2d, 2f, respectively.

From the comparison of the amplitude field shown in **Plate** 2a with that in **Plates** 2e, it is clear that the large high amplitude zone in the central parts of both the Pacific and Atlantic oceans in the northern hemisphere (i.e. the area roughly spanning 20°N to 50°N and 150°E to195°E) is significantly reduced by correcting for the steric effect. We also observe a similar tendency in the southern hemisphere mid latitude regions in both the Pacific and Atlantic oceans, although the degree of changes is small compared with the northern hemisphere. In contrast to this, amplitude changes from the steric correction are not clear in either the Indian ocean or low latitude regions of the Pacific and Atlantic oceans. This is a result of the low coherency between SSH and SST in these regions, as seen in **Fig.** 23. **Plate** 4c and 4e also indicate that the SST is not the dominant source of the annual SSH change there.

From the comparison between the uncorrected SSH amplitude (**Plate** 4a) and the corrected one (**Plate** 4e), it is apparent that the large extent of high amplitude regions accompanying the two western boundary currents (i.e. Kuroshio and Gulf Stream) is substantially reduced by correcting for the steric effect. However, the steric correction is not so effective on the circumpolar current in the southern high latitude ocean region. On the other hand, we observe an effect of over-correction in the north high latitude regions. As described in the section 3.2, in the north high latitude regions, we have obtained a small mean value for steric coefficient (i.e. about 0.25×10^{-2} m/°C) compared with 0.60×10^{-2} m/°C used here for the correction. The mean amplitude of annual SST changes in that latitude zone is not so small (see **Fig.** 23). This effect is also observed at the northern part of Bering sea or that of Sea of Okhotsk (i.e. a high amplitude region in this case), for example.

Stammar(1997) presents images similar to **Plate** 4, which have been obtained from the 3-year T/P data from repeat cycles 7 through 116 (see **Plate** 6 of his paper). The steric field shown by him, which was computed by integrating the sea surface heat fluxes in time, is more rigorous than that obtained here from only the simple temporal correlation between the SSH and SST fields.

However, the two SSH fields corrected for the steric effect show very similar spacial variations in amplitude. This may be important for practical application to gravity observations when only the SST data are available for the steric correction. For the phase, it is not easy to visibly inspect the difference between Stammer's figures and ours due to the difference in the analysis epoch used. But two computation results by him and us give also similar features in the steric fields. Recently, Leuliette and Wahr (1999) have investigated the time-space coherence between the T/P SSH fields and the SST fields prepared by NCEP (National Centers for Environmental Prediction of USA) by means of a modified EOF analysis called 'coupled mode analysis' (Bretherton et al., 1992), and found that the Indian ocean basin as well as basins at low latitudes have a distinctly different character in the correlation between SSH and SST compared with that in the Pacific and Atlantic basins described above (see their **Fig.** 4 and **Table** 2).

8.6.2. Computation of the Annual Gravity Changes

Plate 5 shows comparison between the variabilities of the annual gravity changes on land, which were respectively estimated from the POCM SSH data uncorrected (**Plate** 5a) and corrected (**Plate** 5b) for the steric effect. 0.60×10^{-2} m/°C was used for the correction. The data are averaged with the grid system of $5°\times5°$. We can see in **Plate** 5a that, in the places close to the oceans, the annual amplitude exceeds the magnitude of 1 μGals and reaches to 1.5 μGals, however, at the most of inland places, it is less than 0.5 μGals in magnitude. While, **Plate** 5b indicates that most of the high amplitude areas (i.e. at where the variance is larger than 1.5 μGals) are removed by correcting for the steric effect. From **Plate** 5b, it is concluded that, except for the coastal or island observation sites, the gravity effect induced by the annual SSH changes is less than 0.5 μGals in amplitude at most inland sites in the world.

Figure 24 shows the comparison between the observed and predicted annual components at the three observation sites, Esashi, Canberra and Syowa Station, respectively. This kind of plot is frequently called ' phasor plot' in the tidal study. The horizontal and vertical axes show the cosine-term and sine term, respectively. Thus, the amplitude is represented by the length of vector and the phase angle as its angle measured from the cosine axis, counter clockwise for a lag. The phases of all vectors shown in this figure are referred to the epoch at 00 h UTC of January 1, 2000. Four effects, the solid tide, ocean tide, polar motion and SSH were used here to estimate the predicted vectors. In **Fig.** 24, the solid tide vectors for the Sa wave were evaluated using Tamura's tidal potential (Tamura, 1987) assuming values of 1.155 and 0.0° as nominal values of the gravity tidal factor and phase lag for the long-period tides, respectively. The ocean tide vectors were evaluated from the global ocean tide model for the Sa wave which was computed by Takanezawa (1998) based on integrating the hydrodynamic equation without assimilating any observed data. The vectors of the annual polar motion effect were evaluated by equation (1) using the amplitude and phase of the annual polar motion effects which were obtained from the IERS EOP data for the 16 year period from 1983 to 1998. A value of 1.155 was also assumed as an amplitude factor. The SSH vectors inferred from the POCM SSH data are illustrated in **Fig.** 24. Three vectors are shown in the figure, differing in the magnitude of steric coefficient used for the correction.

As seen in **Fig.** 24, the effects of both the solid and ocean tides on the Sa wave are very small at Esashi and Canberra located in mid latitudes, but the effect of solid tide is not so small at Syowa Station. The amplitudes at Esashi, Canberra and Syowa Station are 0.109, 0.000 and 0.926 μGals for the solid tide and 0.002, 0.003 and 0.070 μGals for the ocean tide, respectively. In contrast to this, the magnitude of the annual polar motion effect is up to 1.73 μGals at Canberra. **Fig.** 24 also shows that the SSH variations cannot be ignored if gravity observations are made at an accuracy of better than 1 μGal, though the effects of solid tide and polar motion are the dominant part, . As clearly seen in the case of Esashi, an important point for the SSH effect is that its estimation is strongly affected by the magnitude of the steric coefficient used in the computation. As a test, we have compared here three cases respectively used three values for the steric coefficient, i.e. the three of 0.0×10^{-2} m/°C, 0.60×10^{-2} m/°C and 1.0×10^{-2} m/°C. The first case corresponds to no steric effect (the yellow vectors), the second is the preferred value estimated from the POCM SSH and SST data above (the blue vectors), and the last is a test value for comparison (the pink vectors).

Among the three sites, the SSH vectors of Esashi have the largest amplitude and show a large difference in both the amplitude and phase by different values of the steric coefficient. The amplitude of SSH variations is large around Japan (see **Plate** 4a and 4e) and the distance from the sea at Esashi relatively small (about 40 km). These factors may contribute to the large amplitude there. Adding to this is the complex spatial distribution of annual phase in the ocean region around Japan mainly caused by such strong ocean current as Kuroshio (see **Plate** 4b and 4f). This may also contribute to the difference among the estimated SSH vectors because, due to the nature of both the Green's functions for the attraction and loading, the gravity effect from each ocean mesh is not simply proportional to its loading distance. The observation at Canberra in mid latitude also indicates the similar results with those for Esashi. For Syowa Station, however, it is more difficult to judge which steric coefficient of 0.60×10^{-2} m/°C or 1.0×10^{-2} m/°C is favored by the observation. At least, we can say that the SSH vector estimated by ignoring the steric effect shows the largest discrepancy in the phase. For this site, we must note that (1) the observation is affected by the maintenance works made at a frequency of about twice a year as described in the sections 4.4 and 5.1, (2) the observation site is very close to sea (i.e. within 0.5 km) and (3) the value of 0.60×10^{-2} m/°C that was determined for the seas in mid latitude may be not suitable for the steric coefficient of the sea around Syowa Station, which is in high latitude. Related with (2) and (3), the ETOPO5 digital map used here and the SSH data in high latitude may be not enough to estimate the effect at Syowa Station accurately. Further investigation is needed for this site.

For comparison, we have also evaluated a phasor plot similar to **Fig.** 24 using SSH vectors derived from the T/P data, and it is shown in **Fig.** 25. Because the Syowa Station is located at 69°S latitude, beyond the ±66° limit of the T/P data, we extrapolated SSH variations for a few degrees into the area around Syowa Station from the nearby oceans by means of a spline method. The results from the T/P data indicate a very similar dependence on the magnitude of the steric coefficients used in the computation. At Esashi, for example, both the amplitude and phase of the SSH vector obtained using 0.60×10^{-2} m/°C are intermediate in magnitude between those obtained using 0.0×10^{-2} m/°C and 1.0×10^{-2} m/°C. However, compared with the vectors estimated from the POCM data, the amplitudes estimated from the T/P data are systematically small by about 10 % to 40% and the phases also show a systematic difference of about 20° in the sense of advance. It is noting that Canberra in mid latitude also indicates the similar tendency as seen in Esashi. We suspect that these differences may be mainly due to the coarseness in spatial resolution of the T/P which was averaged over 2° by 2° grid cells. In general, the ocean region up to 30° to 40° distant has the dominant effect on a gravity observation at a site near the oceans (approximately 80 % to 90 % of the total oceanic effect). Of cause, this percent is changed by several factors as described above. For example, in the case of the gravity effect of the M2 ocean tide on the Esashi observation, it is known that the loading in the ocean region less than 20° supplies the contribution more than 80 % (Sato and Hanada, 1984). Therefore, an SSH field with a spatial resolution of 1° by 1° or better may be necessary to explain the observed SSH effect to an accuracy at 0.1 μGals level for some observation sites near the seas.

Although there exist some systematic differences between the estimations from the POCM and those from the T/P and Syowa Station is affected by the local problems, **Fig.** 24 and 25 show that the agreement between the observation and prediction is excellent for the mid latitude sites. The present results indicate that we can reproduce the observed annual gravity changes at the accuracy of the order of 0.1 μGals. It is worth noting that the observations favor a steric coefficient of 0.60×10^{-2} m/°C. This means that the gravity observations made in the mid latitudes support the steric coefficient which was independently estimated from the SSH and SST data in the mid latitude ocean regions. We will discuss the observational errors for the annual component from the point of view of the correlation among the model parameters in the section 8.7.5.

8.6.3. Effect of Correction for Ocean Volume

As described in the section 6.7.3, we have applied the correction for the ocean volume to the SSH data in order to avoid a possible computation error which is caused by the unconserved ocean volume (i.e. correction for volume conservation). Importances of this correction are: (1) for most observation sites on land, the correction gives a similar effect in magnitude, and (2) the magnitude of the correction is not so much small compared with that of estimated gravity effect, (3) this correction makes a systematic error in both the estimations of amplitude and phase. For example, for (1), the variation of 1×10^{-3} m in an uniform ocean height (i.e. here the thickness of the unconserved sheet mass to be subtracted from the SSH data) makes an estimation error of 0.052 μGals, 0.045 μGals and 0.045 μGals at Esashi, Canberra and Syowa Station, respectively. As an example at a mid continent, we also computed the effect at 45°N and

90°E (i.e. near the west end of the Altai Mountains in Mongolia), and obtained a value of 0.027 μGals. In our case using the SST data for the 3.2 years, the range of the temporal variations of the unconserved steric height is about 2 $\times 10^{-3}$ m in peak-to-peak magnitude. This makes an error of about 0.1 μGals in our gravity estimation using the POCM SSH data, if the volume correction has been ignored. As seen in **Fig.** 24 or 25, the amplitude of the most favorable annual SSH vector at Esashi is about 0.4 μGals in magnitude, and the error of 0.1 μGals corresponds to 24 % of the estimated annual amplitude. It is sure that all of this magnitude does not straightly reflect to the estimated annual amplitude but it is also evident that treatment of the ocean volume gives a significant effect.

Compared **Fig.** 25 with **Fig.** 24, the annual SSH vectors evaluated from the T/P data show the systematic differences with those from the POCM data in both the amplitude and phase. We have discussed some possibilities of this difference in the previous section. In addition to these, there is a possibility that the atmospheric pressure correction applied to the T/P data assuming the IB hypothesis may be also an error source. Because the error in the estimation of the spatial mean pressure over the ocean has the similar effect with the correction for ocean volume and this kind of correction is one of the candidates which can make a common error on the estimations at the three observation sites considered here. The changes in the mean pressure themselves do not affect on the pressure response of the actual ocean as a consequence of volume conservation in the ocean (Wunsh and Stammer, 1997), however, the error of the mean pressure load applied to the T/P data does contribute to our gravity estimation. It is known that the spatial mean over the ocean has a dominant periodic component of 1 year and of about 1.2 hPa in amplitude, but the accuracy of the estimated amplitude is not known well (Wunsh and Stammer, 1997). According to their estimation, the standard deviation of the curve of the mean pressure changes is about 0.54 hPa in magnitude. The error of 0.54 hPa (i.e. 5.4×10^{-3} m in height change of the ocean) corresponds to an estimation error of about 0.26 μGals at Esashi at the most. Further study inclusive of the problem on volume conservation is needed in order to clear the meanings of the difference between the two SSH data shown here.

8.6.4. Statistic Error for the Observed Annual Component

The formal errors (i.e. internal error) of the annual components listed in **Table** 13 are the 1-σ error estimated from the standard deviation (SD) of the residuals after fitting the data to equation (2). However, the magnitude of the errors, which were derived from a linearized least squares fit, may be somewhat optimistic from the point of view of the correlation among the unknown parameters. As seen in **Fig.** 24, the observed annual vectors favor the SSH vectors computed using a steric coefficient of 0.60×10^{-2} m/°C. In order to verify this statement, we examined the confidence interval of the observed annual vectors based on Monte Carlo simulation. Since the effect of SSH variations at the Esashi site is largest among the three sites, we describe here the results for Esashi.

As a test, we generated the 1000 hypothetical data sets by adding Gaussian random errors to each data point of a model time series which was computed using the optimum parameter values and equation (2). The variance of the added noise is the same as that observed at Esashi and the data length of each hypothetical data set is the same as that of the observed data. However, in the simulation we did not include the step-like changes (offsets) sometimes seen in the actual data. The correlation matrix indicates that the annual component shows a relatively high correlation (i.e. 30 % to 50 %) with the Chandler component and some of the offsets. Moreover, the correlation between the cosine-term and the amplitude factor of the Chandler component (i.e. b_3 and

b_7 in equation (2)) is higher than that with the time delay (i.e. b_8). These are considered to be due to the interference problem between the two components of the annual and Chandler. We, therefore, estimated here the confidence interval of the annual amplitude from the distribution in the two dimensional parameter space $b_3 - b_7$. For the same reason, the confidence interval of the phase was estimated from the distribution in $b_4 - b_8$ space (i.e. the sine term of annual component and the time lag of Chandler component). **Figure** 26 shows the correlation in the $b_4 - b_8$ space (top) and that in the $b_3 - b_7$ space (bottom). In this figure, the mean value of each parameter (i.e. expected value used in the simulation) is subtracted in this figure. The simulation suggests that, at the 90 % confidence level, the confidence intervals of b_3 and b_4 are at ±0.21 μGals and ±0.14 μGals, respectively. Using these values, we obtain a range of 1.09 μGals to 1.52 μGals and -9.7° to 4.9° for the observed amplitude (1.30 μGals) and phase (-2.1°), respectively. Comparing these confidence intervals with the difference between the observed vector and the three predicted vectors in **Fig.** 24, we see that, even with the correlation of the parameters taken into account, our observation still prefers the SSH vector estimated from the steric coefficient of around 0.60×10^{-2} m/°C rather than other two values, when we use the POCM SSH data for the estimation.

Leuliette and Wahr (1999) considered the coupled coefficients of the principal first mode for the seasonal SSH and SST variations in the Pacific and Atlantic basins. Based on the T/P SSH data and NCEP SST data of about 5 years in length, they obtained values of 0.79×10^{-2} m/°C and 0.94×10^{-2} m/°C for Pacific and Atlantic, respectively (see their **Table** 2). The values of 0.60×10^{-2} m/°C or 0.52×10^{-2} m/°C, which are estimated here from the POCM and from the T/P respectively, are about 40 % lower than their values. It is not easy to identify the reasons for the difference in the magnitude of steric coefficient between the two estimations, since there are great differences in the analysis method and data length used in each study. Moreover there is a difference in the exact sea regions which are used in each computation. However, the difference may be significant. Our value is clearly preferred by the actual gravity observations, especially by those made at the mid latitude sites, but the SSH vectors estimated from the T/P data are systematically small compared with those estimated from the POCM data. Therefore, the different values for the steric coefficient may point to a way of improving our knowledge of the effect of SSH variations on gravity by further studying the relation among the gravity, POCM and T/P data. On the other hand, in order to clear the differences between the estimations from the POCM and T/P, it is also needed to analyze the data obtained at other SG sites and to compare with the results obtained here.

8.6.5. Effect of the Sea Ice

As an error source in the estimation of the ocean tide effect on the SG observation at Syowa Station, which is not experienced in the observation made at the mid latitudes, we may point out the effect of the sea ice. Lutzo Holm Bay surrounding Ongul Islands is covered with sea ice year-round. The thickness of the sea ice reaches to about 2 m at maximum. We included the observed ocean tides at Syowa Station with the ocean bottom pressure gage (OBPG) in order to improve the accuracy of the correction for the ocean tides. Sato et al. (1995b) examine the effect of sea ice on the tides measured with OBPG.

According to the observation by Sato et al.(1995b), there is a clear seasonal variation in the amplitude ratio between the variations in the sea ice height and the pressure changes observed with BPG. They suspect the seasonal variation in the sea water density around BPG (or in the bay), because the hardness of the sea ice and its thickness becomes significantly weak and thin in the summer season. We suspect that the state of sea ice might affect on the hydrodynamics in the sea of Lutzo Holm Bay through the changes in the surface friction to the tidal current as a boundary condition. This problem is still opened to study, but it is needed further study for this sea ice effect on the ocean tide, especially on the seasonal variation of the SSH at around Ongul Island. Recently, Aoki (2000, personal communication) carried out the measurement of the vertical motion of sea ice at the similar position where Sato et al. (1995b) done with a GPS (Global Positioning System) receiver, and obtained a result that the actual changes in the sea water density including the sea ice affect on the tidal amplitude observed by the BPG.

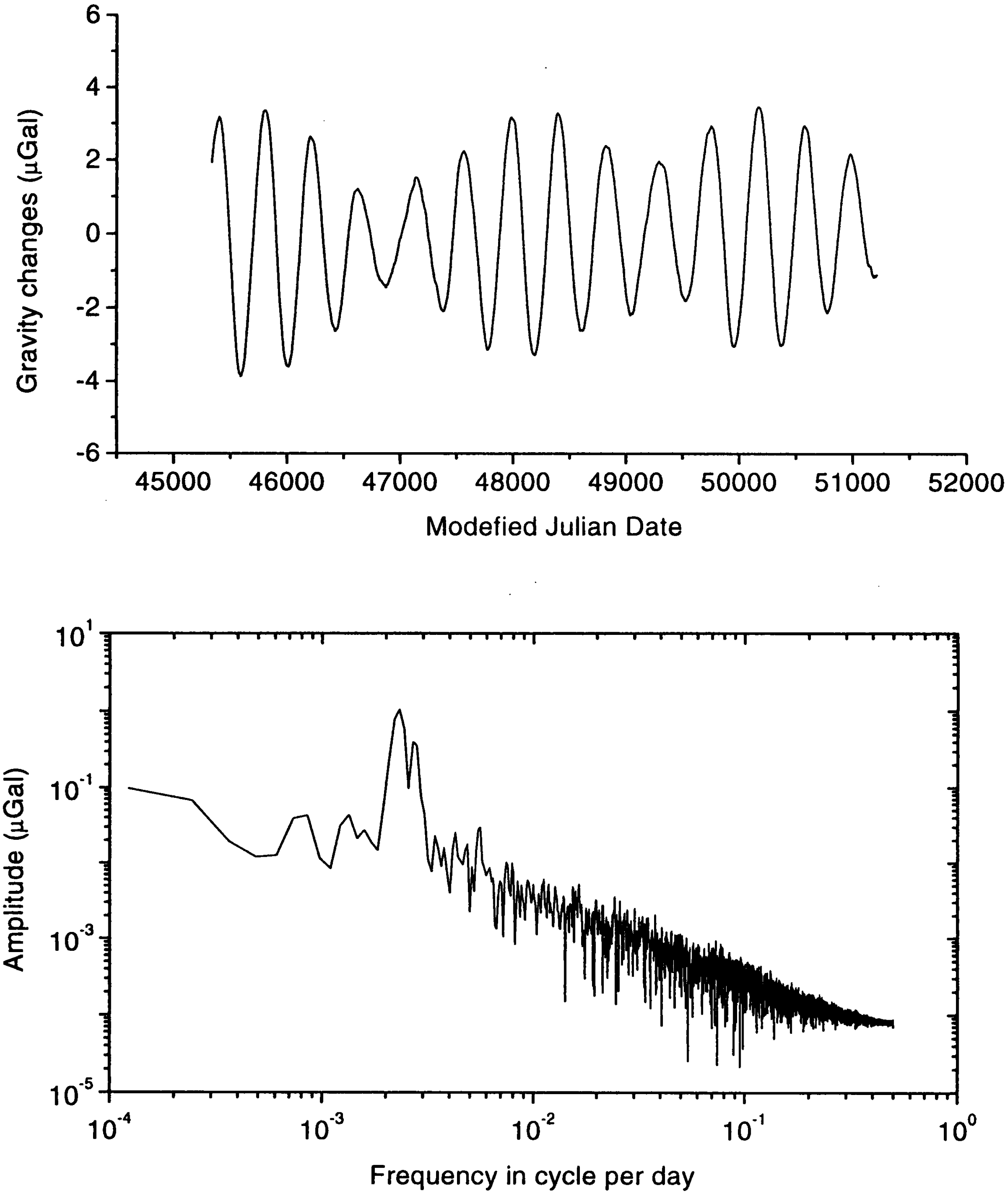

Fig. 17. Polar motion effect at Syowa Station. top: time variation in gravity changes for the period of about 17 years from January, 1983 to May, 1999. The computation was carried out using EOPC04 data of IERS by assuming the δ-factor of 1.155 as a nominal value. bottom: amplitude spectrum estimated from data shown in the above.

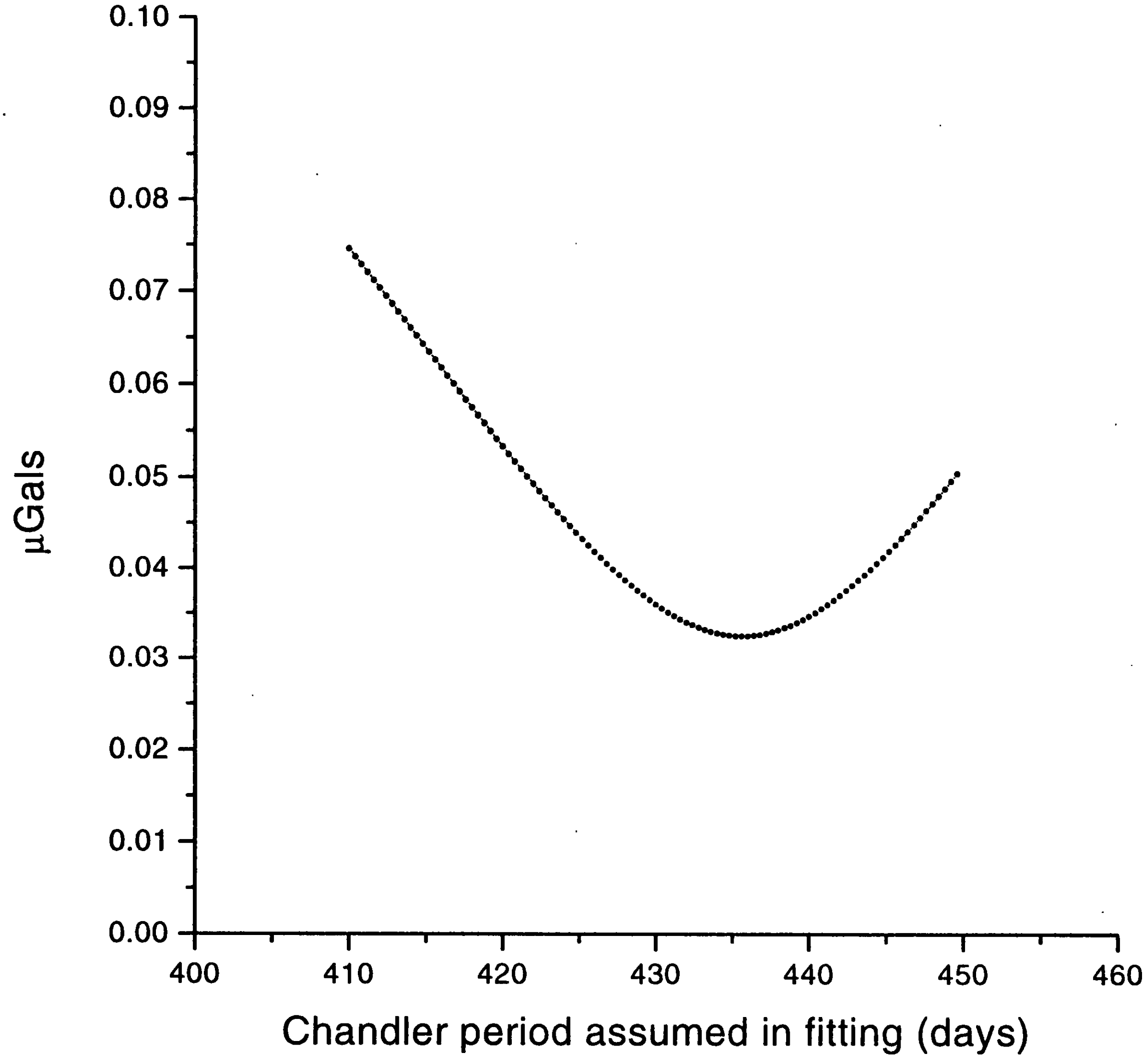

Fig. 18. Changes of standard deviations against to the Chandler period assumed in the analysis. The EOP data for the period from 1993 to 1999 were used for the analysis. This graph shows that the standard deviations take its minimum value at around the period of 435 days as expected.

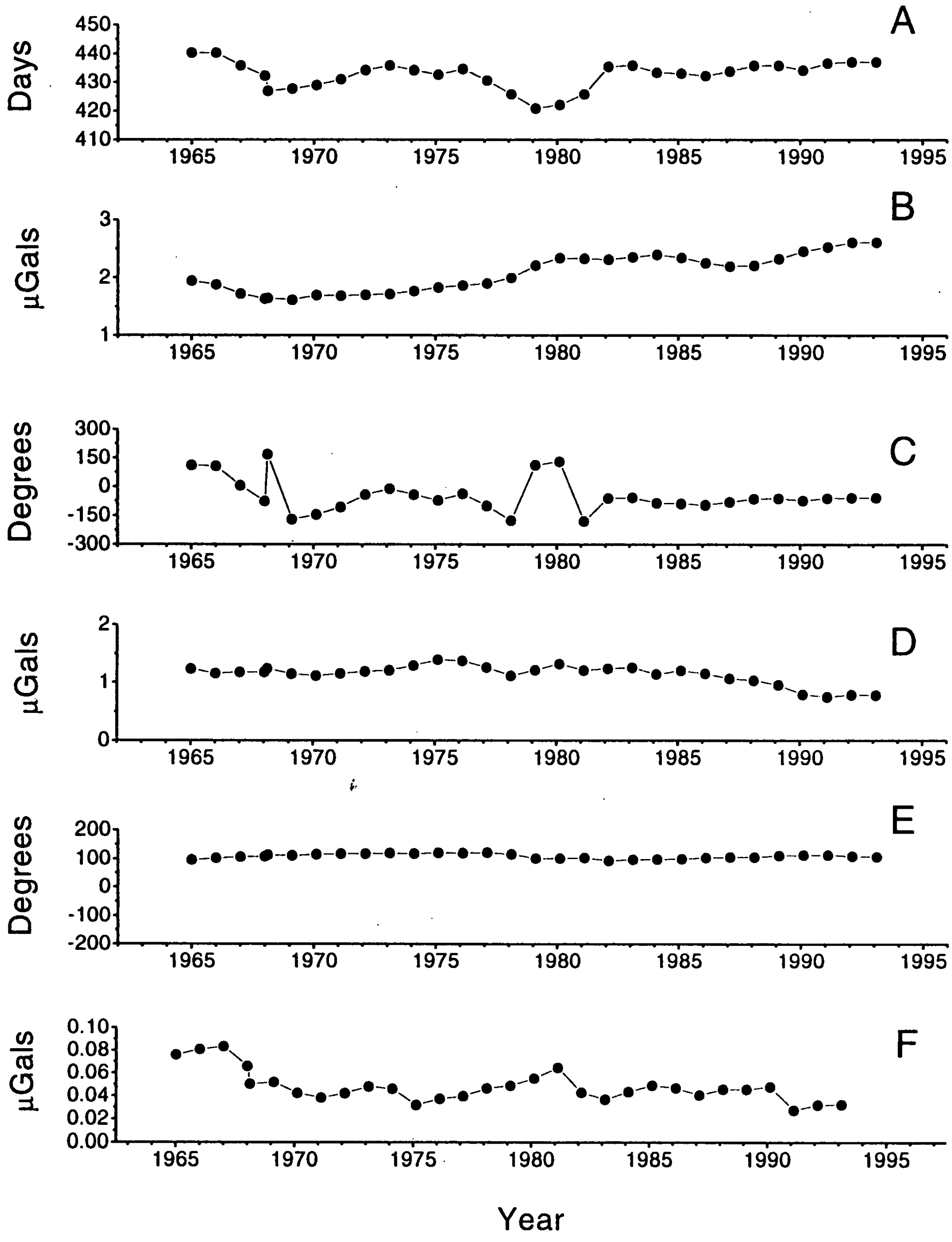

Fig. 19. Temporal variation in the polar motion effect at Syowa Station. From the top: A: Chandler period, B: amplitude of the Candler component; C: its phase; D: amplitude of the annual component; E: its phase; F: standard deviation of the residuals. These figures are obtained from the anlaysis using the 38-years IERS polar motion data by successively shifting the analysis epoch by 1 year. The data span is 6 years in length for each analysis.

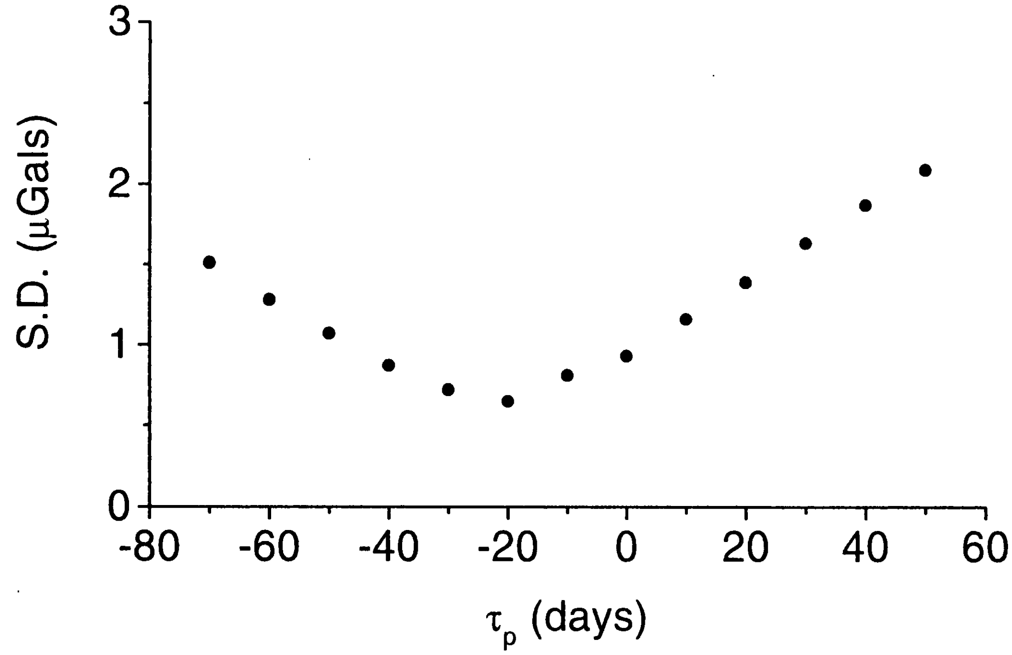

Fig. 20. Changes of the standard deviations of residuals by the time difference τ_p assusmed in the analysis that is based on the equation (37) shown in the txt.

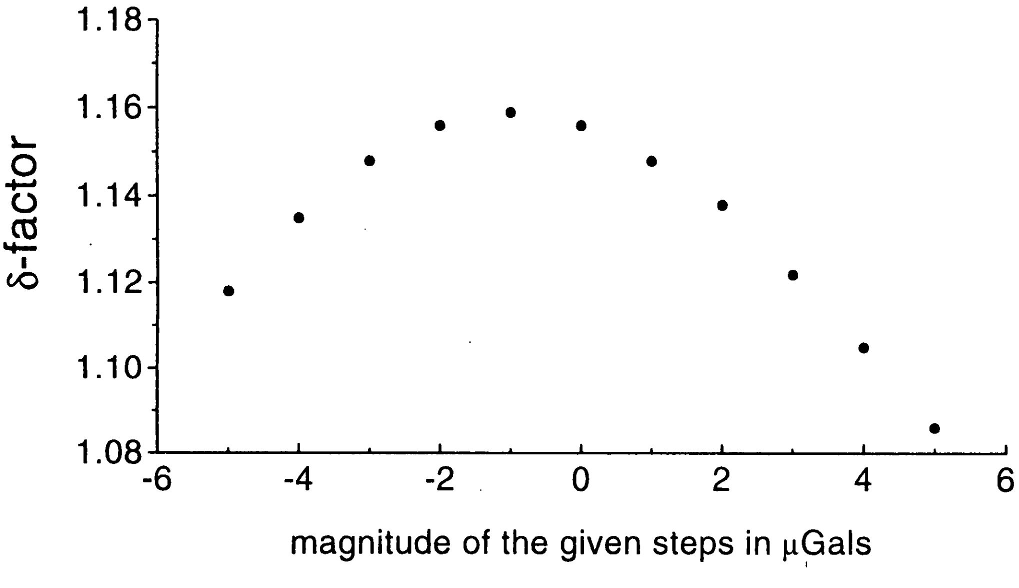

Fig. 21. Dependency of the estimated δ-factor on the magnitude of the given steps.

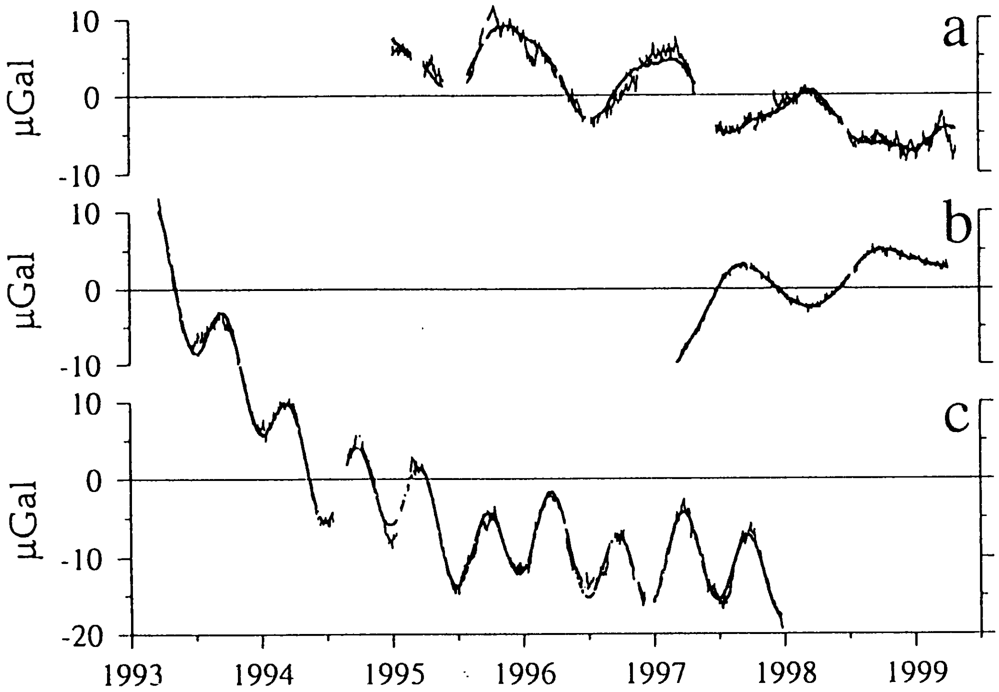

Fig. 22. The observed daily trends and the results for fitting. Equation (38) shown in the text is used for fitting. From the top, a, b, c are the results for Esashi, Canberra and Syowa Station, respectively. The zigzag lines show the observed daily trends and the smooth lines show the fitted curve. In the case a (Canberra), the two kinds of the curves are not clearly identified with the scale of this figure.

a: 1st mode

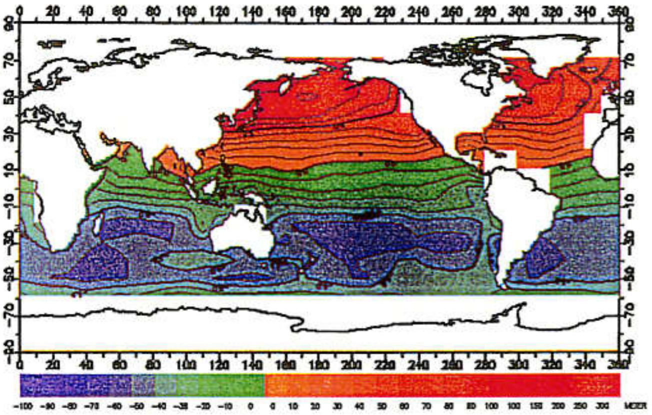

b: 2nd mode

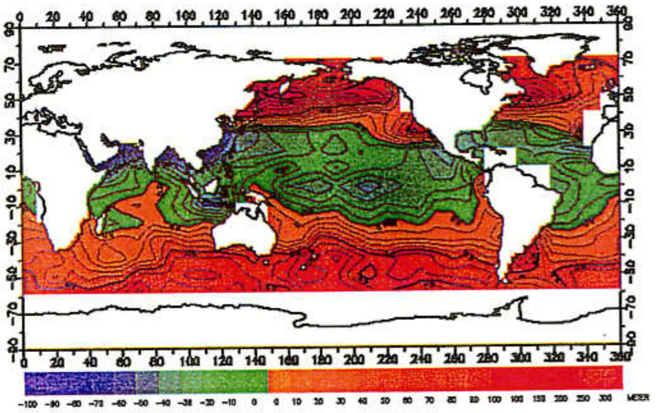

c: 3rd mode

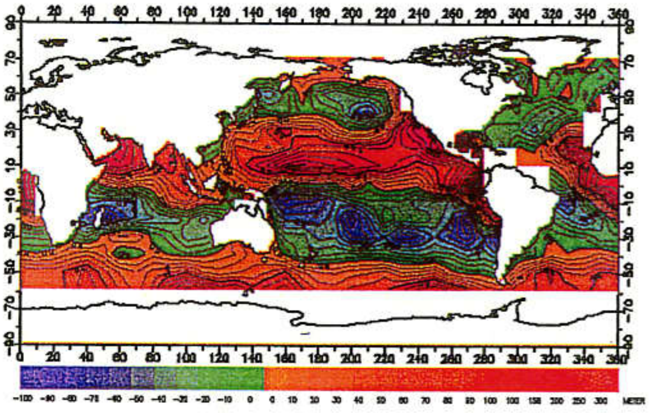

Plate 1. EOFs (Empirical Orthogonal Functions) of the SST data. This figure draws the SST variations converted to the thermal steric variations which were computed using the constant coefficient of 0.60E-2 m/degree, therefore, the color scale is given in unit of meter. From the top, the first, second and third modes of the principal components are displayed in Plate 1a, Plate 1b and Plate 1c, respectively.

a: 1st mode

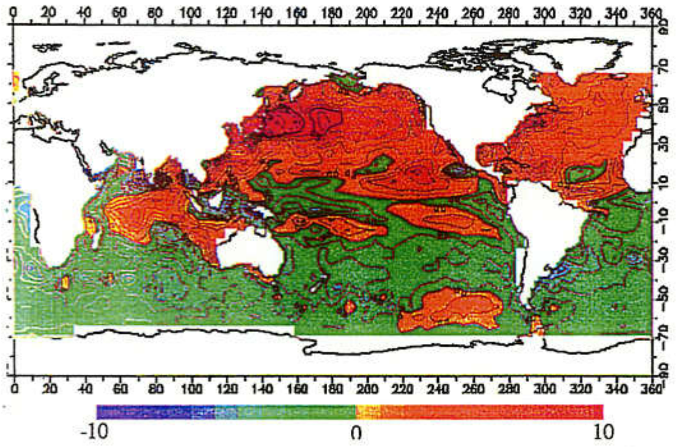

b: 2nd mode

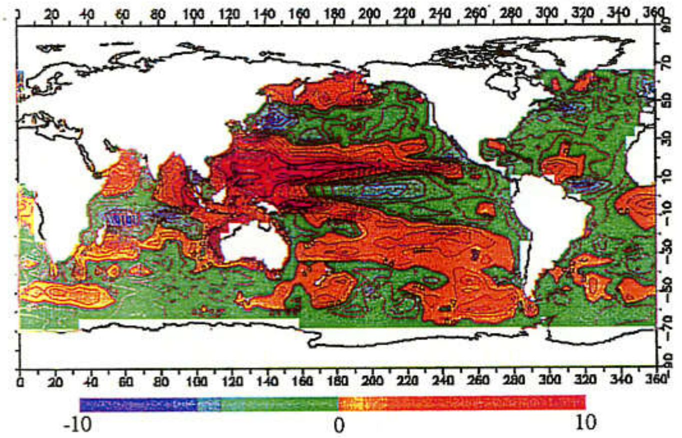

c: 3rd mode

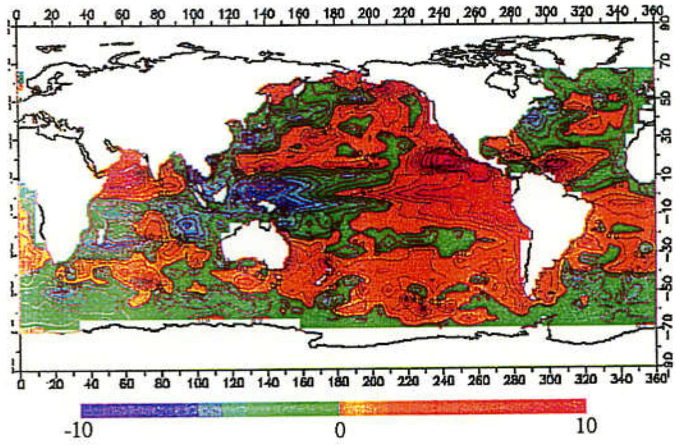

Plate 2. EOFs evaluated from the POCM SSH data without correcting for the steric component. From the top, the first, second and third modes of the principal components are displayed in Plate 2a, Plate 2b and Plate 2c, respectively.

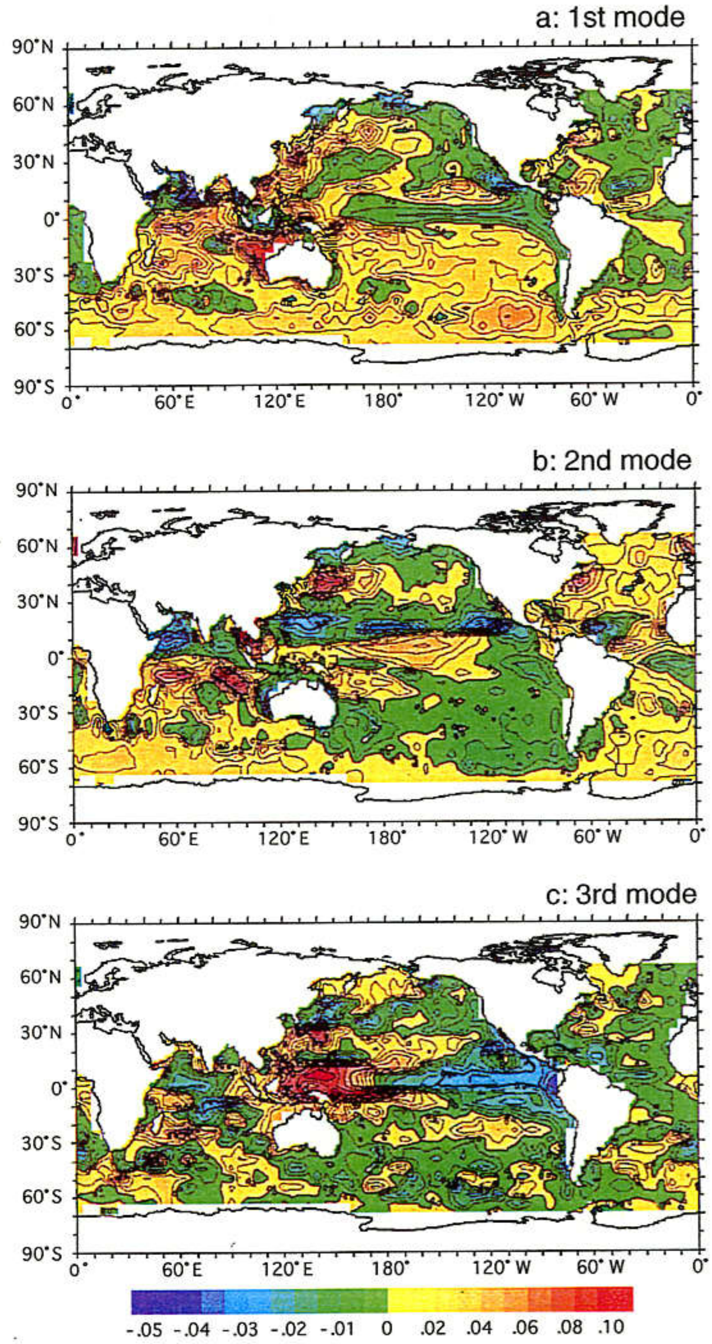

Plate 3. Similar plate as Plate 2, but the POCM SSH data corrected for the steric effect using the coefficient of 0.60E-2 m/degree. From the top, the first, second and third modes of the principal components are displayed in Plate 3a, Plate 3b and Plate 3c, respectively.

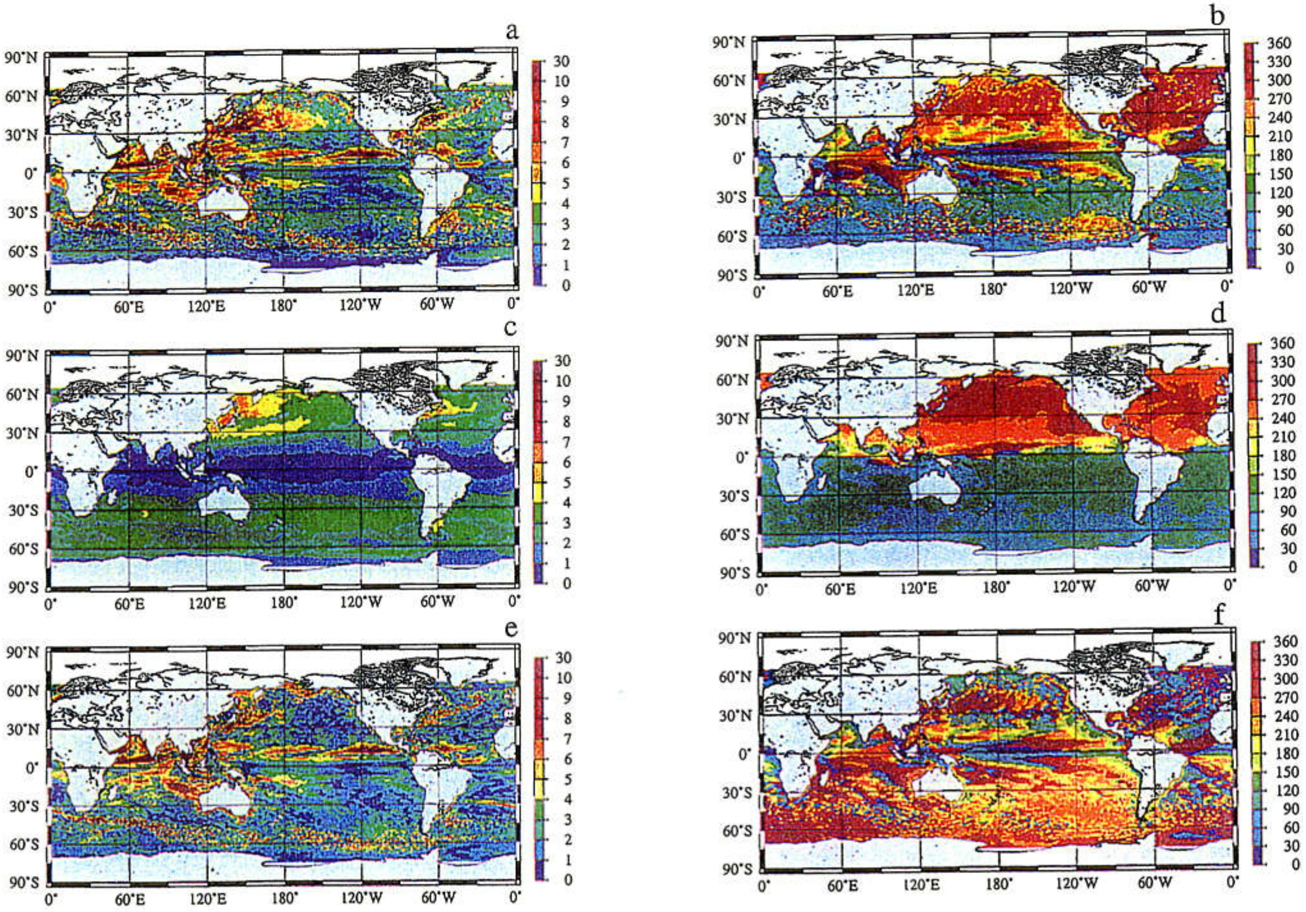

Plate 4. **Amplitude and phase of the annual SSH fields evaluated from the POCM SSH and SST data. Three fields are displayed: from the top, the original field, the steric field and the field corrected for the steric effect. The coefficient of 0.60E-2 m/deg was used for the correction. The amplitude fields are shown in Plate 4a, Plate 4c and Plate 4e in the order of the original, steric and corrected fields, respectively. The phase fields are shown in Plate 4b, Plate 4d and Plate 4f in the same order. The units of color bars are in 1E-2 m for the amplitude and in degree of arc for the phase.**

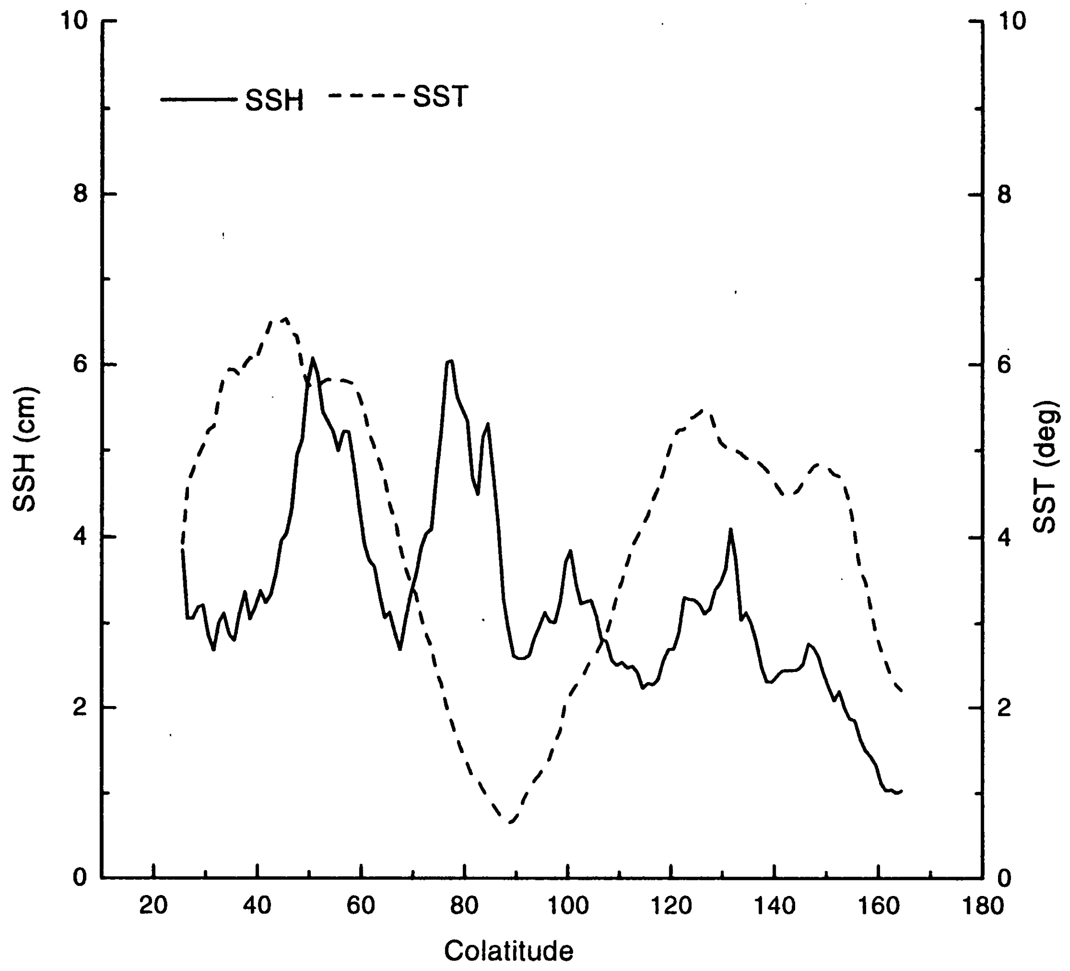

Fig. 23. Latitude dependency of the zonal averaged annual amplitudes of the POCM SSH and SST data. These show the mean values averaged over each latitude belt of 1.0 degree in width. Solid and broken lines show the averages of the POCM SSH and SST data, respectively.

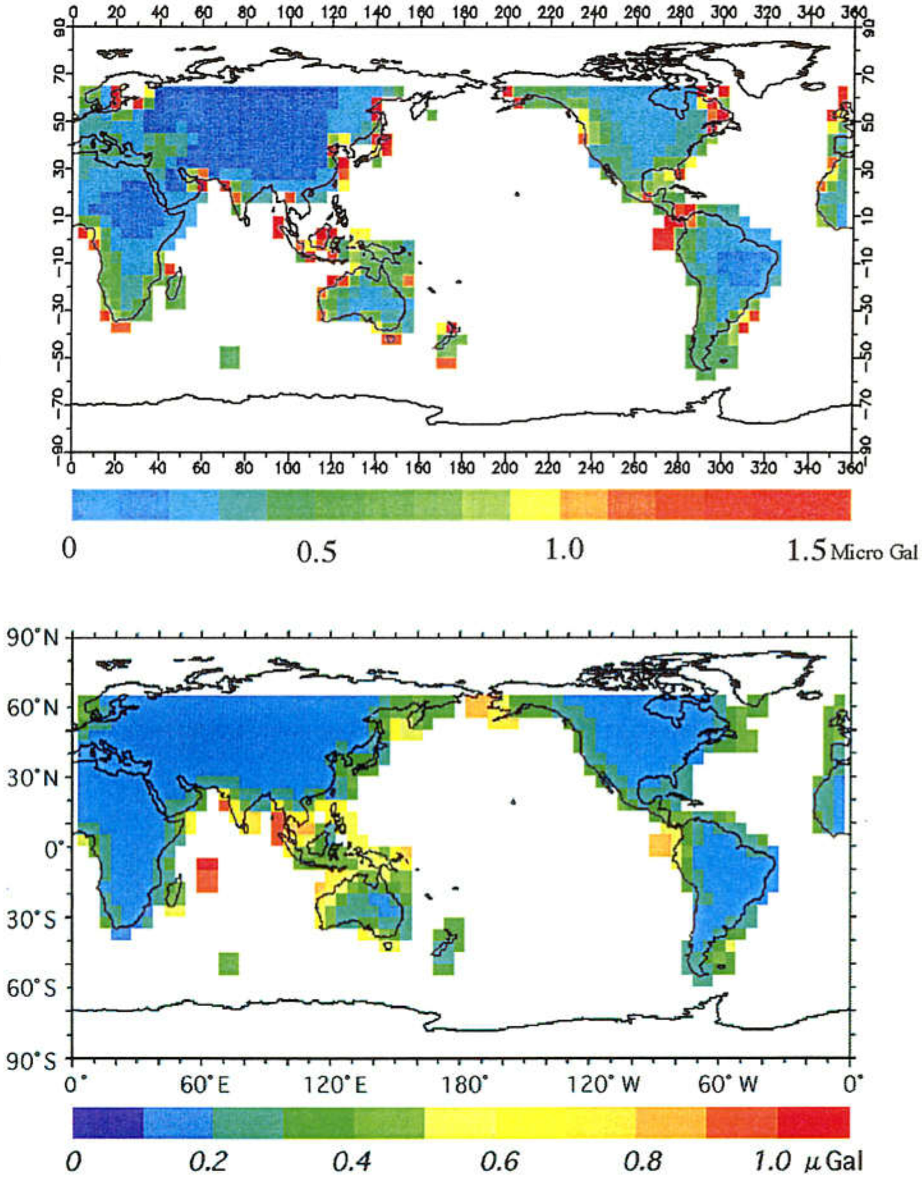

Plate 5. Variability of the annual gravity changes induced by the SSH variations. The variabilities were computed based on the POCM SSH data. Top: valiability computed using the SSH data without correcting for the steric effect. Bottom: that corrected for the steric effect using the coefficient of 0.60E-2 m/degree.

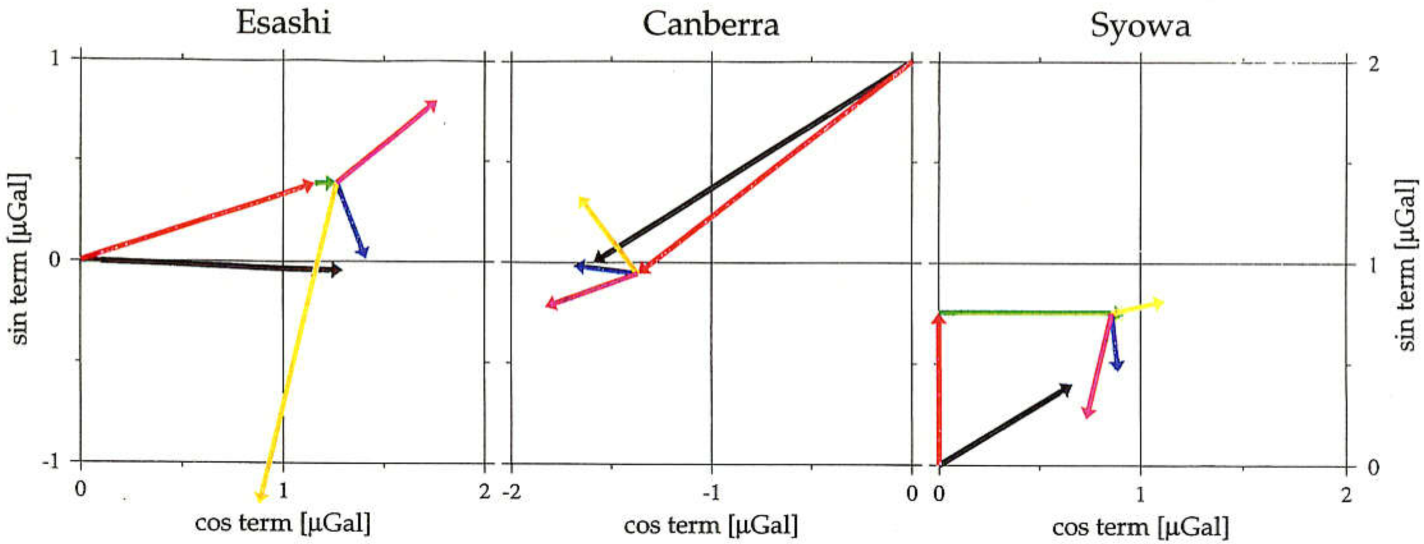

Fig. 24. Phasor plots of the observed annual components and predicted ones. The horizontal and vertical axes correspond to the cosine and sine terms, respectively. The phase angle of each vector is referred to an analysis epoch of 00h UTC, January 1, 2000, and the angle is measured from the cosine axis, counter clockwise for a lag. From the left, the results for Esashi, Canberra and Syowa are displayed. The three vectors of black, red and green show the observation, the polar motion effect and the effect of solid tide, respectively. The effects of the Sa ocean wave are very small to display with the scale of this plot. Its effect is only displayed in the plot for Syowa as the small vector picked with white seeing at the top of the solid tide vector. The three vectors of yellow, blue and pink show the effect of SSH variations evaluated using the steric coefficients of 0.0E10-2 m/deg, 0.60E-2 m/deg and 1.0E-2 m/deg, respectively.

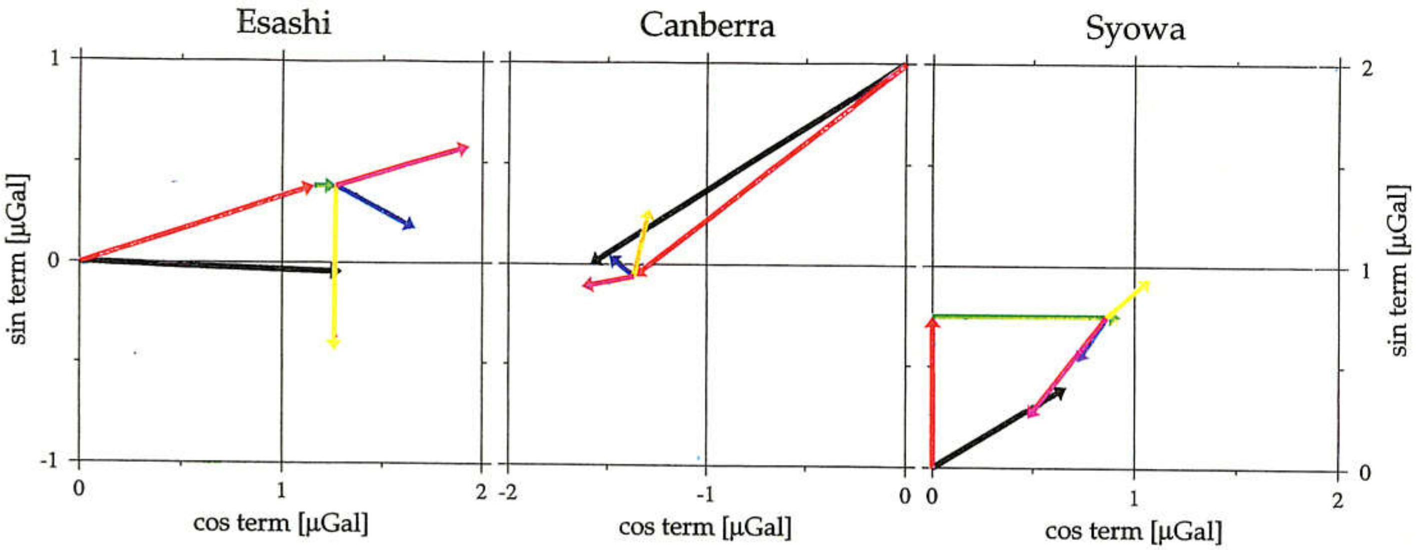

Fig. 25. Similar plots as Fig.24, but the SSH vectors evaluated from the TOPEX/POSEIDON data are displayed.

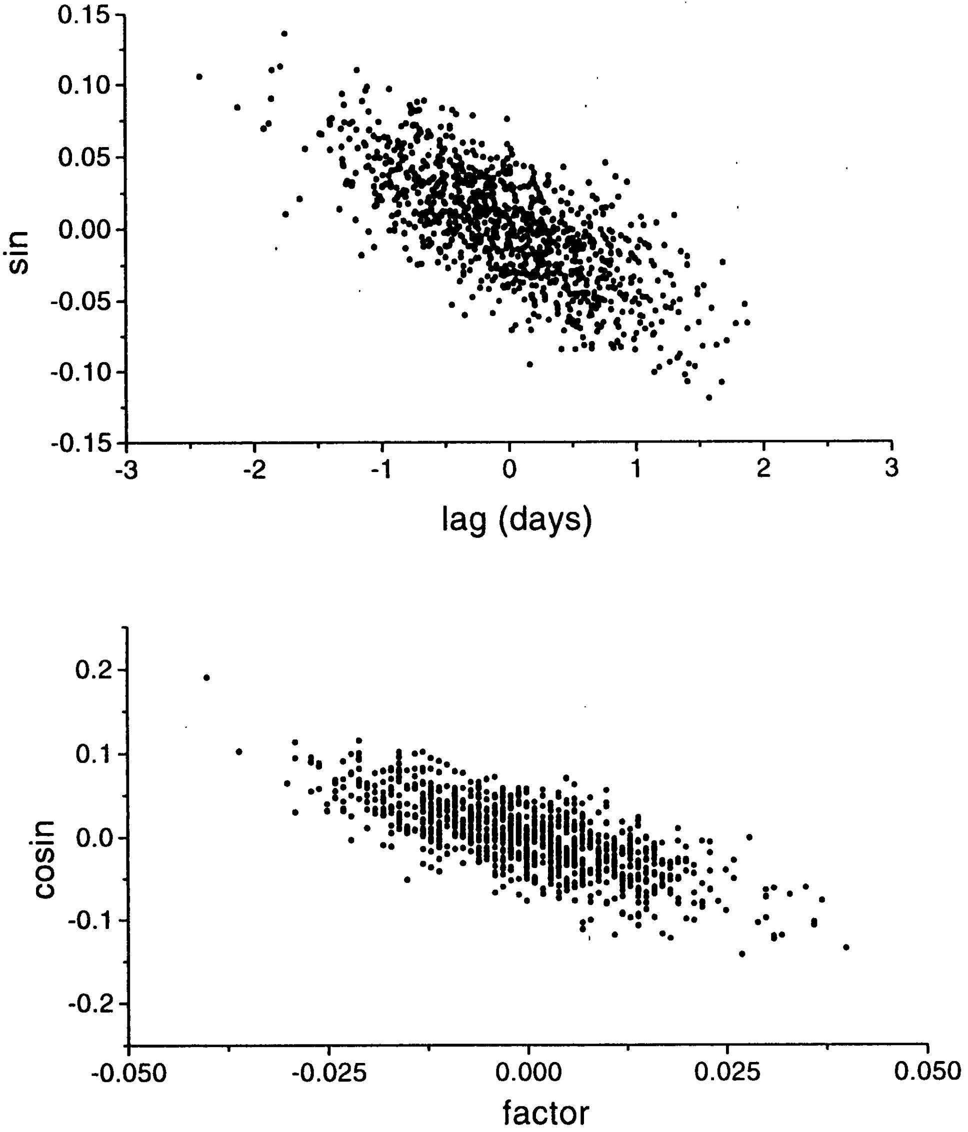

Fig. 26 An example for the correlation between the model parameters which was obtained from Monte Carlo simulation. The correlations between the parameters of the annual and Chandler components are shown in the figures. top: sine term of the annual component vs time lag of the Chandler term. bottom: cosine term of the annual component vs the δ-factor of Chandler term. The mean value for each parameter is subtracted.

Chapter 9.
Conclusions

In Chapters 6 and 7, we estimated the effect of the ocean tides on both the short-period and long-period gravity tides, mainly, based on the SG data obtained at Syowa Station. Further, in Chapter 8, we evaluated the effect of the ocean surface height variability at the period of one year and compared it with the SG observations made at the three sites of GGP-Japan Network including Syowa Station. One of the objectives of Chapter 8 is examining reliability of the SG observations as a measure to study the earth's responses at the period much longer than those treated in the previous chapters. From this point of view, it is clearly shown from our results that the SG observations provide a basis to study the earth's response to the polar motion as a long-period gravity change.

The results for the present studies are summarized as follows.

(1) On the short-period gravity tides at Syowa Station:

Based on the SG data, we obtained the values of 1.144, 1.127, 1.157 and 1.111 as the δ-factors for the four short-period tidal waves of O_1, K_1, M_2 and S_2, respectively, where the ocean tidal effects were corrected by means of the MAT ocean tide model (Matsumoto et al., 1995) and also in taking account of the detailed digital topographic maps in the computation. It was made clear that, when the computations are made without using the finer third- and fourth-order meshes, the estimated ocean tide effects likely to be underestimated by 30-50 %. Further, compared with the ocean tide effects estimated from the MAT model, those estimated from the SCH model (Schwiderski, 1987) are systematically small by about 10% for any of the four waves considered here. However, the observed amplitudes themselves obtained from three different observation periods, namely, Ogawa et al. (1991), Kanao and Sato(1995) and by the present study, are consistent each other within the discrepancy of 1.8 % for all of the four waves. Moreover, the observations corrected for the ocean tide effects by using the MAT model are more consistent with the theoretical δ-factors predicted at the latitude of Syowa Station. From these results, it can be concluded that the discrepancy between the observation and theory, which exceeds 10 % in the semidiurnal δ-factors as pointed out by Ogawa et al. (1991), is mainly caused by their inadequate estimation of the ocean tide effects.

It is also concluded that the MAT model is more consistent with the observation than the SCH, because the discrepancy between the observation and the theory is remarkably reduced by correcting for the ocean tide effects with the MAT model when compared with the SCH model. Further, it is indicated that the Wahr's (1981) theory explains more consistently the observation at Syowa Station than the Dehant's (1987) theory. This is an important result obtained in the present paper, although there still remains a problem on the uncertainty in calibrating the scalar factor of the SG. In order to draw more affirmative conclusion concerning latitude dependency of the δ-factor, and more comparison is required between the results obtained at Syowa Station and those obtained at other SG sites distributed worldwide.

A point of ambiguity in confirming the latitude dependency of δ-factors is the discrepancy of the observed semidiurnal δ-factors between M_2 and S_2 tides. A possible cause is inadequacy of the ocean tide correction applied i this paper. Quite recently, the MAT model was revised using the TOPEX/POSEIDON altimeter data covering much longer period than that used in 1995 (Matsumoto, 2000, private communication). It may be worth while to reestimate the δ-factors using the newly revised MAT model in order to identify the origin of the difference in the semidiurnal δ-factors.

(2) On the long-period gravity tides at Syowa Station:

Using the 2-year SG data, we obtained the amplitudes and phase lags of 11.642±0.035 μGal and -0.12°±0.17° for the Mf wave, and 6.143±0.030 μGal and 0.33°±0.54° for the Mm wave, respectively. By means of the existing five global ocean tide models, we estimated the ocean tide effects as the connection of the observed long-period gravity tides. Then the corrected δ- factors were compared with two theoretical values which are predicted using the elastic earth model and the anelastic one, respectively.

Due mainly to the differences of the five ocean tide models, the corrected δ-factors vary within the ranges of 1.157 to 1.169 and 1.163 to 1.169 for the Mf and Mm waves, respectively. The mean of the five ocean models were 1.162±0.023 for the Mf wave and 1.165±0.014 for the Mm wave. Although the errors of our δ- factors are still large, it is noted that both Mf and Mm δ- factors indicate slightly larger values than those expected from the theory of the elastic tides. In order to give a more reliable constraint with respect to the mantle anelasticity from our observation, it is needed to improve the accuracy of calibration of the gravimeter, as well as the ocean tide models, as in the case of the short-period tides.

(3) On the gravity effects due to the sea surface height variations:

Finally, we evaluated the effect of Sea Surface Height (SSH) variations on the observed gravity changes, mainly focusing on the annual variation. On these purposes, we first estimated the spatial distribution of the gravity response to SSH variations by using SSH data corrected for the steric effect. The steric coefficient employed is 0.60 $\times 10^{-2}$ m/°C, which were obtained by averaging the steric coefficients over the central parts of the Pacific and Atlantic oceans. The estimated gravity changes have an amplitude of more than 1 μGal in some coastal areas.

Then the observed annual gravity changes at the three SG sites were compared with the predicted gravity changes evaluated by taking account of the effects of solid tides, ocean tides, polar motion and SSH variations. It was suggested that, at all three sites, more than 80 % of the annual gravity changes can be explained by the sum of these four effects. The present comparison also suggests that the effect of SSH variations composes an important parts of the observed annual changes, and further the gravity observation supports the steric coefficient around 0.60×10^{-2} m/°C, which was obtained independently by the relation between the SSH and the SST (Sea Surface Temperature).

After careful applying these corrections, we could successfully reproduce the observed annual gravity changes at an accuracy of 0.1 μGals. This also indicates that there is a possibility to study the excitation and dumping of the Chandler motion by using gravity data covering an enough span to separate the Chandler and the annual components. The present results also suggest that the annual SSH variation is one of the major origin making a large phase difference between the observed gravity changes and those predicted from the IERS data. In dealing with the polar motion effect in the long-period gravity changes, it is important to carefully maintain the zero point of the SG record, as well as accurately estimate the data offsets. In order to reduce ambiguity due to the data offsets, it is desirable to maintain the SGs by comparison with an absolute gravimeter at least twice a year.

Chapter 10.
Concluding Remarks

The results of this paper clearly indicate that the SGs could precisely detect the ocean signals related to various phenomena covering the wide periodic ranges up-to one year. Further it was confirmed that we can recover the observed gravity changes at the accuracy of better than 1 μGal based on recent our knowledge of the solid tides, ocean tides, polar motion and SSH variations.

Regarding the effect of the SSH variations at other frequency bands which were not discussed in this paper, gravity changes induced by the ENSO-like oscillation in the oceans (**Plate** 3c) are of further interest. The convolution results using the corrected SSH data suggest existence of a seesaw-like oscillation of the gravity changes in the Pacific ocean. Our analysis also suggests that the ENSO-like ocean oscillations produce an effect of 2 to 3 μGals in peak-to-peak amplitude at an observation point in the equatorial region of the Pacific ocean. Although some of the SSH variations are considered to be contaminated by variations due to baroclinic currents which should cause no gravity changes, these seesaw-like gravity changes are consider to be detectable by careful observations with a superconducting gravimeter network, such as GGP and GGP-Japan network. Further, GRACE (Gravity Recovery and Climate Experiment) scheduled for lunch in 2001 under the joint project of USA and Germany) will provide us with more detailed data. Thus , combination of the gravity data, the satellite altimeter data and the ocean bottom pressure gauge data will produce accurate steric information. it would be emphasized again that gravity observations can possibly be used to constrain the amount of mass changes in the oceans, which is deeply related to the problems on the excitation and damping of the polar motion.

For the short-period tides, one of the important targets of the SG observations at Syowa Station is to determine the parameters of free core resnance (FCR) by stacking with the data obtained at other worldwide SG sites. On this standing point, as described in Chapter 6, the SG data of Syowa Station are sufficiently accurate for this purpose. However, in order to use the data fully, we still need to improve the estimation accuracy of the ocean tide effects. Fortunately, it is obvious that, by using the high accurate altimeter data such as produced by TOPEX/POSEIDON altimeter, the modeling for the short-period ocean tides has been remarkably improved. Use of the improved ocean tide models and comparison with the obtained convolution results should revise our knowledge of the FCR parameters previously obtained by Sato et al. (1994) based on the SG data at the three sites in Japan.

However, as regards the observation at Syowa Station which is located at high latitude place where the TOPEX/POSEIDON altimeter does not cover, it is indispensable to improve the ocean tide model by comparing the actual gravity observations with the predicted ocean tide effects. In implementing the ocean tide model around Syowa Station, effects of the sea ice on the tide should be carefully evaluated.

In this paper, we mainly examined the gravity changes whose periodicity is known. We believe that detecting and interpreting the periodic phenomena provide us with a base to clarify any other gravity changes whose temporal nature is still not clearly understood. From this viewpoint, we could say that the SG at Syowa Station is certainly detecting the gravity changes due to any of the short-period tides, the long-period tides and the long-period SSH variations within an accuracy better than 1 μGal. Further, the drift of the SG at Syowa Station shows seems to a tendency of decreasing with time. Therefore, it is highly possible to observe non-tidal gravity changes accompanying with such crustal motion as related to the motion of the glaciers around Syowa Station, for instance.

Acknowledgments

The author would like to thank many who made this work possible. The author would like to express his thanks to Prof. K. Kaminuma of National Institute of Polar Research (NIPR), Prof. K. Shibuya of NIPR and Prof. M. Ooe of National Astronomical Observatory (NAO), who supported the SG observation project at Syowa Station. Prof. K. Shibuya and Prof. Y. Fukuda of Kyoto University (KU) supported the preparations and setting up the SG at Syowa Station. I would like to express my thanks also to Dr. Y. Tamura and Mr. K. Asari of NAO, who are working on the SG observations with me. Dr. Y. Tamura helped the data analysis and Mr. K. Asari completed the data acquisition system used in the SG observations at Syowa Station, Canberra and Esashi. The figures 22, 24 and 25 shown in this thesis are the results for the cooperative work with Dr. Y. Aoyama of the Graduated University for Advanced Studies (GUAS). While, the plates 1, 2 and 3 are the results for the cooperative work with Prof. Y. Fukuda.

The SG observation at Syowa Station could not be started without the support of the members by JARE 33 (leader Prof. K. Fukuchi) and JARE 34 (leader Prof. N. Sato) and could not be continued without the support by JARE. The authors express thanks to Dr. K. Okano of University of Tokyo, Dr. N. Sawagaki of Hokkaido University, Prof. M. Funaki of NIPR and Dr. I. Ishikawa of Kyoto University, who maintained the SG with T. Sato and Dr. K. Nawa of Nagoya University. The scale factor of the SG was calibrated with a FG5 absolute gravimeter from January to February in 1995 by Geographical Survey Institute.

The SG data used in Chapter 8 are those obtained from the GGP-Japan Network including Syowa Station. This SG network is being operated in cooperation with Ocean Hemisphere Project as Y. Fukao of University of Tokyo as the conductor (Grant in Aid for Scientific Research No. 09NP1101 of the Ministry of Education, Culture, Science and Sports). Prof. Y. Hamano encouraged and supported the commencement the observation at Canberra, and I would like to thank for Prof. K. Yokoyama of NAO and Prof. S. Takemoto of KU, who encouraged the SG observations all times. They critically read the thesis and also kindly pointed out parts to be revised. The observation at Canberra as a site of GGP-Japan Network is continued under a cooperative project between NAO and the Research School of Earth Sciences of the National Australian University. The scale factor of the SG at Canberra was calibrated in September, 1998 with the assistance of Prof. Mike Gladwin of the Division of Exploration and Mining of the Commonwealth Scientific and Industrial Research Organization.

Drs. K. Matsumoto of NAO and T. Takanezawa of GSAS kindly provided us their ocean tide models for the short-period tides and the Sa tide, respectively. Drs. R. Dickman of New York University, R. J. Eanes of Texas University and S. H. Desai of Colorado University kindly provided us their ocean tide models for the long-period tides. The Parallel Ocean Climate Model of Sea Surface Height and TOPEX/POSEIDON data were provided by Naval Postgraduate School (NPS) of USA. Sea Surface Temperature data were kindly offered by Dr. Robin Tokmakian of NPS.

A part of this research was financed by the Grant in Aid for International Science Program No. 06044223 from the Ministry of Education, Culture, Science and Sports, and was also supported by a Grant in Aid for the Cooperative Research Program of NAO (No. 9705, No. 9805 and No. 9905). The support by the Grant in Aid for Science Program of the Graduated University for Advanced Studies was helpful to exchange the data acquisition system of Syowa Station to a new one.

Last, I would like to express my thank to my family who are supporting me all times.

References

Agnew, D.C., 1983. Conservation of mass in tidal loading computations, Geophys. J. R. astr., Soc., 72: 321-325.

Agnew, D.C., Berger, J., Farrell, W.E., Gilbert, F., Masters, G. and Miller, D., 1986. Project IDA: a decade in review. EOS, Trans. Am. Geophys. Union, 67: 203–212.

Akaike, H., 1974. A new look at the statistical model information, IEEE, Trans. Auto. Control, AC-19, 716-723.

Akaike, H., 1980. Likelihood and Bayes procedure. In: Bernado et al., (Editors), Bayesian statistics, Univ. Press, Valencis, pp. 143–166.

Alterman, Z., Jarosh, H. and Pekeris, C.L., 1961. Propagation of Rayleigh waves in the earth. Geophys., J., Vol. 4, 219-241.

Aoyama, Y., Nawa, K., Yamamoto, H., Doi, K., Shibuya, K. and Sato, T., 1997. Calibration of the SG at Syowa Station using an absolute gravimeter FG5. In: K. Kaminuma and Y. Imanishi (Editors), Proc. 6th Workshop on SG: 48-49 (in Japanese).

Boedecker, G. and T. Fritzer, 1986, International Absolute Gravity Basestation Network, Status report March 1986, International Association of Geodesy Special Study Group 3.87, Veroffentlichungen der Bayerischen Kommission fur die Internationale Erdmessung der Bayerischen Akademie der Wissenschaften Heft Nr. 47, 68 pp.

Bretherton, C.S, Smith, C. and Wallace, J.M., 1992. An intercomparison of methods for finding coupled patterns in climate data. J. Climate, 5: 541-560.

Cartwright, D.E. and R.T., Tayler, 1970, New Computations of the Tide-Gagenerating Potential, Geophys. J. R. astr. Soc., 24, 45-74.

Cartwright D.E. and Anne C. Edden, 1973, Corrected Tables of Tidal Harmonics, Geophys. J. R. astr. Soc., 33, 253-264.

Chao, B.F., Merriam, J.B. and Tamura, Y., 1995. Geophysical analysis and zonal tidal signals in length of day. Geophys. J. Int., 122, 765-775.

Crossley, D., 1988, THE EXCITATION OF CORE MODES BY EARTHQUAKES, Geophysical Monograph 46, Structure and Dynamics of Earth's Deep Interior, eds. D.E. Smylie and R. Hide, IUGG Volume 1, 41-50.

Crossley, D., Hinderer, J., Casula, G., Francis, O., Hsu, H.-T., Imanishi, Y., Jentzsch, G., Kaarrianen, J., Merriam, J., Meurers, B., Neumeyer, J., Richter, B., Shibuya, K., Sato, T. and van Dam, T., 1999. Network of Superconducting Gravimeters Benefits a Number of Disciplines. EOS, Trans. American Geophys. Union., 80, 11(121): 125-126.

Cummins, F. and J.M. Wahr, 1993, Astudy of the Earth's free core nutation using International Deployment of Accelerometers gravity data, J. Geophys. Res., 98, 2091-2103.

Dehant, V. and Ducarme, B., 1987. Comparison between the theoretical and observed tidal gravimetric factor. Phys. Earth Planetary Inter., 49, 192-212.

Dehant, V. and Zschau, J., 1989. The effect of mantle inelasticity on tidal gravity. Geophys. J., 97: 549-555.

Delcourt-Honorez, M., 1986. Earth tides response and barometric effect in three well-aquifer systems. The effect on gravity of the water-level variations. In: R. Viera (Editor), Proc. of the 10th Int. Symp. on Earth Tides: 843-854.

Desai, S.H. and Wahr, J.M., 1995. Empirical ocean tide models estimated from TOPEX/POSEIDON altimetry. J. Geophys. Res., 100, 25205-25228.

Dickman, S.R., 1989. A complete spherical harmonic approach to luni-solar tides, Geophys. J. Int., 99, 457-468.

Eanes, R.J., 1995, Private communication.

Farrell, W.E., 1972. Deformation of the Earth by surface loads. Rev. Geophys. Space Phys., 10: 761-797.

Farrell, W.E., 1973. Earth tides, ocean tides and tidal loading. Phil. Trans. R. Soc. London A., 274: 253-259.

Fukuda, Y. and Sato, T., (1996); Gravity effect of sea level variation at the superconducting gravimeter sites, estimated from ERS-1 and TOPEX/POSEIDON altimeter data, In: J. Segawa, H. Fujimoto and S.Okubo (Editors), International Association of Geodesy Symposia, 117, 107-114.

Gilbert, F. and Dziewonski, A.M., 1975. An application of normal mode theory to the retrieval of structural parameters and source mechanisms from seismic spectra. Phil. Trans. R. astr. Soc., 81, 319-269.

Goodkind, J.M., 1999, The superconducting gravimeter. Rev. Sci. Instrum., 70, 11: 4131-4152.

Hagiwara, S., 1978, Theory of the Earth's Gravity, Kyoritsu Shuppann Co. Ltd, pp. 242 (in Japanese).

Harrison, J.C. and L.J.B. LaCoste, 1978, The Measurement of Surface Gravity, Proceedings of the Ninth Geodesy/Solid Earth and Ocean Physics (GEOP) Research Conference, ed. I.I. Mueller, Report No. 280 of 'Reports of the Department of Gedetic Science' published by The Ohio State University, 239-243.

Harrison, J.C. and Sato, T., 1984. Implementation of electrostatic feedback with a LaCoste–Romberg model G gravity meter. J. Geophys. Res., 89, 7957-7961.

Harrison, J.C., 1985, Earth Tides, Benchmark Papers in Geology Series, Vol. 85, Van Nostrand Reinhold Co. Inc., pp. 419.

Imanishi, Y., T. Sato, M. Kumazawa, M. Ooe and Y. Tamura, Observation of Seismic core modes from a superconducting gravimeter record, Physic. Earth and Planetary Int., 72, 249-263, 1992.

International Earth Rotation Service, home page, http//hpiers.obspm.fr/iers/eopc04/EOPC04.GUIDE.

Ishiguro, M., H. Akaike, M. Ooe and S. Nakai, 1981, A Bayesian Approach to the Analysis of Earth Tides, Proc. 9th Int. Symp. on Earth Tides in New York, 283-292.

Ito, K., Ikami, A., Shibuya, K. and Kaminuma, K., Shibuya, 1984. Upper crustal structure beneath the Ongul Islands, East Antarctica. Mem. National Inst. Polar Res., Ser. C15: 3-12.

Jeffreys, Sir H., 1970, the section 7.02 in the fifth ed. of 'THE EARTH', Cambridge Univ. Press, pp. 525.

Kanao, M. and Sato, T., 1995. Observation of tidal gravity and free oscillation of the earth with a LaCoste\&Romberg gravity meter at Syowa

Station, East Antarctica. In: H.T. Hsu (Editor), Proc. 12th Int. Symp. Earth Tides, Science Press, Beijing, pp. 571-580.

Kaneko,Y., Sato, T. and Sasao, T., 1974. Periodic variation of Earth's gravity due to the polar motion and possibility of its observational detection by means of absolute gravimetry. Proc. Int. Latit. Obs. Mizusawa, 14, 24-25.

Kobayashi, N. and K. Nishida, 1998, Continuous excitation of planetary free oscillations by atmospheric disturbances, Nature, 395, 357-360.

Lambeck, K., 1988, Geophysical Geodesy, Oxford Scientific Publ., pp718.

Love, A. E. H., 1909, The yielding of the earth to disturbing forces, Proc. R. Soc. London, Ser. A, vol. 82, 73-88.

Love, A. E. H., 1911, Chapter IV 'GENERAL THEORY OF EARTH TIDE' in 'Some Problems of Geodynamics', Cambridge Univ. Press (reprinted by Dover in 1967, New York, pp.180).

Loyer, S., Hinderer, J. and Boy, J., 1999. Determination of the gravimetric factor at the Chandler period from Earth orientation data and superconducting gravimeter observations. Geophys. J. Int, 136: 1-7.

Ma, X.C., Shum, R.J., Eanes, R.J. and Tapley, B.D., 1994. Determination of ocean tides from the first year of TOPEX/POSEIDON altimeter measurements. J. Geophys. Res., 99, 24809-24820.

Matsumoto, K., Ooe, M., Sato, T. and Segawa, J., 1995. Ocean tide model obtained from TOPEX/POSEIDON altimeter data. J. Geophys. Res., 100, 25319-25330.

Melchior, P., 1983, The Tides of the Planet Earth, Pergamon Press, pp. 641.

Melchior, P., Ducarme, B. and Francis, O., 1996. The response of the Earth to tidal body forces described by second- and third-degree spherical harmonics as derived from a 12 year series of measurements with the superconducting gravimeter GWR/T3 in Brussels. Phys. Earth Planet. Inter., 93, 223-238.

Mukai, A., Higashi, T., Takemoto, S., Nakagawa, I. and Naito, I., 1995. Accurate Estimation of Atmospheric Effects on Gravity Observations Made with a Superconducting Gravity Meter at Kyoto. Phys. Earth Planet Inter. 91: 149-159.

Mukai, A., Takemoto, S., Fukuda, Y., Higashi, T. and Tanaka, T., 1999. Effect of the change in underground water on determination of the parameters of pole tide at Kyoto. In: K. Kaminuma and Y. Imanishi, Proc. 9th Workshop on SG: 56-59 (in Japanese).

Nakagawa, I., K. Shibya, K. Kaminuma, S. Fujiwara, K. Watanabe, M. Murakami, I. Ishihara, T. Tsubokawa, H. Hanada and K. Yokoyama, 1994, Absolute gravity measurements at Syowa Station during the Japanese Antarctic Research Expedition, Bull. d'inform BGI, 75, 41-56.

National Geophysical Data Center, 1988. ETOPO-5 bathymetry/topography data, Data Announc. 88-MGG-02, Nation. Oceanic and Atmos. Admin., U.S. Dep. Commer., Boulder, Colorado.

Nawa, K., N. Suda, Y. Fukao, T. Sato and K. Shibuya, 1998, Inscessant excitation of the Earth's free oscillations, Earth Planet Space, 59,3-8.

Odamaki, M. and Kuramoto, S., 1989. Ocean tides at Syowa Station. in: K. Kusunoki (Editor), Science in Antarctica, \bf 8\rm, Oceanography, Kokin–Shyoin, Tokyo, pp. 51–62 (in Japanese).

Ogawa, F., Fukuda, Y., Akamatsu, J. and Shibuya, K., 1991. Analysis of tidal variation of gravity observed at Syowa and Asuka Stations, Antarctica, J. Geod. Soc. Jpn, 37, No.1, 13-30 (in Japanese).

Okubu, S., 1983, personal cominucation.

Preisendorfer, R.W. and Mobely, C., 1988. Principal Component Analysis in Meteorology and Oceanography, Elsevier, 425pp.

Prothero, W.A. Jr., 1967. A Cryogenic Gravimeter, PhD thesis.

Prothero, W.A.Jr and Goodkind, J.M., 1968. A superconducting gravimeter. Rev. Sci. Instr., \bf 30\rm: 1257-1262.

Press, W.H, Flanney, B.P., Teukolsky, S.A. and Vetterling, W.T.,1989. Numerical Recipes 'The Art of Scientific Computing'. Cambridge Univ. Press, 818pp.

Richter, B., (1985). Three years of registration with the superconducting gravimeter. Bull. Inf. Marees Terrestres, 94, 6344-6352.

Richter, B., 1990. The long period elastic behavior of the earth. In: D.D. McCarthy and W.E. Carter (Editors), Geophys. Monograph IUGG, 9, Variation in Earth Rotation: 21-25.

Richter, B., Wenzel, H.G., \"{Z}urn, W. and Klopping, F., 1995a. From Chandler wobble to free oscillations: comparison of cryogenic gravimeters and other instruments in a wide period range. Phys. Earth Planet. Inter., 91, 131-148.

Rydelek, P.A. and Knopoff, L., 1982. Long-period lunar tides at the South Pole. J. Geophys. Res., 87, 3969-3973.

Saito, M., 1967, Exitation of Free oscillation and Surface waves by a Point Source in a Vertically Heterogeneous Earth, J. Geophys. Res., 72, 3689-3699.

Sapiro, R., 1990; Smoothing, filtering, and boundary effect. Rev. Geophys., 8: 358-387.

Spratt, R. S., 1981. Measurements of Secular Variations in Gravity, PhD thesis.

Sasao, T., S. Okubo and M. Saito, 1980, A simple theory on the dynamical effects of a stratified fluid core upon nutational motion of the Earth, proc. IAU Sympos. 78, '*Nutation and theEarth'srotation*', eds. E. P. Fedrov, M. L. Sumith and P. L. Bender, 165-183.

Sato, T., 1977, On an instrumental phase delay of the LaCoste & Romberg Gravimeter Prod. Int. Lat. Obs. Mizusawa, 16, 36-50 (in Japanese).

Sato, T., Ooe, M. and Sato, N., 1980, Observations of the Tidal Strain at the Esashi Earth Tides Station, J. Geodetic Soc. Japan, 26, No.1, 35-49 (in Japanese).

Sato, T. and Hanada, H., 1984. Computer program 'GOTIC' for the computation of oceanic tidal loading effects, Publ. Int. Latit. Obs. Mizusawa, 18: 29-47.

Sato,T., Tamura, Y., Kikuchi, N. and Naito, I., 1990. Atmospheric pressure effect on gravity observation and its application to geophysical problems. In: T. Sato, M. Ooe and Y. Ida (Editors), Proc. Workshop on the Earth's Central Core: 27-31 (in Japanese).

Sato, T., 1991, Fluid core resonance measured by quartz tube extensometers at the Esashi Earth Tides Station, Proc. 11th Int. Sympos. on Earth Tides, 573-582.

Sato, T., Shibuya, K., Okano, K., Kaminuma, K. and Ooe, M., 1993. Observation of Earth tides and Earth's free oscillations with a superconducting gravimeter at Syowa Station (status report). Proc. NIPR Symp. Antarct. Geosci., 6, 17-25.

Sato, T., Shibuya, K., Tamura, Y., Kanao, M., Ooe, M., Okano, K., Fukuda, Y., Seama, N., Nawa, K., Kaminuma, K., Ida, Y., Kumazawa, M. and Yukutake, T., 1995a. One year observations with a superconducting gravimeter at Syowa Station, Antarctica. J. Geod. Soc. Japan, 41, 75-89.

Sato, T., Okano, K., Sawagaki, T. and Enomoto, H., 1995b. Tidal displacement of sea ice observed at NISHI–NO–URA cove on East Ongul Island, Antarctica. Proc. NIPR Symp. Antarct. Geosci., 8, 43-48.

Sato, T., Shibuya, K., Nawa, K., Matsumoto, K. and Tamura, Y. 1996a, On the diurnal and semidiurnal tidal factors at Syowa Station, Antarctica. J. Geod. Soc. Japan, 42, No.3, 145-153.

Sato, T., Tamura, Y., Okubo, S. and Yoshida, S., 1996b. Calibration of the scale factor of superconducting gravimeter at Esashi using an absolute gravimeter FG5. J. Geodetic Soc. of Japan, 42, 4: 225-232.

Sato, T., Nawa, K., Shibuya, K., Tamura, Y., Ooe, M., Kaminuma, K. and Aoyama, Y.,1997a. Polar Motion Effect on Gravity Observed with a Superconducting Gravimeter at Syowa Station, Antarctica. In: J. Segawa, H. Fujimoto and S.Okubo (Editors), International Association of Geodesy Symposia, 117: 99-106.

Sato, T., M. Ooe, K. Nawa, K. Shibuya, Y. Tamura and K. Kaminuma, 1997b, Long-period tides observed with a superconducting gravimeter at Syowa Station, Antarctica, and their implication to global ocean tide modeling, Phys. Earth Planetary Interiors, 103, 39-53.

Sato, T., Takemoto, S. and Imanishi, I., 1999. GGP and GGP-Japan Network. In: K. Kaminuma (Editor), Superconducting Gravimeter Network, Chikyu Monthry, 21, 8: 474-477 (in Japanese).

Sato, T., Y. Fukuda, Y. Aoyama, H. McQueen, K. Shibuya, Y. Tamura, K. Asari, K. Shibuya, and M. Ooe, 2000, On the observed annual gravity variation and the effect of sea surface height variations, submitted to Phys. Earth Planetary Interiors.

Seama, N., Y. Fukuda and J. Segawa, 1993, Superconducting Gravimeter Observations at Kakioka, Japan, J. Geomag. Geoelect. 45, 1383-1394.

Shibuya, K.,1993, Syowa Station; Observatory for global geodesy in Antarctica (a review), Proc. NIPR Symp. Antarct. Geosci., 6, 26-36.

Shida, T. and M. Matsuyama, 1912, Change of Plumb Line refered to the Axis of the Earth as found from the Result of the International Latitude Observations, in On the Elasticity of the Earth and Earth's Crust, Mem. Coll. Sci. Engng, Kyoto Imperial Univ., Vol. IV, No. 1, 277-284.

Stammer, D., Tokmakian, R., Semter, A. and Wunsh, C., 1996. How well does a 1/4° global circulation model simulate large-scale oceanic observations?. J. Geophys. Res., 101, C10: 25779-25811.

Stammer, D., 1997. Steric and wind-induced changes in TOPEX/POSEIDON large-scale sea surface topography observation. J. Geophys. Res., Vol.102, No.C9: 20987-21009.

Schwiderski, E.W., 1980. On charting global ocean tides. Rev. Geophys. Space Phys., 18, 243-268.

Suda, N., K. Nawa and Y. Fukao, 1998, Earth's background free oscillations, Science, 279, 2089-2091.

Takahashi, F., T. Kondo and Y. Tkahashi, 1997, VLBI technics, p184, Ohmusha, pp285 (in Japanese).

Takanezawa, T., 1998. Dynamical Response of Global Ocean to Long Period Tidal Force. thesis for PhD.

Takeuchi, H., 1951, On the Earth Tide in the Compressible Earth of Varing Density and Elasticity, J. Faculty of Science, Section II, Vol. II, Part II, Univ. of Tokyo, pp.1-152.

Tamura,Y., 1987. A harmonic development of the tied-generating potential. Marees Terrestres Bulletin d'Informations, 99: 6813-6855.

Tamura, Y., Sato, T., Ooe, M. and Ishiguro, M., 1991. A procedure for tidal analysis with a Bayesian information criterion. Geophys. J. Int., 104: 507-516.

Tamura, Y., Y. Aoyama and K. Nawa, 1997, Gravimeteric tidal factors at Syowa Station obtained from three-year observations with a superconducting gravimeter, Proc. NIPR Sympo. on Antarctic Geosciences, No. 10, 1-10.

Tanimoto, T., J. Um, K. Nishida and K. Kobayashi, Geophys. Res. Lett., 25, 1553-1556.

Tokmakian, R, 1998. personal communication.

Tsubokawa, I., T. Sugawa, K. Hosoyama, S. Nakai, T. Sato, H. Ishii, T. Mishina, S., Hagiwara, K. Tajima, S. Izutsuya, M. Yanagisawa, T. seto, and I. Nakagawa, 1977, Simultaneous Observation of Earth Tides Performed by LaCoste and Romberg Graavimeters at Mizusawa, J. Geodetic Soc. of Japan, Vol. 23, No. 3, 165-173.

Valliant, H.D., 1991. Gravity meter calibration at LaCoste and Romberg. Geophysics, \bf 56\rm: 705–711.

van Dam, T.M. and Francis, O., 1998, Two years of continuous measurments of tide and nontidal variations of gravity in Boulder, Colorado. Geophys. Res. Letters, 1.25, 3: 393-396.

Wahr, J.M., 1981. Body tides of an elliptical, rotating, elastic and oceanless earth. Geophys. J. R. astr. Soc. 64: 677-703.

Wahr, J.M., and Bergen, Z., 1986. The effect of mantle anelasticity on nutations, Earth tides, and tidal variation in rotation rate. Geophys. J. R. astr. Soc.: 87,633-668.

Warburton, R. and Brinton, E., 1995. Recent developments in GWR Instruments 'Superconducting Gravimeters'. In: C. Potvin (Editor), Proc. of Second Workshop on Non-tidal gravity changes, Concel de Europe Cahiers du Centre Europeen de Geodynamique et de Seismologie, 11: 23-56.

Wunsh, C. and Stammer, D., 1997. ATOMOSPHERIC LOADING AND THE OCEANIC "INVERTED BAROMETER" EFFECT. Rev. Geophys., 35, 1: 79-107.

Zurn, W., Rydelek, P.A., Knopoff, L. and Smith, W.D., 1995. Gravity studies at the South Pole. In: H.T. Hsu (Editor), Proc. 12th Int. Symp. Earth Tides, Science Press, Beijing, pp. 539-545.